Electroanalysis *via* Accumulation

A thesis submitted for the degree of
Doctor of Philosophy
in Physical & Theoretical Chemistry

Rita Nissim
St John's College

Michaelmas Term 2015

Abstract

This thesis is concerned with the exploitation of carbon paste electrodes and heterogeneous mixtures, such as emulsions or solutions only containing miceller structures, for the accumulation or trapping of analytes of interest and their subsequent electroanalysis.

In Chapter 4, the reduction of oxygen is studied in aqueous solutions of pH 6.22 - 8.01, at a carbon paste electrode fabricated from dioctyl phthalate (oil) and graphite. Two two-electron voltammetric waves are usually seen on carbon electrodes, associated with the formation of hydrogen peroxide and water, respectively. However, an additional signal is seen on the carbon paste electrode, which is attributed to the initial formation of the superoxide radical anion, $O_2^{\cdot -}$. Data is presented to show that the predominant source of oxygen for this reaction is that dissolved in the carbon paste material, rather than in the aqueous solution, and that the superoxide is likely formed at the graphite/oil/water triple phase boundary. Kinetic and thermodynamic parameters for the O_2/ $O_2^{\cdot -}$redox couple are reported.

In Chapter 5, a novel electrochemical procedure is developed that allows the amount of oxygen in cetyltrimethylammonium bromide (CTAB) micelles to be effectively titrated and hence the oxygen solubility in the micelles to be determined. The electroreduction of oxygen is studied in aqueous phosphate buffer solutions, using a microelectrode. The addition of micelle forming surfactants to solutions pre-saturated with oxygen leads to a reduction of the oxygen signal allowing the oxygen uptake by the micelles to be measured. For CTAB micelles, a concentration of oxygen of 6.7 ± 0.72 mM was observed, and shown to remain constant with increasing CTAB concentration in the bulk solution. The method has general applicability.

In Chapter 6, the electrochemistry of nitroblue tetrazolium chloride (NBTC) is investigated in aqueous solutions of pH 6.97, on a glassy carbon macroelectrode and at a carbon fibre microelectrode; the adsorption properties of the electrochemically produced diformazan are also studied. A reduction and overall mechanism is proposed based on the analysis of the obtained results. A carbon paste electrode, fabricated using dioctyl phthalate and graphite powder, is then used as a non-enzymatic sensor. The sensitivity of the diformazan oxidation signal to the presence of superoxide is taken advantage of to detect superoxide. The paste electrode is first immersed in aqueous superoxide solutions. It is subsequently equilibrated with NBTC, by immersing it into aqueous NBTC solutions. The reduction of NBTC (by superoxide) thus takes place *in* the paste so allowing the quantification of the superoxide in the aqueous phase by means of the diformazan oxidation signal. A value for the practical limit of detection of 0.059 nM is obtained.

In the final chapter (Chapter 7), a carbon paste recipe is optimised for the detection of phenols via a procedure in which phenols are allowed to accumulate in the paste via transfer from an aqueous solution prior to electro-oxidation. Importantly, the use of such paste electrodes is shown to substantially overcome the "self-passivating" behaviour of the phenol oxidation which usually constrains the electrode process to low concentrations and single-shot experiments. Here, 4-phenoxyphenol could be detected in the range from 2.5 to 40 μM, phenol from 2.5 μM to 60 mM and 4-methoxyphenol from 5.0 to 40 μM. The electrodes were re-usable without surface renewal for phenol concentrations up to 1.0 mM. The use of a bulk phenol solution for pre-concentration via absorptive uptake into a bulk phase followed by electrochemical quantification represents a new form of electroanalysis which is here termed "absorptive stripping voltammetry". This novel approach is complementary to "adsorptive stripping voltammetry", where accumulation

occurs via adsorption on an electrode surface.

The value of absorptive stripping voltammetry is demonstrated through the application of the approach to the sensitive detection of Δ^9-tetrahydrocannabinol (THC) in both aqueous solutions of pH 10.0 and in synthetic saliva solutions; an optimised carbon paste electrode, fabricated from graphite powder and mineral oil, is here utilised. Practical limits of detection of 0.50 μM and 0.10 μM are determined for THC in stationary and stirred aqueous borate buffer solutions, respectively, while THC concentrations as low as 0.50 μM are detected in synthetic saliva solutions. "Absorptive Stripping Voltammetry" can thus be reliably applied to the detection of Δ^9-tetrahydrocannabinol, after suitable optimisation of the assay.

The research in this thesis comprises of work presented in the following articles; these are in order of appearance in the text.

- R. Nissim and R. G. Compton, *PhysChemChemPhys*, 2013, 15, 11918
- R. Nissim, C. Batchelor-McAuley and R. G. Compton, *ChemElectroChem*, 2015, DOI: 10.1002/celc.201500380
- R. Nissim and R. G. Compton, *ChemElectroChem*, 2014, 1, 763
- R. Nissim and R. G. Compton, *Analyst*, 2014, 139, 5911
- R. Nissim and R. G. Compton, *Chemistry Central Journal*, 2015, 9, 41

Acknowledgements

Firstly, an incredibly big thank you must go to Professor Richard Compton for his advice and encouragement throughout my Part II year and the three years of my DPhil. Your continuous support and guidance have been invaluable.

Thank you must also go to the rest of the Compton Group, past and present. Thank you for you friendship, for being around in times of both frustration and celebration. Special thanks to my office neighbour Patty for making me laugh more times than I can count, Eddy for unforgettable Plush memories, Lior for knowing when an update was needed, Chris for all his help whenever I needed it and Eden for being an absolute rock and bringing me raviolli and raspberries at crucial times.

The past seven years in this city have been both challenging but also rewarding when I look at the people I have met. Even if our paths have now split, you played a big part in me being here and growing as much as I have during this experience - so thank you. More importantly, though, if you've managed to stick so far, it must be for a good reason and be sure you have contributed more than you know in me being as happy as I have been in Oxford! Stefano, Andreas, Anna, Christos, Lisa, Tim, Marina, Ben - from volleyball in the park, amazing souvlaki nights and hikes through the wilds of Kea to walks through Apollo's temple, Plush nights, oreo ice cream sessions at G&Ds and cocktails at Angels, thank you for being a continuous source of support. Benjamin - though your time in Oxford was short, those were two of the best terms I have had in Oxford and I am incredibly lucky to count you as my friend. Thank you for, amongst other things, introducing me to Bordeaux wine and chocolate and cinnamon muffins! Timber may sadly no longer be high on the charts but it shall forever be our song! Ross - our friendship over

the past year has greatly shaped me as a person. Thank you for being there for me, for exploring Spain and Croatia with me, for introducing me to sushi and granadillas and for being the best dance partner I could have hoped to find! And, of course, Karine - I don't even know where to start. You are literally on the other side of the planet but that hasn't changed our friendship the tiniest bit. You always ask the right questions and help me the best version of myself. I am looking forward to our adventures in Mexico and Brazil and to more than 200 years in Kea!

Last but not least, I would like to thank my parents and my amazing sister, who have always believed in me. None of this would have been possible without your love and support! Lara should also be thanked for always being willing to test my electrochemistry knowledge and for giving the best welcomes of anyone I know!

Glossary

Where appropriate, symbols are defined in terms of the generic species i or the reduction $\mathrm{A} + \mathrm{e}^- \rightleftharpoons \mathrm{B}$.

Roman Symbols

Symbol	Definition	Units
A	Electrode area	cm^2
A_d	Double layer area	cm^2
C_i	Concentration of species i	mol cm^{-3}
C_d	Differential capacitance	μF cm^{-2}
C_p	Droplet concentration	mol cm^-3
D_i	Diffusion coefficient of species i	cm^2 s^{-1}
d	Density	g mL^{-1}
E^0	Standard electrode potential	V
$E_\mathrm{f}^\ominus$	Formal potential	V
$E_{\frac{1}{2}}$	Half wave potential	V
F	Faraday constant ≈ 96485	C mol^{-1}
G	Gibbs Energy	J mol^{-1}
i	Current	A
$I_\mathrm{A/C}$	Anodic/ Cathodic current	A
i_p	Peak Current	A

Continued on next page

i_{ss}	Steady State Current	A
j	Flux	mol cm^{-2} s^{-1}
k_0	Standard electrochemical rate constant	cm s^{-1}
k_B	Boltzmann constant $\approx 1.381 \times 10^{-23}$	J K^{-1}
$k_{red/ox}$	Rate constant for reduction/oxidation	cm s^{-1}
m	Mass	g
N_A	Avogadro constant $\approx 6.022 \times 10^{23}$	mol^{-1}
n	Total number of electrons transferred	Dimensionless
n'	Number of e^-s transferred before the rate determining step	Dimensionless
R	Gas constant ≈ 8.314	J K^{-1} mol^{-1}
r	Electrode radius	cm
r_0	Microelectrode radius	cm
T	Temperature	K
t	Time	s
V	Volume	mL
$v(x)$	The solution velocity in the x direction	cm s^{-1}
x	Displacement of a species	cm
z_i	The charge of a species i	C

Greek Symbols

Symbol	Definition	Units
α and β	Butler-Volmer transfer coefficients	Dimensionless
$\alpha_{A/B}$	Activities of species A and B	Dimensionless
$\gamma_{A/B}$	Activity coefficients of species A and B	Dimensionless
η	Overpotential	V
η_i	Viscosity	Pa s^{-1}
ν	Scan rate	V s^{-1}
$\phi_{(m)/(s)}$	Electrical potentials of the electrode and solution	V

Contents

Chapter 1

Electrochemistry Fundamentals

Electrochemistry can be a powerful tool in the investigation of fundamental properties of a redox active species, such as its kinetics or thermodynamics [1–3], but electrochemical techniques also provide attractive methodologies for analytical purposes such as the assessment of the concentration of an analyte of interest [4, 5]. In both cases, researchers often use solid electrode substrates to study the electrochemical response of an analyte dissolved in a solution. The electrochemical reactions that are followed thus take place at the two-phase boundary that exists between the electrode and the solution.

This chapter introduces and develops some basic electrochemical concepts, as well the electrochemical techniques used throughout this thesis, before moving on to a discussion of the electrode materials used in experiments in Chapter 2.

1.1 Electrochemical Equilibrium

When an electrode is immersed in a solution, electrons transfer across the two phases - the solution and the electrode - a potential difference builds up at the electrode surface and electrochemical equilibrium is attained. Considering the following case of an electrochemical equilibrium between species A and B,

$$A_{(aq)} + e^-_{(m)} \rightleftharpoons B_{(aq)} \tag{1.1}$$

where A is the oxidised form of B, the electrode potential that is established across the electrode/solution interface can be quantified by the Nernst Equation [6]:

$$\phi_{(m)} - \phi_{(s)} = \frac{\Delta\mu^0}{F} + \frac{RT}{F} ln \frac{\alpha_A}{\alpha_B} \tag{1.2}$$

where $\phi_{(m)}$ and $\phi_{(s)}$ refer to the electrical potentials (V) of the electrode and the solution respectively, $\Delta\mu^0$ is the difference between the standard chemical potentials of species A and B (J mol^{-1}), F is the Faraday constant (96,485 C mol^{-1}), R is the gas constant (8.314 J K^{-1} mol^{-1}), T is the temperature (K), and where α_A and α_B are the activities of the oxidised and reduced species, A and B, respectively (mol kg^{-1}).

The insertion of a second reference electrode is, however, needed to complete the circuit and act as a reference against which the potential drop built up at the working electrode can be measured; it is thus arbitrarily assigned a zero electrode potential. The Nernst equation then becomes:

$$E = E^0 + \frac{RT}{F} ln \frac{\alpha_A}{\alpha_B} \tag{1.3}$$

where E^0 is the standard electrode potential (V) and where the rest of the terms have been previously defined. However, since activities are often unknown, Equ. 1.3 can more usefully be written in terms of the concentrations of the electroactive species. This is possible since the activities of the two species can be expressed as follows:

$$\alpha_A = \gamma_A C_A \tag{1.4}$$

$$\alpha_B = \gamma_B C_B \tag{1.5}$$

where γ_A and γ_B are the activity coefficients (dimensionless) and C_A and C_B are the concentrations of species, A and B, respectively (mol cm^{-3}). The following alternative expression of the Nernst Equation can thus be derived, which is applicable for dilute solutions where the activity coefficients are ca. 1:

$$E = E_f^{\ominus} + \frac{RT}{F} ln \frac{\alpha_A}{\alpha_B} \tag{1.6}$$

where $E_f^{\ominus}$ is the formal potential (V) that is given by Equ. 1.7 and describes the composition of the studied solution and where the rest of the terms have been previously defined.

$$E_f^{\ominus} = E^0 + \frac{RT}{F} ln \frac{\gamma_A}{\gamma_B} \tag{1.7}$$

While a two-electrode system finds application in the measurement of a variety of thermodynamic parameters [7], such measurements are carried out at the equilibrium potential at which the rates of electron transfer from the electrode to species A and from species B to the electrode are equal, i.e. negligible currents flow. Non-equilibrium electrochemistry provides one with more versatility with regards to the types of experiments that can be completed and hence the type of information that can be obtained.

Under non-equilibrium conditions, since a sufficiently large (positive or negative) po-

tential is applied such that a current flow is induced, a third counter electrode becomes necessary. The counter electrode prevents the current from passing through the reference electrode. This ensures that the chemical composition of the reference electrode does not change, allowing the potential drop at the working electrode to be controlled.

Importantly, under these conditions, the current flow through the cell causes changes in the interfacial structure as well as the electrode surface concentrations of the analytes in question. We thus turn to discuss the structure of the electrode/solution interface as well as the kinetics of electrochemical reactions and the modes of transport of species in solution.

1.2 Faradaic and Non-Faradaic Processes

This section introduces faradaic charge transfer reactions and non-faradaic, capacitative, processes. These are the two types of processes that occur at electrodes when an external potential difference is applied, the distinction being whether or not electrons cross the electrode solution interface.

1.2.1 Capacitative Current and the Double Layer

The application of a potential to an electrode induces the build-up of a charge at the electrode/solution interface. This charge is usually held near the electrode surface (< 1 Å[8]) and is balanced by the migration of ions of opposite charge towards the electrode surface. To a first approximation, the double layer that is formed can be viewed as a parallel-plate capacitor, where a potential drop exists between two oppositely charged plates, as shown in Fig. 1.1; this simple model was proposed by Helmholtz [9, 10].

However, more realistic models have been developed, since, unsurprisingly, the physical structure of the double layer has been extensively studied [11–14].

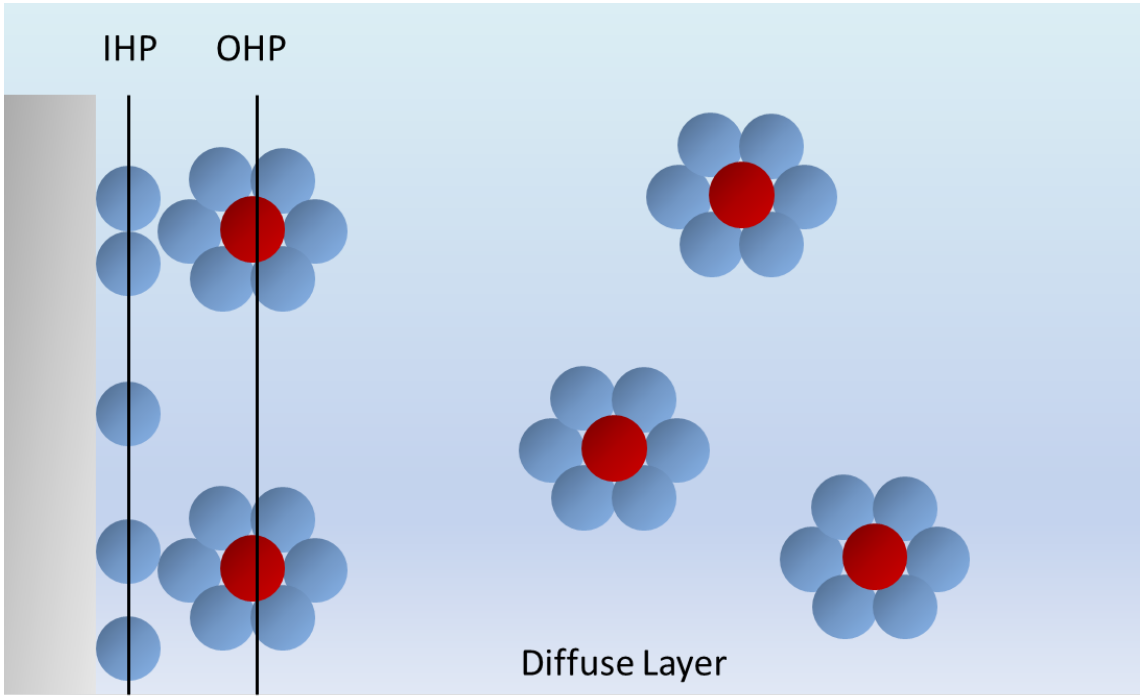

Figure 1.1: Visualising the electrochemical double layer, where the OHP and IHP are the Outer and Inner Helmholtz planes, respectively, as defined in the main text.

The main features of the solution side, as described by the Gouy-Chapman-Stern model [13, 14], include two distinct layers; the compact region, which comprises of the Inner and Outer Helmholtz Planes (IHP and OHP) and in which the potential drops linearly, and the diffuse region where the potential decreases approximately exponentially, as the net charge density returns to its bulk solution value of zero [8]. The IHP is then defined as the plane through the centres of those ions that are specifically adsorbed onto the electrode surface, i.e. that are in direct contact with the electrode. In contrast, when an ion cannot lose its solvation shell, its closest approach to the electrode surface is more hindered. The plane through such ions that are non-specifically adsorbed then defines the OHP. Although more refined models do exist [15, 16], the above description of the

interfacial region is considered adequate. The charging current due to ion migration is termed "capacitative" and can be described by

$$i = \frac{dQ}{dt} = C_d \frac{dE}{dt} = C_d A_d \nu \tag{1.8}$$

where C_d is the differential capacitance (μF cm^{-2}), specific to the electrode, A_d is the double layer area (cm^2) and ν is the voltage scan rate (V s^{-1}).

Importantly, the scale of the double layer varies as a function of the electrolyte concentration. This is of particular significance for electrochemical experiments since, first, most electrochemical techniques are modelled assuming diffusion-only conditions and, second, an electron transfer can only readily take place within an electron tunnelling distance (c.a. 10-20 Å) and when the full potential drop between the electrode and the solution is "felt". The use of sufficient amounts of inert supporting electrolyte (concentrations at least fifty times larger than any analyte concentration [17, 18]) ensures that both the above criteria are fulfilled. The double layer is then compressed to within 10-20 Å, which ensures that the migration of charged species is suppressed as well as that the full potential drop is available to drive the reaction. Added desirable advantages of using a supporting electrolyte include the reduction of the resistivity of the solution and the maintenance of near constant ionic strength, which fixes the activity coefficients, γ_A and γ_B, at near unity values and hence fixes the formal potential.

1.2.2 Faradaic Processes

Proceeding to faradaic processes, the same one-electron reaction as in Section 1.1 (Equ. 1.1) is next considered, this time under non-equilibrium conditions. The total current may be described by Equ. 1.9, where I_a and I_c are the anodic and cathodic currents

respectively (A), n is the total number of electrons transferred, F has been previously defined, A is the electrode surface area (cm^2) and j is the flux of material through the electrode surface (mol cm^{-2} s^{-1}). At the same time the flux, which is equal to the rate of the electrochemical reaction, is given by Equ. 1.10, where k_{red} and k_{ox} are the heterogeneous rate constants for the reduction and oxidation reactions respectively (cm s^{-1} for a one-electron reaction) and $[A]_0$ and $[B]_0$ are the surface concentrations of species A and B respectively (mol cm^{-3}).

$$i = I_a + I_c = FAj \tag{1.9}$$

$$j = k_{red}[A]_0 - k_{ox}[B]_0 \tag{1.10}$$

Through the use of Transition State Theory [6, 8], k_{red} and k_{ox} can both be related to Gibbs energies. The well-known Butler-Volmer Equation can thus be derived [19, 20].

$$j = k_0[A]_0 \exp\left[\frac{-\alpha F}{RT}\eta\right] - k_0[B]_0 \exp\left[\frac{\beta F}{RT}\eta\right] \tag{1.11}$$

$$\text{with} \quad k_{red} = k_0 \exp\left[\frac{-\alpha F}{RT}\eta\right] \quad \text{and} \quad k_{ox} = k_0 \exp\left[\frac{\beta F}{RT}\eta\right] \tag{1.12}$$

where k_0 is the standard electrochemical rate constant (cm s^{-1}), which represents the magnitude of k_{red} and k_{ox} at the formal potential, and α and β are the transfer coefficients (dimensionless), which indicate the position of the transition state between reactants and products; α and β sum up to unity in the case of one-electron reactions. Lastly, η is the overpotential (V) defined as $(E - E_f^{\ominus})$; the rest of the terms have been previously defined. Even though the Butler-Volmer Theory is phenomenological, it can satisfactorily describe

effect of electrode kinetics for the systems investigated.

Substitution of Equ. 1.11 into 1.9, results in the Tafel Law [6, 8]:

$$i = FAk_0\left(\exp\left[\frac{-\alpha F}{RT}\eta\right][A]_0 - \exp\left[\frac{\beta F}{RT}\eta\right][B]_0\right) \tag{1.13}$$

where all the terms have been previously defined. Importantly, in the situations where $E \gg E_f^{\ominus}$ and $E \ll E_f^{\ominus}$, in which the flux depends on the rate of oxidation or reduction respectively, the first or second term can respectively be neglected. Tafel analysis, i.e. plots of $\ln|i|$ versus η, then yields plots where the gradient is proportional to the transfer coefficient in question.

We next turn to discuss the three modes of mass transport of analytes from the bulk solution to the electrode surface, before the last part of this section, which deals with the principles behind the electrochemical techniques that have been used for the completion of experiments.

1.3 Mass Transport

Three contributions to the movement of species from the bulk solution to the electrode surface can be separated; diffusion, convection and migration. Even though the majority of the processes here studied are diffusional and, unless otherwise stated, measures are taken to minimise the effect of convection and migration, it is nevertheless important to establish an understanding of both the random motion of the molecules in solution, as well as any motion that is a response to the application of an external stimulus. Collectively, these three modes of mass transport can be quantified by the one-dimensional form of the Nernst-Plank Equation [6, 8],

$$j_{\mathrm{i}}(x) = -D_{\mathrm{i}}\frac{\partial C_{\mathrm{i}}(x)}{\partial x} + C_{\mathrm{i}}\nu(x) + \frac{z_{\mathrm{i}}F}{RT}D_{\mathrm{i}}C_{\mathrm{i}}\frac{\partial \phi_{\mathrm{i}}(x)}{\partial x} \tag{1.14}$$

where the flux, $j_{\mathrm{i}}(x)$ has units of mol cm^{-2} s^{-1}, as in Equ.1.10, D_{i} is the diffusion coefficient of the species that gives a measure of how far a particle can travel during a period time (cm^2 s^{-1}), C_{i} is the analyte concentration (mol cm^{-3}), $\nu(x)$ is the solution velocity in the x direction (cm s^{-1}), z_{i} is the charge of the species in question (C) and where the rest of the terms have been previously defined.

1.3.1 Diffusion

The first form of mass transport that can affect electrochemical experiments is diffusion, the natural movement of a species down a concentration gradient, which arises from the tendency of any system to maximise its entropy. Mathematically, the rate of diffusion is given by Fick's First Law, which was derived experimentally by Adolf Fick via experiments with salt solutions [21].

$$j_{\mathrm{i}}(x) = -D_{\mathrm{i}}\frac{\partial C_{\mathrm{i}}(x)}{\partial x} \tag{1.15}$$

where $\frac{\partial C(x)}{\partial x}$ is the concentration gradient (mol cm^{-4}), where the negative sign indicates that particles diffusion *down* the gradient and where the remaining terms have been previously defined.

From Fick's First Law, Fick's Second Law [6, 8] can be derived which shows how the concentration varies as a function of time. Equs. 1.16 and 1.17 quantify that relationship in one and three dimensions, respectively.

$$\frac{\partial C_{\mathrm{i}}}{\partial t} = D_{\mathrm{i}} \frac{\partial^2 C_{\mathrm{i}}}{\partial x^2} \tag{1.16}$$

$$\frac{\partial C_{\mathrm{i}}}{\partial t} = D_{\mathrm{i}} \left(\frac{\partial^2 C_{\mathrm{i}}}{\partial x^2} + \frac{\partial^2 C_{\mathrm{i}}}{\partial y^2} + \frac{\partial^2 C_{\mathrm{i}}}{\partial z^2} \right) \tag{1.17}$$

1.3.2 Convection

Convective currents can be either natural or forced. The former are the result of, for example, thermal gradients that can exist in the solution and which unpredictably perturb it. The latter are caused by external stimuli such as mechanical stirring. Such fluxes are thus not entirely predictable but are given by Equ. 1.18 [6, 8]:

$$j_{\mathrm{i}}(x) = C_{\mathrm{i}} \nu(x) \tag{1.18}$$

where all the terms have been previously defined. Given the experimental irreproducibility that natural convective currents can lead to, it is desirable to minimise their effect; this can be done by limiting the time frame of experiments or by preventing the electrochemical cell from vibrating. In contrast, when the application of forced convection is controlled, it can be taken advantage of in the delivery of electroactive species to the electrode surface; this can be done using for example a rotating disc electrode [22–24].

1.3.3 Migration

As briefly discussed in Section 1.2.1, migration is the transfer of charged species through the solution, as a result of the presence of an electric field, such as the one created when the double layer is formed. Migratory fluxes may be quantified by the following equation

[6, 8],

$$j_{\mathrm{i}}(x) = \frac{z_{\mathrm{i}}F}{RT} D_{\mathrm{i}} C_{\mathrm{i}} \frac{\partial \phi_{\mathrm{i}}(x)}{\partial x} \tag{1.19}$$

where all the terms have been previously defined. As can be seen, the direction of these fluxes can be either towards or away from the double layer, depending on whether the species are positively or negatively charged. An important note is that such currents are complex and hence difficult to model, leading to the need of a supporting electrolyte, such as KCl, at concentrations at least fifty times larger than that of any of the electroactive species [17, 18], as discussed in Section 1.2.1. These high support conditions are used throughout this thesis; relatively few studies have focused on low support conditions due to the difficulty in extracting physically meaningful results.

1.4 Macro vs. Microelectrodes: Linear vs. Radial Diffusion

As the name suggests, the difference between macro and microelectrodes is their dimension. While macroelectrodes usually have radii in the millimetre range, microelectrodes have at least one diameter in the micrometre range.

This difference has important implications with regards to the diffusion regime that is followed under the usual voltammetric timescales, summarised in Fig. 1.2. Due to the small size of microelectrodes, the thickness of the diffusion layer that is formed during an electrochemical experiment is much larger than its radius. The electrode can thus be viewed as not uniformly accessible, with the hemispherical diffusion layer that is created leading to this radial diffusion regime. Conversely, the radius of a macroelectrode is much

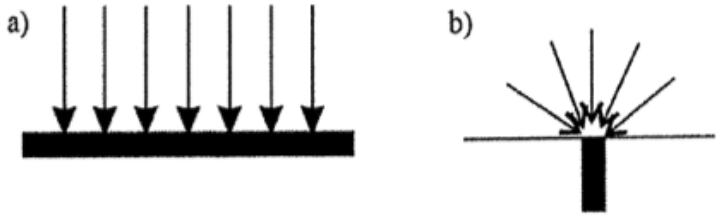

Figure 1.2: a) Linear diffusion at a macroelectrode. b) Radial diffusion at a microelectrode.

larger than the diffusion layer thickness. The diffusion can hence be considered to be linear and normal to the electrode surface. The main point that should be highlighted is that radial diffusion is much more efficient than linear diffusion, which has practical consequences that are elaborated on in the following section.

1.5 Electrochemical Techniques

Bringing together the electrochemical principles discussed so far, this last introductory section goes through the electrochemical techniques that are used in the experiments discussed in the following chapters; cyclic voltammetry, potential step chronoamperometry and square wave voltammetry. What they all have in common is that they probe the effect of the perturbation of the applied potential on the obtained current response. Where they differ is the way in which the applied potential is varied with time. Stripping voltammetry - a technique whose key feature is that it involves a pre-concentration step prior to the current sampling step - is also briefly introduced.

1.5.1 Cyclic Voltammetry

Starting with cyclic voltammetry, during a cyclic voltammetric scan, the applied potential is varied linearly with time, at a constant scan rate (V s^{-1}), starting from potential E_1,

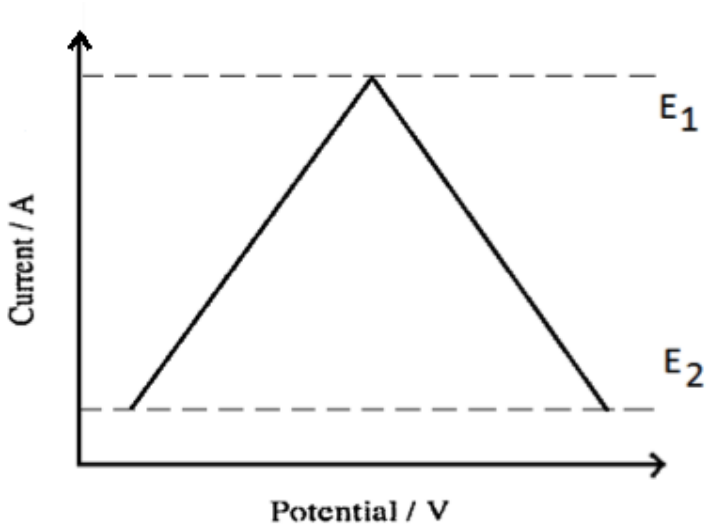

Figure 1.3: The variation of the applied potential with time during a cyclic voltammogram.

usually chosen to be such that the electrochemical reaction under consideration is not yet driven, to an end potential E_2, at which the reaction is fully driven. At potential E_2, the potential is reversed and swept back at the original value at which the potential was held, as shown in Fig. 1.3.

Considering any voltammetric response, since, at potential E_1, the electrochemical reaction under consideration is not yet driven, no current is generated. As the potential is then swept to higher values that are large enough to induce the electron transfer, a current is seen to flow, which increases approximately exponentially. For electrochemically reversible systems (see later), this reflects the formation of the product at the electrode surface as predicted by the Nernst Equation (Equ. 1.6). Conversely, for irreversible systems (again see later), this is the stage at which the electrochemical reaction is controlled by electrode kinetics; the current increase thus here follows the Butler-Volmer Equation (Equ. 1.11). However, as the redox species is consumed near the electrode surface, the surface concentration of the electroactive species decreases. This results in the diffusion layer thickness - the distance that the redox species has to travel to reach the electrode

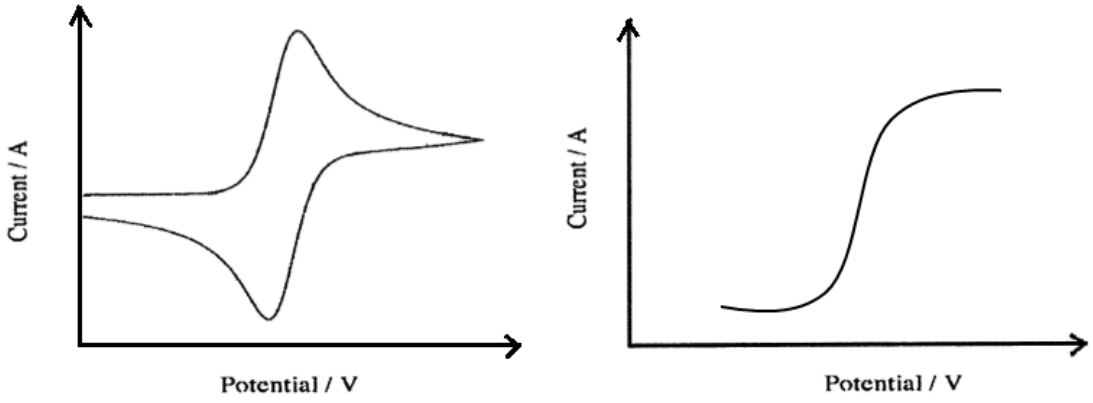

Figure 1.4: Left: Typical cyclic voltammetric response ontained at a macroelectrode. Right: Typical cyclic voltammetric response obtained at a microdisc electrode.

surface - increasing. As a concentration gradient is formed between the electrode surface and the bulk solution, the kinetics become diffusion controlled.

However, this will be reflected differently on the resultant voltammogram, depending on the size of the electrode; in the case of a macroelectrode, the current is seen to decrease as the diffusion layer thickness increases and the reactant near the electrode is depleted over the time frame of the experiment. In contrast, when a microelectrode is used, a steady state current is reached, due to radial diffusion being more efficient than linear diffusion. It is at this point, where the reaction is fully driven, that the scan direction is reversed and the potential is returned to the original value of E_1, the same principles holding during this reverse scan. A typical wave-shaped cyclic voltammetric response obtained on a macroelectrode is shown in (Fig. 1.4 - left), compared to a typical sigmoidal response obtained on a microelectrode (Fig. 1.4 - right).

Importantly, apart from the size of the electroactive surface, the overall electrode kinetics of a system will also be reflected on the shape of the obtained voltammetric response. Matsuda and Ayabe [25] considered three regimes, according to the magnitude of the electrochemical rate constant relative to the voltage scan rate that is used. These

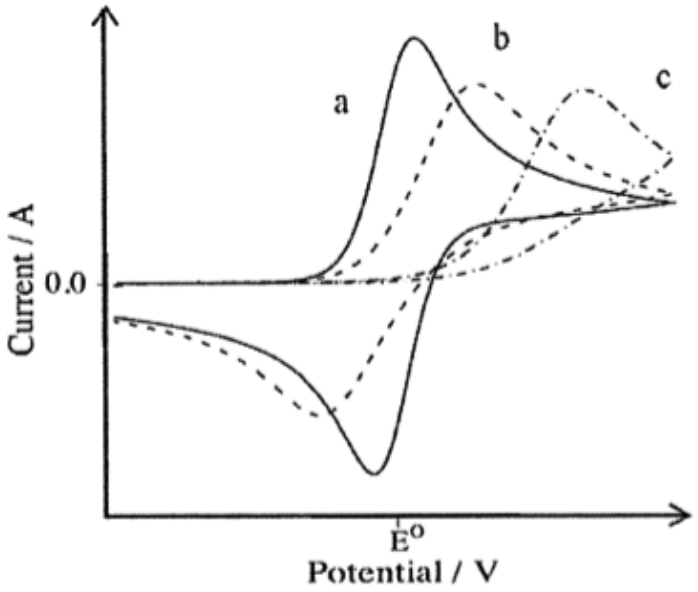

Figure 1.5: a) A fully "reversible" system. b) A "quasi-reversible" system. c) An "irreversible" system.

are classified as "reversible", "irreversible" and "quasi-reversible" (Fig. 1.5) and can be summarised in Table 1.1. In the case of reversible reactions, an equilibrium is attained at the electrode surface. Such reactions require low overpotentials and, in the case of macroelectrodes, voltammetric responses are characterised by peak separations of 57 mV at 25° C [6]. For irreversible reactions, the rate of mass transport is high enough that the redox species is able to diffuse away from the electrode surface, in the timescale of the experiment, before equilibrium can be attained. This is reflected in the larger peak separations that are recorded. With regards to quasi-reversible systems, these exhibit features that lie in between those observed for reversible and irreversible systems.

Lastly, the effect of increasing the rate at which the potential is varied during a cyclic voltammogram should also be considered, especially since scan rate studies are a common way to characterise a system and obtain values of for example the diffusion coefficient of an analyte. Quantitatively, this effect can be understood through Einstein's theory of

diffusion as described by Equ. 1.20 [26]. This relates the root mean square displacement of a species to the experimental time frame and implies an inverse dependence of the extent of the diffusion layer on the square root of scan rate.

	Classification Boundary
Reversible	$k_0 \geq 0.3v^{\frac{1}{2}}$ cm s^{-1}
Quasi - Reversible	$0.3\ v^{\frac{1}{2}} > k_0 > 2$ x 10^{-5} cm s^{-1}
Irreversible	$k_0 \leq 2$ x 10^{-5} cm s^{-1}

Table 1.1: Criteria of reversibility according to Matsuda and Ayabe [25]

$$\sqrt{< x^2 >} = \sqrt{2Dt} \tag{1.20}$$

Given that the flux of a species to the electrode is inversely proportional to the diffusion layer thickness, it is directly proportional to the square root of the scan rate. At the same time, the current density is directly proportional to the flux, i.e. directly proportional to the square root of scan rate, meaning that upon increasing the voltage scan rate, higher currents will be observed.

The equations used to describe peak (Equs. 1.21 and 1.22 [6, 11]) or steady-state currents (Equ. 1.23 [6]) for macro- or microelectrodes, respectively, are the following. For macroelectrodes, the reversible form of the Randles-Ševčik Equation (Equ. 1.21) is used if the system under consideration is an electrochemically reversible one, while the irreversible form (Equ. 1.22) is used for electrochemically irreversible systems.

$$i_p = (2.69 \quad \text{x} \quad 10^5) n^{\frac{3}{2}} \nu^{\frac{1}{2}} A C_{\text{i}} D_{\text{i}}^{\frac{1}{2}} \tag{1.21}$$

$$i_p = (2.99 \quad \text{x} \quad 10^5) n(n^{'} + \alpha)^{\frac{1}{2}} A C_{\text{i}} D^{\frac{1}{2}} \tag{1.22}$$

$$\text{and} \quad i_{ss} = 4nFD_{\text{i}}C_{\text{i}}r_0 \tag{1.23}$$

In the above equations, which are only applicable when the experiments are carried out at 25° C, $n^{'}$ is the number or electrons transferred before the rate determining step (RDS), α_{RDS} is the transfer coefficient of the RDS, and r_0 is the radius of the microelectrode (cm); the rest of the terms have been previously defined.

1.5.2 Potential Step Chronoamperometry

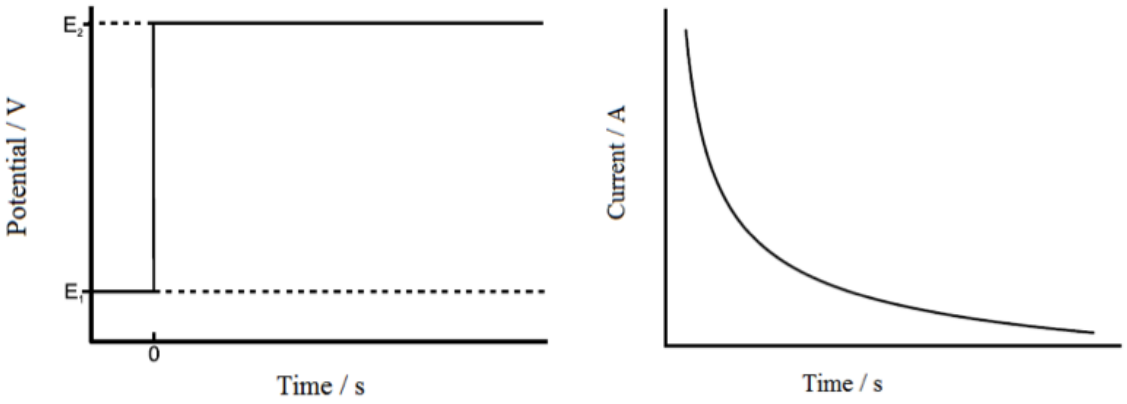

Figure 1.6: Left: The variation of the applied potential with time during a potential step chronoamperogram. Right: Typical chronoamperometric response.

In the case of potential step chronoamperometry, instead of a linear variation of the applied potential with time, a sufficiently high overpotential is instantaneously applied such that the reaction under consideration is fully "driven" and all the electroactive species adjacent to the electrode surface is consumed (Fig. 1.6 - left). The potential is then held constant and the current time response is recorded. A sharp current increase is observed

immediately after the potential jump, followed by steady decrease due to the depletion of the electrode surface concentration of the redox species (Fig. 1.6 - right). When a macroelectrode is used, the current during a chronoamperogram decreases to zero as a function of time, while on a microelectrode, the current stabilises at a steady state value; this is due to the different diffusion regimes that are followed.

Importantly, if a microelectrode is utilised, the independent determination of D_{i} and (nC_0) can be achieved, through fitting of experimental data with the Shoup and Szabo Equation [27, 28], which describes the time dependence of the current.

$$i = 4nFD_{\mathrm{i}}C_{\mathrm{i}}rf(\tau) \tag{1.24}$$

$$f(\tau) = 0.7854 + 0.4431\tau^{-0.5} + 0.2146\exp(0.39115\tau^{-0.5}) \tag{1.25}$$

$$\text{where} \quad \tau = \frac{Dt}{r^2} \tag{1.26}$$

If a macroelectrode is used, the Cottrell Equation [29] can be used to quantify the current recorded at its surface, where t is the time during which the measurement takes place (s) and where the rest of the terms have been previously defined. This equation also allows the determination of D_{i} and C_{i}, though attention must be paid to the timescales used, since if they are long enough, convection can cause non-negligible perturbations.

$$i(t) = \frac{nFAD_{\mathrm{i}}^{\frac{1}{2}}C_{\mathrm{i}}}{\pi^{\frac{1}{2}}t^{\frac{1}{2}}} \tag{1.27}$$

1.5.3 Square Wave Voltammetry

Proceeding to square wave voltammetry (SWV), it is a technique where a square wave is superimposed on a staircase, as shown in Fig. 1.7 (left). During a measurement, the current is sampled at the end of the forward and reverse pulses, with both being recorded as a function of staircase potential. The difference between them, which is larger than each individual current component, is then calculated; a typical square wave voltammogram is shown in Fig. 1.7 (right).

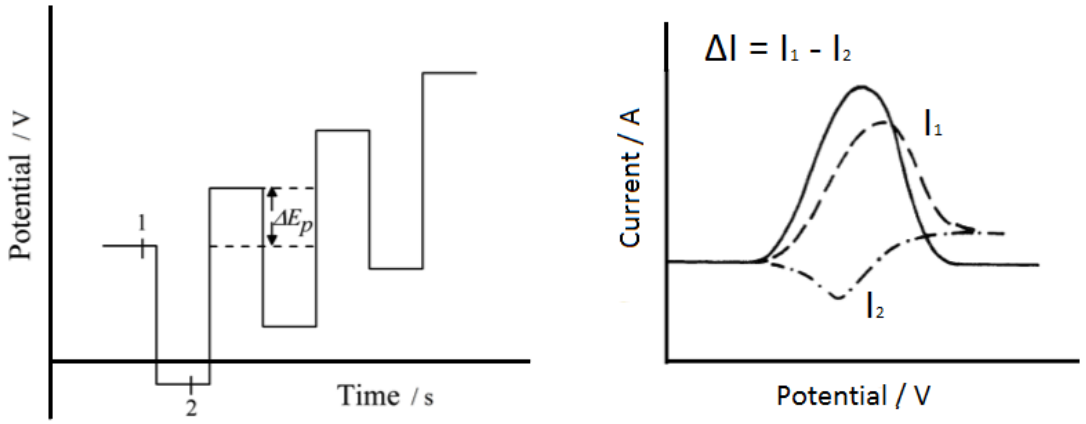

Figure 1.7: Left: Sum of a staircase and a square wave. Right: A typical square wave voltammogram.

Notably, since the capacitative current recorded during both pulses will apparently remain constant, due to the small potential ranges utilised, the capacitative contribution can be subtracted from the overall current potential response. This is of particular importance in electroanalysis where the exclusion of such non-faradaic currents allows more sensitive methods to be developed. Other advantages of square wave voltammetry include the versatility of the technique with regards to being able to optimise for the frequency (Hz), step potential (mV) and amplitude (mV), which can further decrease the achievable limits of detection of the redox active species of interest as well as increase the sensitivity

of the sensor.

1.5.4 Stripping Voltammetry

Finally, stripping voltammetry is here discussed, a term which refers to a set of techniques where a pre-concentration step is carried out prior to the determination step, to allow the analyte to accumulate at the electrode surface before it is stripped off during a scan. This pre-concentration step can be completed under open circuit conditions or under the application of fixed potentials that are usually chosen to ensure maximum surface coverage. During the determination step, the potential is swept - in any of the ways described above - to voltammetrically observe the accumulated redox active species under investigation; the generated current is then proportional to the surface coverage of the species and hence the concentration of the species in the bulk solution. Depending on the nature of the pre-concentration step, three types of stripping voltammetry can be identified; anodic stripping voltammetry, cathodic stripping voltammetry and adsorptive stripping voltammetry.

While the nature of the pre-concentration step can differ, all three can be used in electroanalytical studies to ensure low limits of detection can be achieved. For example, antimony concentrations as low as 40 nM can be detected through anodic stripping voltammetry at unmodified carbon electrodes [30]. With regards to cathodic stripping voltammetry, its application to the detection of manganese, at a boron doped diamond electrode, has yielded a detection limit of 0.01 nM [32], though it should be noted that the technique has been explored to a relatively lesser extent [31],.

The three types of stripping voltammetry are briefly discussed below.

1.5.4.1 Anodic and Cathodic Stripping Voltammetry

In anodic stripping voltammetry (ASV), reductive potentials are applied to induce specific ions to accumulate on the electrode, usually by reduction of metal ions to metals (Equ. 1.28). A commonly used electrode material in this case is mercury (Hg) - either in the form of a standing or mercury drop or as a thin film covering substrates such as glassy carbon - due to its larger potential window in the negative range.

$$\mathrm{M}^{n+} + ne^- \rightleftharpoons \mathrm{M}_{\mathrm{Hg}} \tag{1.28}$$

The above reaction is then reversed during the determination step.

On the other hand, in the case of cathodic stripping voltammetry (CSV), it is oxidative potentials that are used to promote analyte build-up; CSV is thus the inverse of ASV. CSV is usually chosen for the measurement of matrials such as halide ions or thiols, as these species form sparingly soluble Hg salts. The deposition step can be described by:

$$\mathrm{A}^{n-} + \mathrm{Hg} \rightleftharpoons \mathrm{HgA} + ne^- \tag{1.29}$$

which, as with ASV, is reversed during the determination step.

1.5.4.2 Adsorptive Stripping Voltammetry

Finally, adsorptive stripping voltammetry is often the preferred pre-concentration method for organic analytes and is also often used for trace metal analysis [33, 34]. This approach doesn't require potential control during the pre-coconcentration step, though it is often applied to ensure full coverage of the electrode surface. Where the adsorption of the analyte is irreversible, the electrode can be transferred to a supporting electrolyte solution

in order for the determination step to be carried out with minimum interferences.

References

[1] Aldrich, A. P.; den Berg, C. M. G. V. *Electroanalysis* **1998**, *10*, 369.

[2] Kumar, A. S.; Swetha, C., P.; Physicochemical, S. A.; Aspects, E. *Colloids and Surfaces A: Physicochemical and Engineering Aspects* **2011**, *384*, 597.

[3] Ji, X.; Banks, C. E.; Crossley, A.; Compton, R. G. *ChemPhysChem* **2006**, *7*, 1337.

[4] Wang, C.; Yu, C. *Rev. Anal. Chem.* **2013**, *32*, 1.

[5] Chen, S.; Zhang, L.; Long, F., Y.and Zhou *Electroanalysis* **2014**, *26*, 1236.

[6] Compton, R. G.; Banks, C. E. *Understanding Voltammetry, 2nd ed.*; Imperial College Press: London, 2011.

[7] Fisher, A. C. *Electrode Dynamics*; Oxford University Press: Oxford, 1991.

[8] Bard, A. J.; Faulkner, L. R. *Electrochemical Methods: Fundamentals and Applications of Electrochemistry, 2nd ed.*; Wiley & Sons: New York, 2001.

[9] von Helmholtz, H. L. F. *Ann. Phys.* **1853**, *165*, 211.

[10] von Helmholtz, H. L. F. *Ann. Phys.* **1879**, *243*, 337.

[11] Gouy, G. *J. Phys.* **1910**, *9*.

[12] Gouy, G. *Compt. Rend.* **1910**, *149*, 654.

[13] Chapman, D. L. *Philos. Mag.* **1913**, *25*, 475.

[14] Stern, O. *Z. Electrochem.* **1924**, *30*, 508.

[15] Bockris, J. O. M.; Devanathan, M. A. V.; Mueller, K. *Proc. Phys. Soc. Ser. A* **1963**, *274*, 55.

[16] Grahame, D. C. *Chem. Rev.* **1947**, *41*, 441.

[17] Belding, S. R.; Limon-Petersen,; J. G, D.; F., E. J.; G., C. R. *Angewandte Chemie International Edition* **2010**, *49*, 9242.

[18] Dickinson, E. J. F.; Limon-Petersen, J. G.; Rees, N. V.; Compton, R. G. *The Journal of Physical Chemistry C* **2009**, *113*, 11157.

[19] Butler, J. A. Z. *Trans. Faraday Soc.* **1924**, *19*, 729.

[20] Erdey-Gruz, T.; Volmer, Z., M. *Physik. Chem.* **1930**, *150*, 203.

[21] Fick, A. *Poggendorffs Annel. Physik.* **1855**, *94*, 59.

[22] Concepcion, J. J.; Binstead, R. A.; Alibabaei, L.; Meyer, T. J. *Inorg. Chem.* **2013**, *52*, 10744.

[23] Herranz, J.; Garsuch, A.; Gasteiger, H. A. *J. Phys. Chem. C* **2012**, *116*, 19084.

[24] Lu, Y.; He, Q.; Gasteiger, H. A. *J. Phys. Chem. C* **2014**, *118*, 5733.

[25] Matsuda, H.; Ayabe, Y. *Z. Electrochem.* **1995**, *59*, 494.

[26] Einstein, A. *Ann. Phys.* **1905**, *17*, 549.

[27] Nicholson, R. S.; Shain, I. *Analytical Chemistry* **1964**, *36*, 706.

[28] Shoup, D.; Szabo, A. *Journal of Electroanalytical Chemistry* **1982**, *140*, 237.

[29] Cottrell, Z. ., F. G. *Physik. Chem.* **1902**, *4*, 385.

[30] Lu, M.; Toghill, K. E.; Phillips, M. A.; Compton, R. G. *Intern. J. Environ. Anal. Chem.* **2013**, *93*, 213.

[31] Jones, S. E. W.; Chevallier, F. G.; Paddon, C. A.; Compton, R. G. *Anal. Chem.* **2007**, *79*, 11.

[32] Saterlay, A. J.; Foord, J. S.; Compton, R. G. *Analyst* **1999**, *124*, 1791.

[33] Paneli, M. G.; Voulgaropoulos, A. *Electroanalysis* **1993**, *5*, 355.

[34] Zuhri, A. Z. A.; Voelter, W. *Fresenius Journal of Anal. Chem.* **1998**, *360*, 1.

Chapter 2

Electrode Materials and Electrochemical Systems

Carbon electrodes are widely used in electrochemistry, not least because of their wide potential window, relatively inert electrochemistry, ease of modification and low cost [1, 2]. They are also of interest due to the very different physical properties and surface structures that different forms can exhibit [3]. In this thesis, three types of carbon electrodes are utilised; glassy carbon, carbon fibre and carbon paste electrodes. This chapter describes these carbon materials, with particular emphasis on the properties of carbon paste electrodes. The fundamental principles behind the formation of micelles and emulsions are also covered to establish an understanding of the heterogeneous mixtures that are used in the experiments discussed in Chapter 5.

2.1 Solid Carbon Materials

Graphite is a semi-metal comprising of hexagonal lattices in which the carbon atoms are sp2 hybridised. These lattices arrange themselves and form parallel planar sheets, a process referred to as "graphitisation". Two graphitic materials were here utilised - polycrystalline graphite and nanocarbon. These exhibit some degree of order, with

observed interplanar spacings ranging between 10 and 100 nm in the case of polycrystalline graphite and with smaller spacings of 1-10 nm being seen in nanocarbon [4]. Different degrees of order can be achieved depending on the pre-treatment conditions.

Similarly, the method chosen for the fabrication of carbon fibres can control the different degrees of order that they can exhibit; for example heat treatment increases the degree of graphitisation , hence decreasing the interplanar spacing [3]. In general, the graphite planes in carbon fibres can be found in a radial, "onion" or random orientation [4, 5]. In radial fibres, the sheets "radiate" out from the centre of the fibre, while "onion" fibres consist of concentric graphene cylinders. Mainly due to their small "footprint" - they usually have diameters of 5 - 50 μm - these types of electrodes are often selected for "in vivo" experiments [6–8].

Conversely, glassy carbon does not completely graphitise. This is because it is formed by heating aromatic polymers [9] to temperatures that are high enough to result in the evaporation of all the heteroatoms, and thus in the formation of a carbon-only structure, but which cannot cause the C-C bonds to break. This limits the size of the graphitic planes that are formed and leads to interplanar spacings that are larger than those seen with the graphitic materials described above [10]. It was originally thought that the glassy carbon structure was both diamond- and graphite-like, with both sp2 and sp3 hybridised carbon atoms and with short oxygen bridges linking the graphitic domains [11]. An improved model was then developed by Jenkins and Kawamura [12] who suggested that the crystalline material consisted of interwoven graphite ribbons that contained highly conjugated sp2 carbon atoms. Further characterisation of the glassy carbon surface has since shown that glassy carbon is made from fullerene-like structural units [13, 14], though the exact details of its structure are still under debate [15, 16].

We next introduce carbon paste electrodes on which the majority of the experiments here reported were carried out.

2.2 Carbon Paste Electrodes

As the name suggests, carbon paste electrodes (CPEs) are not solid substrates but are instead fabricated by mixing a carbon powder with a liquid binder to produce a homogeneous paste [17]. The paste can then, as described in Chapter 3, be packed in a "well" at the end of a solid rod (usually Teflon), which has a metal rod (usually copper) running through it for electrical contact, where the diameter of the cavity can be adjusted to fit the needs of the researcher. Materials such as polycrystalline graphite and nanocarbon are usually chosen as the carbon components of the paste, with popular organic pasting liquids including paraffin oils and organic esters [18, 19].

While such electrodes are very easy to make, there are a few considerations that have to be made, with regards to both the solid and liquid paste components. The selected carbon powder should for example have a uniform particle size distribution, with particle sizes not exceeding 20 μm, to ensure the homogeneity and good conductivity of the material [21]. At the same time, the pasting liquid should be chemically inert and non-volatile, in order to prevent changes in the paste composition, as well as immiscible with the solvent used in order for the electrode to remain stable during an electrochemical experiment [22, 23]. The binder should also be electrochemically inactive to avoid additional electrochemical signals interferring with those produced by the redox species under investigation [22, 23]. Importantly, the paste as a whole should also be considered as for example the volatility of the liquid binder can lead to an "ageing" effect whereby the paste becomes unusable after

a certain period of time. These observations illustrate how crucial it is to characterise the paste using a known system not only in terms of the selection of the most appropriate powder-to-liquid ratio but also to confirm that the paste can be used quantitatively. Extensively studied redox couples such as the $[Fe(CN)_6]^{3-}/[Fe(CN)_6]^{4-}$ [24] can be used to that effect.

Given their composition, carbon paste electrodes have a hydrophobic surface, this being the most commonly reported property of such substrates [25–29]. This is because the hydrophobic character of the paste can have a significant effect on the observed reaction kinetics [27], which in turn can also be altered depending on the quality of the utilised graphite as well as the chosen carbon-to-pasting liquid ratio [30]. Another important consequence of the surface of these electrodes being hydrophobic is that they are appropriate for studies in aqueous environments but inapplicable in the case of non-aqueous systems or mixed media [20].

Two of the most important features of carbon paste electrodes, however, are the existence of a carbon-oil (binder)-water triple phase boundary at the electrode/solution interface and the fact that analytes can transfer from the bulk solution into the liquid binder, under open circuit conditions, if they are soluble and stable in it. In combination with the ability to optimise the paste composition to ensure highest uptake, their ease of fabrication and modification, their low background currents and very easy surface renewal, carbon paste electrodes are commonly used in electroanalysis, where the above properties and features can be usefully exploited. The next section aims to give a brief overview of the ways in which these surfaces have been utilised in electroanalytical studies.

2.3 Carbon Paste Electrodes in Electroanalysis

Focusing on the ease with which carbon paste electrodes can be modified, this can be done either by mechanically mixing a modifier into the paste [27] or by dissolving it into the liquid binder [31]; up to 30 % is usually added, the exact amount being dependent on for example its ability to form enough active sites, whether that be in surface functional groups [18] or molecules present in the bulk of the paste [19]. It has also been demonstrated that soaking graphite particles in a solution containing the desired modifier, and subsequently evaporating the solvent, results in the graphite particles being "impregnated" with the modifier [32]. As has been mentioned in the previous section, a modifier can also easily be accumulated in the liquid component of the paste through diffusion, under open circuit conditions. Interestingly, it is additionally possible to fabricate "solid" pastes by for example mixing melted phenanthrene with graphite and allowing the homogeneous mixture to harden [33]; these materials can also easily be modified *in situ*. As classified by Kalcher et al, potential paste modifiers can have four possible methods of operation [22]:

- Selective interaction with desired species
- Mediation of redox reactions through surface adsorbed molecules
- Catalysis
- Changing the surface properties of carbon paste electrodes

Unsurprisingly, carbon paste electrodes have thus been used in conjunction with various modifiers. These have ranged from analytical reagents such as 8-hydroxyquinoline

and compounds with ion-pairing properties such as cetyltrimethylammonium bromide (CTAB), for selective ion accumulation [34] and the detection of metals [35] respectively, to silica-containing matrices [36] and substances obtained from humans [37] or other living organisms [38]. Zeolites are also commonly used [39–41], mainly in the detection of inorganic species, as they can act as both ion exchangers and ion traps [39].

The reliability of these surfaces has also been demonstrated through their wide use in different set ups, including carbon paste-based flow cells [42], potentiometric and amperometric sensors [43, 44] as well as in *in vivo* measurements [45, 46], where, due to organic substances often sticking on the electrode surface, their easy surface renewal makes them attractive substrates. More involved designs have also been developed that allow the periodic renewal of the carbon paste surface through the use of cells with a double carbon paste filling [44].

Having illustrated the practical applicability of carbon paste electrodes, the final section of this chapter summarises the fundamental principles behind the formation of micelles and emulsions, before reporting the chemical reagents and electrochemical set ups that were used to carry out the experiments in this thesis.

2.4 Heterogeneous Mixtures: Micelles and Emulsions

Surfactants, often referred to as surface-active agents, are substances that contain both a non-polar hydrocarbon "tail", which is hydrophobic, and a polar "head" which is hydrophilic. When dissolved in aqueous solutions, surfactants instantly self-assemble to form structures whose shape can vary (e.g. they can be spherical or cylindrical) [47]. Given

the hydrophobic nature of the non-polar "tails", the hydrocarbon chains pack closely together, facing away from the aqueous environment, in an arrangement that ensures the highest possible thermodynamic stability [48]. These structures are called micelles and this spontaneous process is called micellisation.

Micellisation may be treated as a step-wise association process [49–51] and the formed agglomerates (micelles) can be viewed as being in an association-dissociation equilibrium. Considering the thermodynamics of this process in more detail, an equilibrium can be assumed to exist between a monomer, A, and an agglomerate of size n. Therefore:

$$\mathrm{nA} \rightleftharpoons \mathrm{A}_n \tag{2.1}$$

$$\text{and} \quad \mu^0 + k_B T \ln(x) = \mu_n^0 + \frac{k_B T}{n} \ln\left(\frac{x_n}{n}\right) \tag{2.2}$$

where μ^0 and μ_n^0 are the chemical potentials of the monomer and the agglomerate, respectively (J mol^{-1}), k_B is the Boltzmann constant (1.38 x 10^{-23} J K^{-1}), n is the number of monomers, x and x_n are the mole fractions of the monomer and agglomerate (dimensionless), respectively, and T is the temperature (K). It is found that there is a specific concentration below which the surfactant molecules exist almost exclusively as monomers and above which they exist almost exclusively as micelles. This concentration is termed critical micelle concentration (cmc), the word "critical" describing the sudden change in the behaviour of the surfactant molecules.

In qualitative terms, the reason why this abrupt behavioural change occurs lies in the fact that as the surfactant concentration is increased, the interfacial tension between the two phases drops. This continues to happen until the cmc is reached, above which the interfacial tension no longer decreases and micelles form in the bulk solution. At

this stage, the minimum area per molecule is occupied, which is slightly larger than if the molecules were close-packed. Quantitatively, this can be rationalised in terms of μ_n^0 being a function of n, that consists of two terms - one increasing and one decreasing with increasing n. The first arises from the hydrophobic interactions between the surfactant tails and water. The latter is due to the polar heads of the molecules repelling each other.

It is based on this model that for example Israelachvili et al further developed the theory of micelle formation [52]. By considering ionic and zwitterionic surfactants that form spherical micelles and making certain assumptions about the surface area per surfactant molecule and the repulsive forces described above, they evaluated the role of geometric constraints in self-assembly processes. They proposed a model that can be extended to apply to more complicated multicomponent systems.

A common use of surfactants is in the stabilisation of emulsions, disperse solutions that consist of two immiscible phases. They operate by forming a thin film around the dispersed phase, thus reducing the interfacial tension between it and the bulk phase. Different droplet sizes can be achieved depending on the selected emulsification method, with the formation of smaller droplets generally being less facile. Macroemulsions, characterised by an average radius of 1-2 μm, will for example easily be formed if a high-speed stirrer is used, while nanoemulsions whose average radius ranges from 20 to 100 nm require the input of higher amounts of energy. [53]

Importantly, although emulsions might be temporarily stable in the absence of surfactants, they lack long-term stability due to breakdown processes taking place. One such process is Ostwald Ripening, the disappearance of smaller droplets and the deposition of those molecules onto larger droplets which leads to an increase in the average droplet size. Other examples include coalescence, the fusion of droplets into larger structures as

a result of the van der Waals forces being too strong, and flocculation, during which the lack of strong repulsive forces leads to the aggregation of droplets. In addition, creaming or sedimentation, in other words the diffusion of droplets to the top or the bottom of the bulk phase depending on the relative densities of the two liquids, can also occur. Emulsions can also undergo a phase inversion where an oil-in-water emulsion can for example invert to a water-in-oil emulsion. These processes, summarised in Fig. 2.1, may occur simultaneously, though the degree to which each will contribute to the separation of the two phases will depend on factors such as the solubility of the dispersed phase, the droplet size or the particle size distribution. [53]

Nevertheless, it is possible to produce emulsions that are stable long enough for elec-

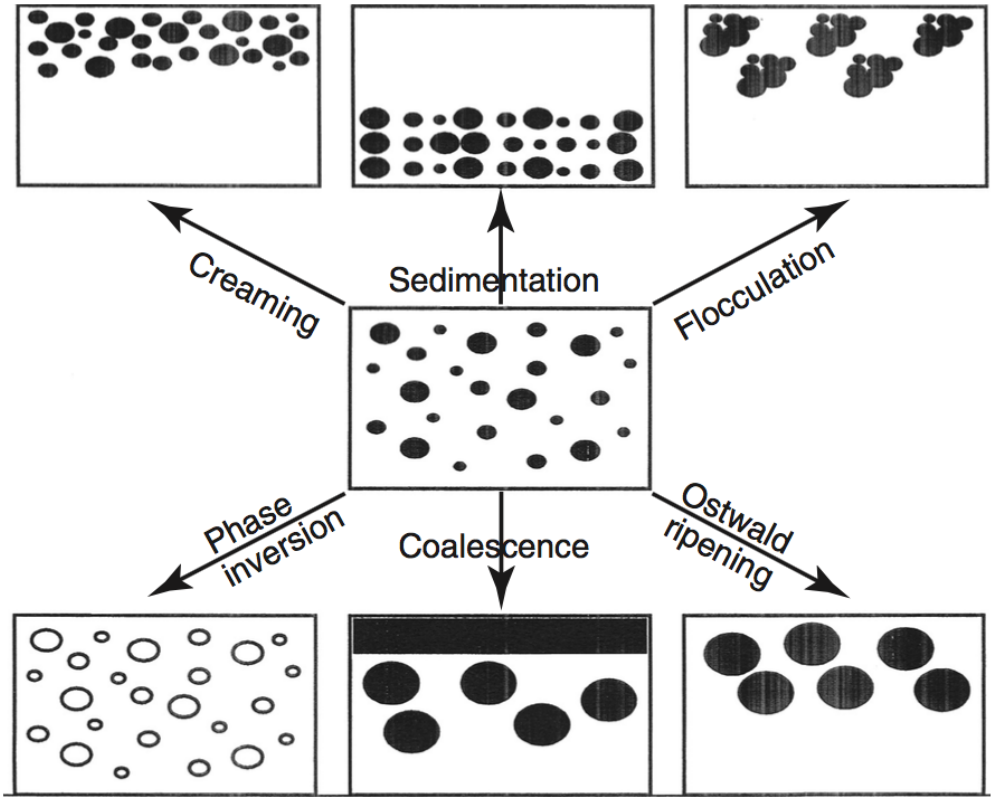

Figure 2.1: Summary of the breakdown processes involved in the separation of the phases of an emulsion. Included from [53] with permission from Wiley.

trochemical experiments to be carried out *without* using surfactants; this can be achieved through acoustic emulsification [54]. This is further discussed in Chapter 5 where the reduction of oxygen is investigated in a heptane-in-water emulsion. Using the observation that oxygen has a higher solubility in organic solvents [55] and hence assuming that much higher amounts of oxygen could be dissolved in the heptane droplets as opposed to the aqueous phase, the aim was to see whether the oxygen mass transport through the aqueous solution would be increased. Given that micelles have also previously been shown to trap oxygen [56–61], Chapter 5 also discusses the uptake of oxygen by CTAB micelles in an aqueous phosphate buffer solution, along with a generally applicable method for the determination of the oxygen solubility within them.

References

[1] Pappis, J.; Blum, S. L. *J. Am. Cer. Soc.* **1961**, *44*, 592.

[2] Pappis, J.; Cvikevich, S.; Hagen, L.; Viola, N. *Metall. Soc. Conf. Proc.* **1963**, *18*, 419.

[3] McCreery, R. L. *Chem. Rev.* **2008**, *108*, 2646.

[4] Bard, A. J. *In Electroanalytical Chemistry*; Dekker, New York, 1991; Vol. 17.

[5] Dresselhaus, M. S. *Graphite Fibers and Filaments*; Springer-Verlag: New York, 1988.

[6] Wightman, R. M. *Science* **2006**, *311*, 1570.

[7] Hermans, A.; Seipel, A. T.; Miller, C. E.; Wightman, R. M. *Langmuir* **2006**, *22*, 1964.

[8] Heien, M. L. A. V.; Johnson, M. A.; Wightman, R. M. *Anal. Chem.* **2004**, *76*, 5697.

[9] Toda, N.; Inagaki, M.; Yamada, S. *J. Non-Cryst. Solids* **1969**, *1*, 285.

[10] Jenkins, G. M.; Kawamura, K. *Polymeric Carbons, Carbon Fibre, Glass and Char*; University Press: Cambridge, England, 1976.

[11] Ergun, S.; Tiensuu, V. H. *Acta Crystallographica* **1959**, *12*, 1050.

[12] Jenkins, G. M.; Kawamura, K. *Nature* **1971**, *231*, 175.

[13] Burian, A.; Dore, J. C. *Acta Physica Polonica* **2000**, *98*, 457.

[14] Harris, P. J. F. *Philos. Mag.* **2004**, *84*, 3159.

[15] McDermott, M. T.; McDermott, C. A.; McCreery, R. L. *Anal. Chem.* **1993**, *65*, 937.

[16] McDermott, C. A.; McCreery, R. L. *Langmuir* **1994**, *10*, 4307.

[17] Adams, R. N. *Anal. Chem.* **1958**, *30*, 1576.

[18] Švancara, I.; Kalcher, K.; Diewald, W.; Vytřas, K. *Electroanalysis* **1996**, *8*, 336.

[19] Švancara, I.; Konvalina, J.; Schachl, K.; Kalcher, K.; Vytřas, K. *Electroanalysis* **1998**, *10*, 435.

[20] Olson, C.; Adams, R. N. *Anal. Chim. Acta* **1963**, *29*, 358.

[21] Švancara, I.; Schachl, K. *Chem. Listy* **1999**, *93*, 490.

[22] Kalcher, K. *Electroanalysis* **1990**, *2*, 419.

[23] Švancara, I.; Vytřas, K. *Chem. Listy* **1994**, *88*, 138.

[24] Bard, A. J.; Faulkner, L. R. *Electrochemical Methods: Fundamentals and Applications of Electrochemistry, 2nd ed.*; Wiley & Sons: New York, 2001.

[25] Švancara, I.; Vytřas, K.; Renger, F.; Smyth, M. R. *Sb. Ved. Pr. Vys. Sk. Chemickotechnol. Pardubice* **1993**, *56*, 21.

[26] Ulakhovich, N. A.; Medyantseva, E. P.; Budnikov, G. K. *Zh. Anal. Khim.* **1993**, *48*, 980.

[27] Kalcher, K.; Kauffmann, J.-M.; J., W.; Švancara,; Vytřas, K.; Neuhold, Z.; Z., Y. *Electroanalysis* **1995**, *7*, 5.

[28] Kalcher, K.; Cai, X.-H.; Koelb, G.; Švancara, I.; Vytřas, K. *Sb. Ved. Pr. Vys. Sk. Chemickotechnol. Pardubice* **1994**, *57*, 5.

[29] Kalcher, K.; Shcachl, K.; Švancara, I.; Vytřas, K.; Alemu, H. *Sb. Ved. Pr. Vys. Sk. Chemickotechnol. Pardubice* **1997**, *3*, 57.

[30] Rice, M. E.; Galus, Z.; Adams, R. N. *J. Electroanal. Chem.* **1983**, *143*, 89.

[31] Metelka, R.; Vytřas, K.; Borbowski, A. *J. Solid State Electrochem.* **2000**, *4*, 348.

[32] Ravinchandran, K.; Baldwin, R. P. *J. Electroanal. Chem.* **1981**, *126*, 293.

[33] Diewald, W.; Kalcher, K.; Neuhold, C.; Švancara, I.; Cai, X.-H. *Analyst* **1994**, *119*, 299.

[34] Zhang, Z.-Q.; Liu, H.; Zhang, H.; Li, Y.-F. *Anal. Chim. Acta* **1996**, *333*, 119.

[35] Stadlober, M.; Kalcher, K.; G., R.; Neuhold, C. *Talanta* **1996**, *43*, 1915.

[36] Walcarius, A.; Despas, C.; Trens, P.; Hudson, M. J.; Bessiere, J. *J. Electroanal. Chem.* **1998**, *453*, 249.

[37] Navratilova, Z.; Kula, P. *Sci. Pap. Univ. Pardubice Ser. A.* **1997**, *3*, 195.

[38] Yao, H.; Ramelow, G. J. *Talanta* **1998**, *5*, 1139.

[39] Švancara, I.; Vytřas, K.; Barek, J.; Zima, J. *Anal. Chem.* **2012**, *31*, 311.

[40] Walcarius, A. *Anal. Chim. Acta* **1999**, *338*, 79.

[41] Walcarius, A.; Mariaaulle, P.; Lamberts, L. *J. Electroanal. Chem.* **1999**, *4653*, 100.

[42] Adams, R. N. *Electrochemistry at Solid Electrodes*; M. Dekker, New York, 1969, 1969.

[43] Taliene, V. R.; Ruzgas, T.; Razumas, V.; Kulys, J. *J. Electroanal. Chem.* **1994**, *372*, 85.

[44] Kulys, J.; Klitgaard, P.; Hansen, H. E. *Mat. Sci. Eng. C* **1996**, *4*, 39.

[45] Wang, H.; Hutchkins, L. D.; Selim, S.; Cummins, L. B. *Biochem. Bioenerg.* **1984**, *12*, 193.

[46] ONeil, R. D. *Analyst* **1994**, *119*, 767.

[47] Kellerman, M.; Bauer, W.; Hirsch, A.; Schade, B.; Ludwig, K.; Bottcher, C. *Angew. Chem. Int. Ed.* **2004**, *43*, 2959.

[48] Taddei, G. *Colloid Polym. Sci.* **1994**, *272*, 1300.

[49] Mukerjee, P. *Adv. Colloid Interface Sci.* **1967**, *1*, 267.

[50] Corkill, J. M.; Goodman, F. *Adv. Colloid Interface Sci.* **1969**, *2*, 97.

[51] Schoda, K.; Nakagawa, T.; Tamamushi, B.; Isemura, T. *Colloidal Surfactants*; Academic Press, New York, 1963.

[52] Israelachvilli, J. N.; Mitchell, D. J.; Ninham, B. W. *J. of the Chemical Society, Faraday Transactions 2: Molecular and Chemical Physics* **1976**, *72*, 1525.

[53] Tadros, T. F. *Emulsion Formation and Stability*; Wiley & Sons: New York, 2013.

[54] Gao, J.; Rusliing, J. F.; Zhou, D. L. *Journal of Organic Chemistry* **1996**, *61*, 5972.

[55] Li, Q.; Batchelor-McAuley, C.; Lawrence, N. S.; Hartshorne, R. S.; Compton, R. G. *Journal of Electroanalytical Chemistry* **2013**, *688*, 328–335.

[56] Matheson, I. B.; King, A. *J. Colloid Interf. Sci.* **1978**, *66*, 464.

[57] Geiger, M. W.; Turro, N. J. *Photochem Photobiol* **1975**, *22*, 273.

[58] Petyaeo, I.; Hunt, J. *Biochim. Biophys. Acta* **1997**, *1345*, 293.

[59] Kameo, Y.; Takahashi, S.; Krieg-Kowald, M.; Ohmachi, T.; Takagi, S.; Inoue, H. *J. Phys. Chem. B* **1999**, *103*, 9562.

[60] An, Y.-J.; Carraway, E. J.; Schlautman, M. A. *Water Res.* **2002**, *36*, 300.

[61] Barillari, J.; Iori, R.; Papi, A.; Orlandi, M.; Bartolini, G.; Gabbanini, S.; Pedulli, G. F.; Valgmigli, L. *J. Agric. Food Chem.* **2008**, *56*, 7823.

Chapter 3

Experimental

3.1 Chemical Reagents

All reagents were purchased from Aldrich (Gillingham, U.K.), at the highest grade available, and were used as received, without any further purification. These were potassium ferricyanide ($K_3Fe(CN)_6$), hexaamine ruthenium (III) chloride ($Ru(NH_3)_6Cl_3$), dioctyl phthalate, mineral oil, graphite powder (particles < 20 μm), nanocarbon powder (particles of 27 nm diameter), cetyltrimethylammonium bromide (CTAB), heptane, nitroblue tetrazolium chloride (NBTC), dimethyl sulfoxide (DMSO), sodium hydroxide (NaOH), potassium superoxide (KO_2), phenol (P), 4-phenoxyphenol (4PP), 4-methoxyphenol (4MP), Δ^9-Tetrahydrocannabinol (THC), synthetic saliva, potassium phosphate monobasic (K_2HPO_4), potassium phosphate dibasic ($K_2H_2PO_4$), sodium tetraborate ($Na_2B_4O_7$) and potassium chloride (KCl).

With regards to the heptane-in-water emulsions used in Chapter 5, the procedure followed for its preparation was based on that reported by Compton et al [1]. Each component was separately saturated with oxygen before emulsification. Heptane (3 % v/v) was subsequently dispersed in the aqueous phosphate buffer component and emulsification was achieved through the use of a 20 kHz sonic horn (Sonics & Materials Inc., VCX400,

U.S.A.) with 3 mm stepped tip (titanium alloy, Jencons, Leyton Buzzard, U.K.)

With regards to the superoxide used to test the sensor developed in Chapter 6, it was synthesised using the method proposed by Hyland et al [2], whereby an air-saturated DMSO solution (here 3 mL) containing 0.55 M H_2O and 5 mM NaOH was prepared. To determine the concentration of the resultant solution, the UV Visible spectra of different KO_2 solutions (0.12 - 1.69 mM) in DMSO were first recorded, using a Hitachi U-2001 spectrophotometer. An extinction coefficient of 1010 L mol^{-1} cm^{-1} was calculated, which was in agreement with literature [3]. The concentration of the superoxide solution prepared as per [2] was thus determined as being 0.22 mM.

All solutions were prepared daily, at 298 K, using deionised water of resistivity of no less than 18.2 MΩ cm (25° C, Millipore UHQ, Vivendi, U.K.) as the solvent and KCl (0.1 M) as the supporting electrolyte. Appropriate K_2HPO_4/ $K_2H_2PO_4$ phosphate buffer solutions (PBS solutions) and NaOH/ $Na_2B_4O_7$ borate buffer solutions (BBS solutions) were used to adjust the pH of the aqueous solutions used to 6.2 - 8.0 and 10, respectively. The pH of each solution was measured using a Hannah pH 213 pH meter.

Where experiments required the absence of oxygen, solutions were deoxygenated using oxygen-free nitrogen (N_2, BOC, Guildford, U.K.), in an air-tight environment, for at least 30 minutes. The measurements themselves were then also done under a light N_2 flow, where attention was paid to not create convective currents. For experiments performed in O_2 saturated solutions, solutions were purged with O_2 (O_2, BOC, Guildford, U.K.), prior and during measurements in the same way as N_2.

3.2 Equipment and Experimental Set-Up

Electrochemical measurements (Cyclic Voltammetry, Potential Step Chronoamperometry and Square Wave Voltammetry) were recorded using a computer controlled Autolab potentiostat (PGSTAT 101, EcoChemie, Utrecht, Netherlands) and were done in a home-built Faraday cage. A standard three-electrode configuration was used, with a glassy carbon macroelectrode (GC, 1.475 mm radius, IJ Cambria Scientific Ltd, Llwynhendy, U.K.), a Carbon Fibre microdisc electrode (CF, 5.82 and 3.56 μm radius, BASi Technicol, West Lafayette, IN), a Carbon Microwire Electrode (CF, 3.50 μm radius, 0.70 and 0.40 mm length, made in-house), a Platinum microdisc electrode (Pt, 5.06 μm radius, BASi, West Lafayette, IN) and a Carbon Paste Electrode (CPE, 1.97 mm radius, 1.00 mm depth, made in-house) acting as working electrodes. A platinum wire (99.99% Good-Fellow, Cambridge, U.K.) was utilised as the counter electrode and a Standard Calomel reference electrode (SCE, Bas Inc, Japan) completed the assembly. All experiments were carried out in a thermostated water bath, at a temperature of 25 $\pm$ 0.1° C.

3.3 Fabrication and Characterisation of the Carbon Paste and Carbon Microwire Working Electrodes

The carbon paste electrode holder was made from a copper rod of radius of 1.97 mm running through a Teflon rod (for electrical contact), leaving a 1.00 mm deep cavity at the edge. The graphite/dioctyl phthalate paste was made with 4.26 g of graphite powder (particles $\langle$ 20 μm) and 1.40 mL dioctyl phthalate. It was characterised in a 0.35 mM $K_3Fe(CN)_6$, phosphate buffer solution containing 0.1 M KCl. A variable scan rate

experiment (25 - 800 mV s^{-1}) gave a diffusion coefficient equal to 7.2 ($\pm$ 0.35) x 10^{-6} cm^2 s^{-1}, in agreement with the literature value of 7.6 x 10^{-6} cm^2 s^{-1} [4], indicating that the paste could be used quantitatively; the same ratio of pasting liquid to carbon powder was thus used to make the graphite/mineral oil, the nanocarbon/dioctyl phthalate and the nanocarbon/mineral oil pastes, unless otherwise stated. The nanocarbon particles have also been previously characterised [5]. Their size was determined by field-emission scanning electron microscopy (SEM, Leo Gemini 1530, Zeiss).

The carbon microwire electrodes were fabricated according to the method reported by Compton et al [6]. A carbon fibre (3.50 μm radius, 0.80 and 0.40 mm length, GoodFellow, Cambridge, U.K.) was connected to a conducting metal wire, using silver epoxy (RS Components Ltd, Northants, U.K.). After allowing the adhesive to set by heat treatment (15 min, 60 °C), the wire was threaded through a plastic micro pipette tip, with the fibre extending out of the tip. The intervening space between the fibre/metal wire and the pipette tip was sealed usind a cyanoacrylate adhesive to prevent electrical leakage. The carbon fibre could then be cut to the desired length, which was confirmed through electrochemical characterisation in a 1 mM $Ru(NH_3)_6Cl_3$.

3.4 Working Electrode Surface Preparation

For experiments carried out in Chapters 4 and 6, the glassy carbon macroelectrode, as well as the carbon fibre microdisc, was polished using diamond sprays of decreasing particle size (3.0 μm, 0.1 μm and 0.01 μm Kemet Ltd, U.K.). Both were briefly sonicated in deionised water between each polishing step, to remove any adhered diamond particles.

For experiments carried out in Chapter 5, the carbon fibre and the platinum microdiscs

were polished using alumina particles of decreasing particle size (1.0 μm, 0.3 μm and 0.05 μm, Buehler, U.S.A.). Both were briefly sonicated in a solution containing a 1:1 ratio of ethanol and deionised water, between each polishing step and before a measurement was recorded, to remove any adhered CTAB and alumina particles. This was not done when the effect of CTAB "fouling" the microdisc electrode surfaces was invertigated.

The carbon paste electrodes used in Chapters 4, 6 and 7 did not need to be polished. Their surface was instead renewed between each scan by cleaning the holder and packing fresh paste; this renewal was not done when the effect of "fouling" was investigated (Chapter 7).

3.5 Simulations

The voltammetric simulations carried out in Chapter 4 were achieved through the use of the commercially available software package DIGISIM (version 3.0, BASi Technicol, USA). DIGISIM is based on a fully implicit finite difference (IFD) method as proposed by Rudolph [7, 8]. The voltammetric simulations carried out in Chapter 6 were achieved through the use of in-house simulation programmes [9, 10].

3.6 Deconvolution of Square Wave Voltammetric Responses

The Peak Analyser Function of OriginPro 9 was used to deconvolute square wave voltammetric responses. The function allowed for the voltammogram to be modelled as a sum of three Gaussian functions.

References

[1] Banks, C. E.; Rees, N. V.; Compton, R. G. *Journal of Physical Chemistry B* **2002**, *106*, 5810.

[2] Hyland, K.; Auclair, C. *Biochemical and Biophysical Research Communications* **1981**, *102*, 531.

[3] Matheson, I. B. C.; Lee, J. *Spectrosc. Lett.* **1969**, *2*, 117.

[4] Bard, A. J. A. J.; Faulkner, R. L. *Electrochemical Methods: Fundamentals and Application*; John Willey and Sons: New York, 2001.

[5] Lowinsohn, D.; Gan, P.; Tschulik, K.; Foord, J. S.; Compton, R. G. *Electroanalysis* **2013**, *25*, 2435.

[6] Ellison, J.; Batchelor-McAuley, C.; Tschulik, K.; Compton, R. G. *Sensors and Actuators B* **2014**, *200*, 47.

[7] Rudolph, M. *Journal of Electroanalytical Chemistry* **1991**, *314*, 13.

[8] Rudolph, M. *Journal of Electroanalytical Chemistry* **1992**, *338*, 85.

[9] Alden, J. A.; Hutchinson, F.; Compton, R. G. *J. Phys. Chem. B* **1997**, *101*, 949.

[10] Alden, J. A.; Compton, R. G. *J. Phys. Chem. B* **1997**, *101*, 8941.

Chapter 4

Superoxide Generation from the Reduction of Oxygen at the Carbon-Oil-Water Triple Phase Boundary

When the reduction of oxygen takes place in aqueous systems, two two-electron waves are usually seen, which arise from the reduction of oxygen to hydrogen peroxide and subsequently to water. In this chapter, the high solubility of oxygen in the oil dioctyl phthalate is exploited and the reduction of oxygen to superoixde is carried out at a carbon paste electrode, fabricated by mixing graphite powder with the oil. The generation of superoxide at the carbon-oil-water triple phase boundary is voltammetrically observed and the "new" peak attributed to that redox process is quantitatively studied and discussed. The work herein presented has been published in *Physical Chemistry Chemical Physics* [1].

4.1 Introduction

The electrochemistry of oxygen in water has been extensively studied, not least because of the importance of the reaction in energy conversion (fuel cells, batteries etc) and in bio-

logical media. The process when studied voltametrically generally shows the intermediary of hydrogen peroxide, with the formation of water at more negative potentials:

$$O_2 + 4H^+ + 4e^- \rightarrow H_2O_2 + 2H^+ + 2e^- \rightarrow 2H_2O, \tag{4.1}$$

although the full four-electron reduction to water is possible on some electrodes (e.g. Pt [2]). Otherwise two two-electron waves are generally seen [2], with different formal (reduction) potentials. That said, the formation of hydrogen peroxide from water clearly includes a sequence of separate steps of which the formation of superoxide ions, $O_2^{\cdot -}$, is generally thought to be the first [3–6]. The addition of an electron to molecular oxygen, during that first step, has been viewed as an outer-sphere electron transfer reaction [7].

In this chapter, we investigate the reduction of oxygen at carbon surfaces, with the aim of observing the superoxide intermediate. Although this has previously been seen with modified solid carbon electrodes [8, 9], here we employ a carbon paste electrode as originally developed by Adams [10] and as reviewed by Svancara et al [11]. In such electrodes, a carbon (graphite) powder is mixed with a binder (pasting liquid) to form materials which have been widely used in electrolysis and especially in the development of chemical sensors, usually for use in aqueous solutions, in which the liquid binder is essentially insoluble.

One feature of carbon paste electrodes (CPEs) is that atmospheric oxygen tends to dissolve and accumulate in the liquid binder; often, the oil dioctyl phthalate is used as the latter. This is then electrochemically visible when voltammetry is run using the carbon paste electrode in aqueous solutions [12–14]. The signal usually appears as a broad response due to the irreversible two-step reduction of oxygen [15], between -0.3 V and

−0.8 V (vs. SCE) [11]. It reflects the aqueous solution reduction of oxygen on carbon, after the oxygen has diffused out of the paste into the aqueous solution.

In the present chapter, we build on and develop further these observations and show that, using a phosphate buffer solution and an appropriate carbon paste electrode, a voltammetric feature associated with the formation of the $O_2^{\cdot-}$ intermediate is electrochemically visible, occurring at a much lower reduction potential than the two-electron formation of hydrogen peroxide on carbon. The origin of this observation lies in the possibility of voltammetry occurring at the phase boundary formed between the oil, the graphite powder and the aqueous solvent, as has been observed in other contexts [16–18], notably "oil droplet voltammetry", where droplets of water insoluble electroactive oils are supported on a carbon electrode in an aqueous electrolyte solution. In this latter case, electron transfer occurs at the circumferences of the droplets, where they touch the underlying electrode, since only at that point are electrons (from graphite), analyte (from the oil) and charge balancing counter ions (from the aqueous solution) all available to allow the electrolytic process to take place without violating the principle of electroneutrality (for a review see ref. [19]). We note that a similar possibility exists for carbon paste electrodes, in which material, for example O_2, dissolved in the oil binder can potentially be reduced (or oxidised) if it is within electron tunnelling distance of the graphite/ carbon material within the carbon paste electrode and also near the oil/water interface [20–22]. Under these conditions, electrolysis might occur either in the oil or the water side of the interface and the products could electron transfer to either the aqueous or the oil phase.

In the case of the O_2/ $O_2^{\cdot-}$ reaction, we note that the solubility of oxygen is much higher in non-aqueous media [23] , compared to aqueous ones where the stability of the superoxide ion is low, and that dioctyl phthalate dissolves oxygen [24]. On the other hand,

$O_2^{\cdot-}$ is very rapidly protonated in aqueous solvents [25] leading to $HO_2^{\cdot}$, which is thought to disproportionate, leading to H_2O_2. In the present chapter we explore processes as in the following scheme:

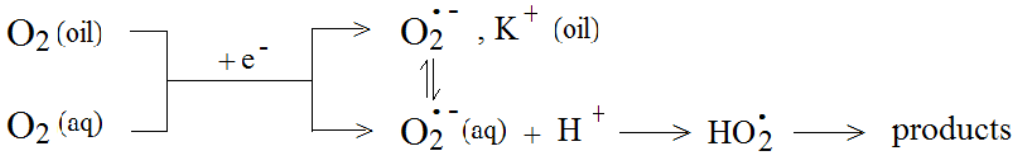

where the K^+ needed for charge neutrality in the oil likely transfers from the electrolyte in the aqueous phase.

4.2 Experimental

Details about the chemical reagents and deoxygenation procedure here utilised can be found in Section 3.1. Cyclic voltammetric and potential step chronoamperometric measurements were carried out using the equipment and experimental set up described in Section 3.2. A glassy carbon macroelectrode (GC) and a carbon paste electrode (CPE), fabricated as described in Section 3.3, were used as working electrodes. A Saturated Calomel Electrode (SCE) and a platinum mesh acted as the reference and counter electrodes respectively. The graphite/dioctyl phthalate paste used was fabricated as per Section 3.3, while the surface of each working electrode was prepared as per Section 3.4. Voltammetric simulations (see Section 3.5) were achieved through the use of the commercially available software package DIGISIM (version 3.0, BASi Technicol, USA). DIGISIM is based on a fully implicit finite difference (IFD) method as proposed by Rudolph [26, 27].

4.3 Glassy Carbon vs. Carbon Paste Electrode - Two Different Routes for the Reduction of Oxygen in Water

The cyclic voltammetric response of an oxygen saturated (pure O_2 - 1.24 mM [28]) phosphate buffer solution (PBS), containing 0.1 M KCl, at pH = 6.98, was recorded both on a glassy carbon macroelectrode and a carbon paste electrode, at an experimental scan rate of 100 mV s^{-1}. Upon comparison of the two results (Fig.4.1), the striking feature is that, while two reduction peaks are seen with the glassy carbon electrode, at -0.70 V and -0.16 V (vs. SCE), three are observed on the carbon paste electrode, at -0.51 V, -1.14 V and -1.59 V (vs. SCE). In addition, a *much* higher current is observed on the carbon paste electrode, compared to the glassy carbon electrode, despite the two electrodes having very similar radii (r_{CPE} = 1.97 mm vs. r_{GC} = 1.48 mm). These observations indicate that oxygen is reduced via a new, additional route on the carbon paste substrate.

Concerning the glassy carbon electrode, the exact steps involved in the process that occurs on its surface are currently under debate [2–6, 29]. Nevertheless, it is agreed that the pathway in some way involves superoxide adsorbed on the glassy carbon surface [3–6], though various different routes have been proposed both for the production of superoxide [3–5] and its subsequent disproportionation into H_2O_2 and O_2 [4, 5]. It has been suggested for example that the superoxide anion can be formed from either adsorbed [5] or free [3, 4] oxygen and that the adsorbed radical must either first migrate to active glassy carbon sites before disproportionating [5] or that a transition to a different type of the anion has to occur before disproportionation [4].

Importantly, however, it is generally accepted that two two-electron steps that form hydrogen peroxide and water take place. The first peak seen at the glassy carbon electrode can, hence, be readily assigned to the two-electron reduction of oxygen to hydrogen peroxide [2, 29], with the second peak corresponding to the further two-electron reduction of hydrogen peroxide to water [2, 29]. This reaction path can be summarised as being:

$$O_2 + 2e^- \rightarrow H_2O_2 \tag{4.2}$$

$$H_2O_2 + 2e^- \rightarrow H_2O \tag{4.3}$$

In the case of the carbon paste electrode, the second and third peaks may be attributed to similar processes as those that give rise to the first and second peaks on the glassy carbon electrode. It is presumed that the first peak corresponds to the one-electron reduction of oxygen to superoxide, probably at the carbon/oil/water triple phase boundary (see below for full arguments). The radical would then rapidly disproportionate into oxygen

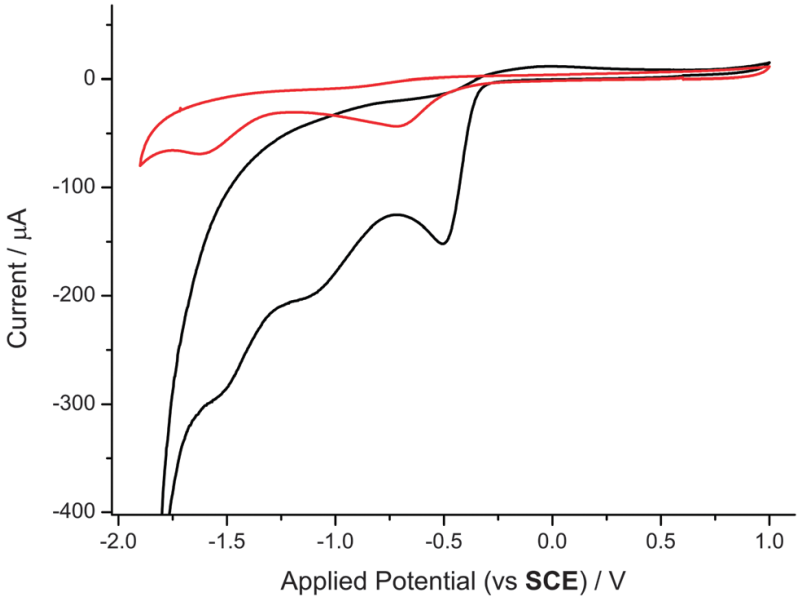

Figure 4.1: The 100 mV s^{-1} cyclic voltammetric response of an oxygen saturated (1.24 mM) phosphate buffer solution of pH = 6.98, on a GC macroelectrode (red, r = 1.48 mm) and a CPE (black, r = 1.97 mm), at 298 K.

and hydrogen peroxide. On or near the glassy carbon surface, possible disproportionation routes would include [3–5]:

$$2O_2^{\cdot -} + H_2O \rightarrow O_2 + HO_2^- + OH^- \tag{4.4}$$

$$O_2^{\cdot -} + H_2O \rightarrow HO_2(ads) + OH^- \tag{4.5}$$

The carbon paste substrate, thus, offers an additional path for H_2O_2 generation, with the reaction pathway being summarised in Fig. 4.2.

Since the oxygen can dissolve in dioctyl phthalate [24], it was inferred that it would build up in the paste prior to electrolysis. Given that the charge transfer event of interest requires electrons, oxygen and charge compensating anions from the supporting electrolyte, it can accordingly be proposed that the reaction occurs at the carbon/oil/water triple phase boundary, especially since the $O_2^{\cdot -}$ radical is known to be stable in organic (aprotic) media [30, 31] but not in water. Favoured generation of superoxide, over that

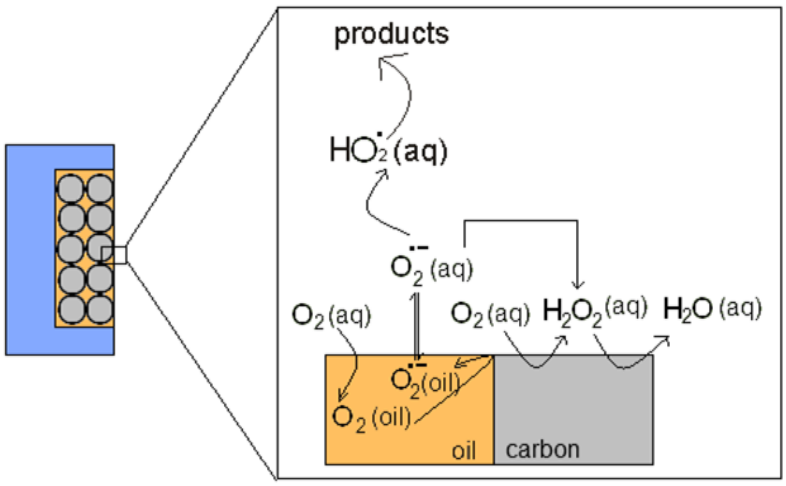

Figure 4.2: Schematic representation of the reaction pathway followed on the carbon paste electrode surface. The presence of the triple phase boundary allows for an additional path for H_2O_2 generation to take place.

of H_2O_2 has also been observed with Hg electrodes covered with hydrophobic surfactants [25, 32], as well as with chemically modified glassy carbon substrates [8, 9]. In the first case, the compact film that such surfactants form over the Hg surface hinders the approach of the H_2O molecules to the adsorbed superoxide [25, 32] and, thus, inhibits HO_2 formation. It has also been proposed that there could be a stabilising interaction between the radical anion and the surfactants [2].

To quantify the accumulation of oxygen in the paste, the first O_2 reduction peak on the carbon paste electrode was investigated by obtaining cyclic voltammograms in a deoxygenated phosphate buffer solution, containing 0.1 M K, at pH = 6.98, after the electrode had been immersed, for different pre-concentration times, in an identical solution that had been previously saturated with oxygen. The results are shown in Fig.4.3, where a clear reduction peak is seen at -0.53 V and a clear oxidation peak is seen in the reverse scan at -0.03 V (vs. SCE). The observation alone that the current, obtained in the deoxygenated solution increases with increasing time of pre-concentration in the oxygen saturated solution, suggests that the origin of most of the O_2 reduced is in the carbon paste electrode. Fig.4.4 reveals that the peak current reaches a plateau at pre-concentration times of approximately eight minutes. It was, thus, concluded that oxygen diffuses into the paste and that the paste is equilibrated with oxygen after eight minutes. Given the known solubility of O_2 in organic media, we infer the oxygen is mostly dissolved in the organic paste.

The above experiment was repeated with the same solutions, but by this time performing single step chronoamperometry in the deoxygenated solution. Results showed a similar relationship of limiting current with pre-concentration time in the oxygen saturated solution, with the paste once again being shown to be equilibrated with oxygen

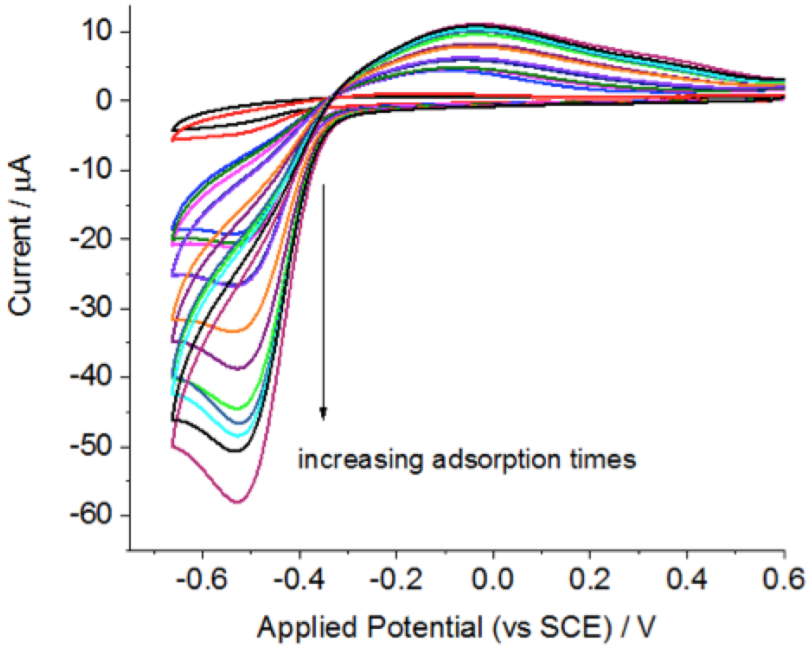

Figure 4.3: 100 mV s^{-1} cyclic voltammetric responses in a deoxygenated phosphate buffer solution of pH = 6.98, containing 0.1 M KCl, for increasing pre-concentration times in an identical solution that had previously been saturated with O_2, at 298 K.

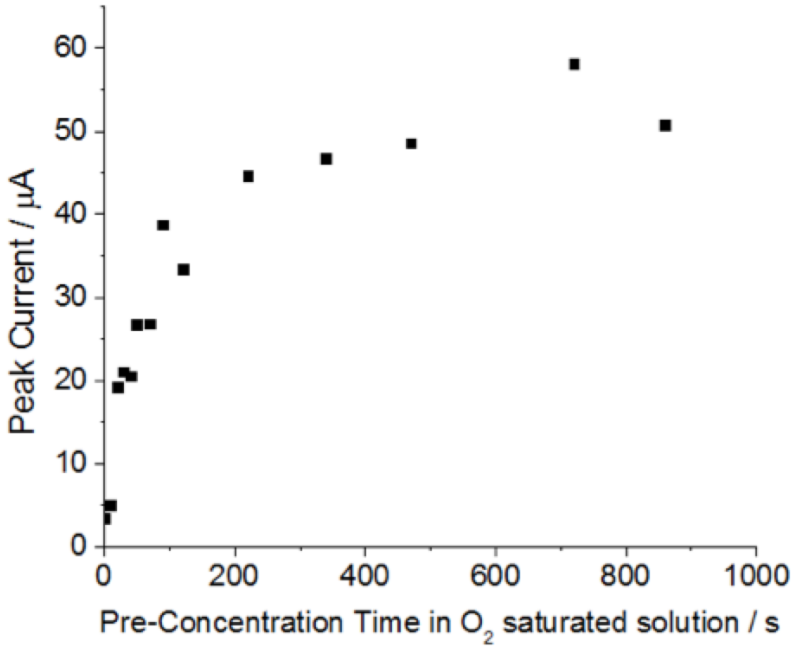

Figure 4.4: The increase of the peak current with increasing pre-concentration time in the O_2 saturated solution, with the plateau being reached after eight minutes.

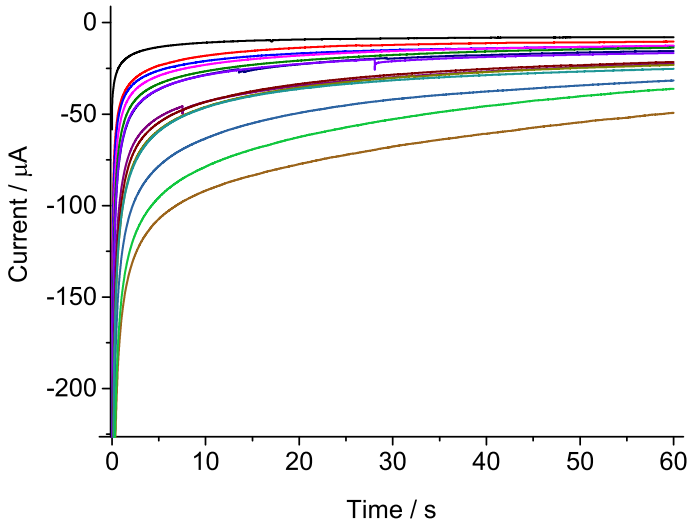

Figure 4.5: Potential step chronoamperometric responses in a deoxygenated phosphate buffer solution of pH = 6.98, containing 0.1 M KCl, for increasing pre-concentration times in an identical solution that had previously been saturated with O_2, at 298 K.

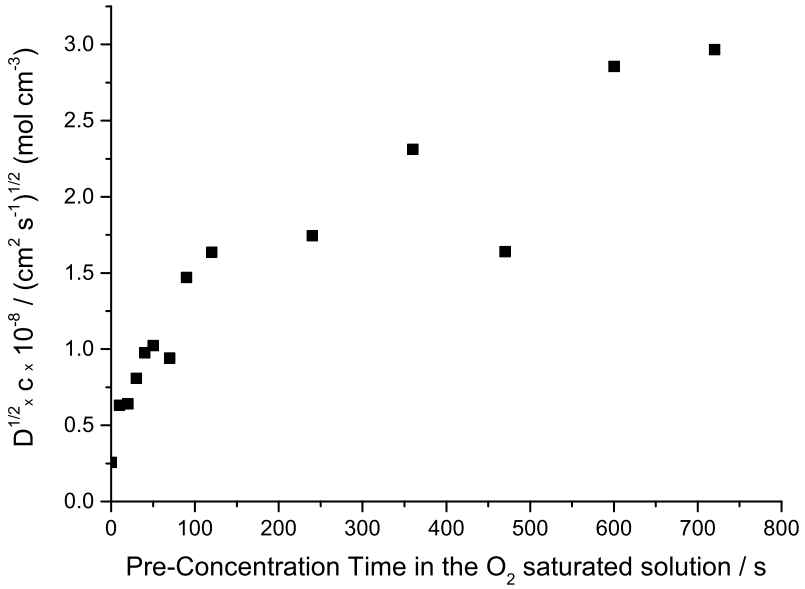

Figure 4.6: The increase of the limiting current with increasing pre-concentration time in the O_2 saturated solution, as reflected through the ($D^{\frac{1}{2}}c$) vs. pre-concentration time plot.

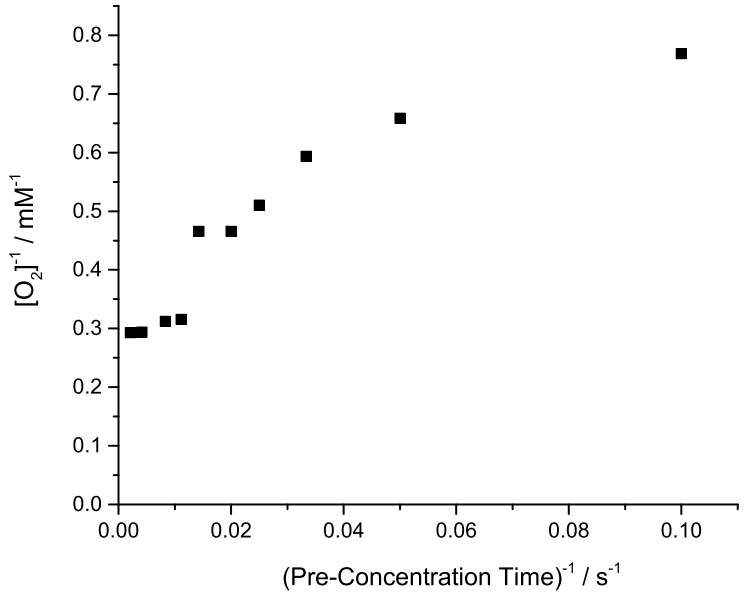

Figure 4.7: Reciprocal plot of the variation of the concentration of O_2 in the paste with pre-concentration time in the O_2 saturated (1.24 mM) phosphate buffer solution.

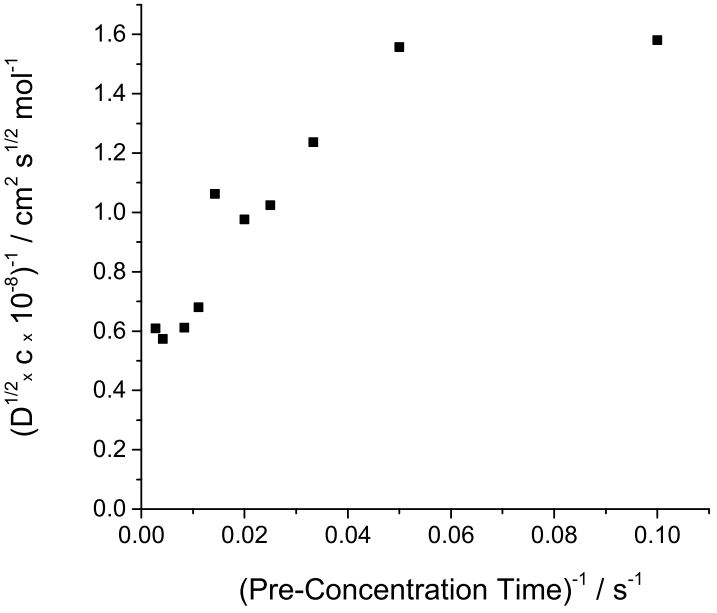

Figure 4.8: Reciprocal plot of the variation of $(D^{\frac{1}{2}}c)$ value with pre-concentration time in the same solution.

at pre-concentration times of approximately eight minutes (Fig.4.5). Cottrell fittings of the chronoamperograms allowed for the determination of the variation of the ($D^{\frac{1}{2}}c$) values with pre-concentration time (Fig.4.6). For the eight minute pre-concentration time, the value of ($D^{\frac{1}{2}}c$) was found to be 1.6 x10^{-8} $(cm^2s^{-1})^{\frac{1}{2}}$ (mol cm^{-3}).

By integrating the chronoamperograms, converting the resultant charge into moles of O_2 present in the paste and estimating the volume of dioctyl phthalate in the carbon paste electrode, the solubility of oxygen in the organic pasting liquid was calculated from the y-intercept of Fig.4.7 as being ca. 3 mM. Given the small depth of the carbon paste electrode, all of the oil in the paste was assumed to be available for the reaction. Having

Solubility / mM	Solvent	Reference
1.24	Water	[33]
6.3	MeCN	[28]
7.71	Toluene	[34]
10	n-Hexane	[35]

Table 4.1: Literature values for the solubility of oxygen in the above solvents, at 298 K. MeCN: Acetonitrile

D / 10^{-5} cm^2 s^{-1}	Solvent	Reference
1.8-2.6	Water	[36]
2.69	Toluene	[37]
3.23	DMSO	[38]
7.05 $*$	MeCN	[39]

Table 4.2: Literature values for the solubility of oxygen in the above solvents, at 298 K. DMSO: dimethyl sulfoxide. MeCN: Acetonitrile. The $*$ refers to measurements carried out at 293 K.

acquired the previously unknown value of the concentration of oxygen in the paste, the y-intercept of Fig.4.8 then allowed for the calculation of the diffusion coefficient of oxygen in the organic medium as being ca. 2.50 x10^{-5} cm^2 s^{-1}. As shown through Tables 4.1 and 4.2, both the solubility and diffusion coefficient of oxygen in dioctyl phthalate are reasonable compared to other similar liquids [6, 25, 30–39].

The oxidation of H_2O_2 was then fingerprinted on the carbon paste electrode. The results are presented in Fig. 4.9, where the oxidation of H_2O_2 (1.09 mM) in a deoxygenated phosphate buffer solution containing 0.1 M KCl, at pH = 6.98, again at an experimental scan rate of 100 mV s^{-1}, is compared to the O_2 reduction cyclic voltammetric response previously obtained on the carbon paste electrode. It can readily be seen that the O_2 reduction back peak at -0.03 V (vs. SCE) does not correspond to the oxidation of H_2O_2, which occurs at the much more positive potential of +1.16 V (vs. SCE).

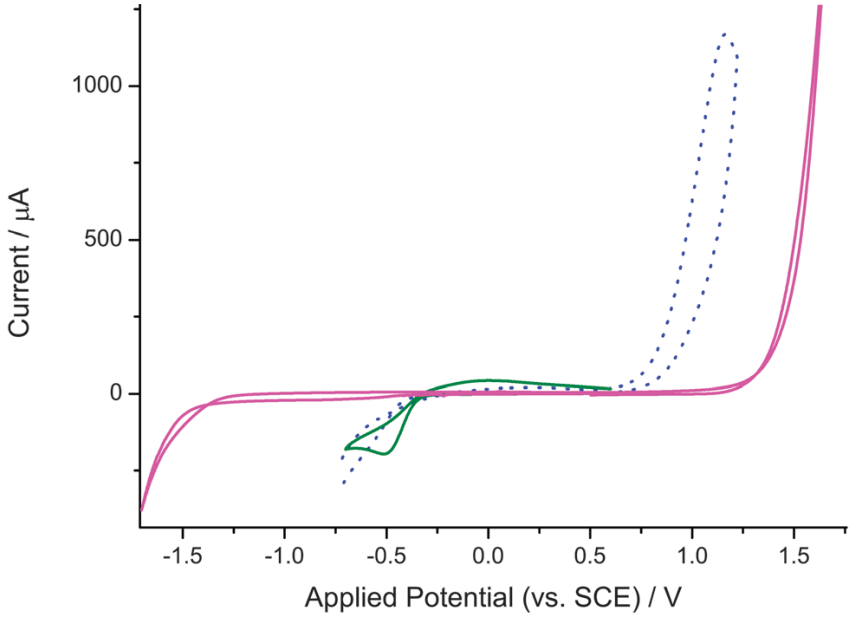

Figure 4.9: The 100 mV s^{-1} cyclic voltammetric responses on the CPE, in an oxygen saturated (1.24 mM) phosphate buffer solution of pH=6.98 (green), a deoxygenated 1.09 mM H_2O_2 phosphate buffer solution of pH=6.98 (dotted blue) and a deoxygenated buffer solution containing of pH=6.98 (magenta).All solutions contained 0.1 M KCl and all measurements were recorded at 298 K.

4.4 Studying the new peak on the carbon paste electrode

We next studied the new (first) reduction peak on the carbon paste electrode, in an oxygen saturated (1.24 mM) phosphate buffer solution of pH = 6.98, containing 0.1 M KCl, at variable scan rates (25 to 800 mV s^{-1}). Oxygen was bubbled for at least eight minutes before getting each voltammogram to obtain stable and reproducible peak currents. The results are shown in Fig 4.10; the O_2 reduction peak is observed between -0.45 V and -0.69 V (vs. SCE), while the oxidation peak is seen between -0.10 V and +0.06 V (vs. SCE). Scans have been performed between +0.6 V to -0.8 V (vs. SCE).

Tafel plots (Fig. 4.11) for the forward peaks gave α values averaging to 0.57, in agreement with literature values for the one-electron reduction of oxygen to produce

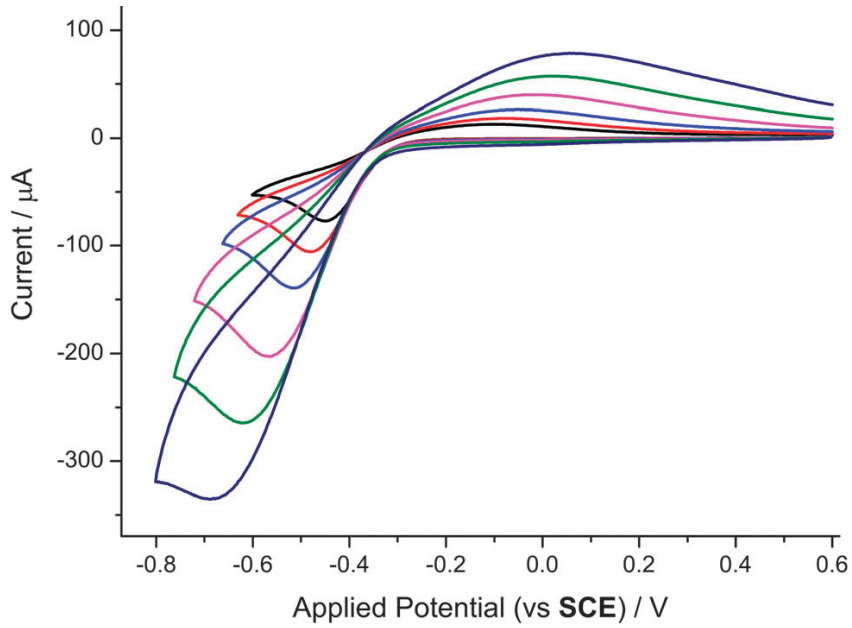

Figure 4.10: The reduction of O_2 on the CPE (1.24 mM O_2 and 0.1 M KCl phosphate buffer solution of pH=6.98), bubbling O_2 for eight minutes before each scan, at variable scan rates (25-800 mV s^{-1}).

superoxide [3, 25, 40–43], which are summarised in Table 4.3. This determined the first step of the process as being the rate determining one. β values from Tafel plots for the back peaks averaged to 0.44, which added to α_{ave} gave a sum of almost exactly 1.0; this suggests that the forward and back peaks are related and may be attributed to:

$$O_2 + e^- \rightleftharpoons O_2^{\cdot -} \rightarrow \quad \text{products} \tag{4.6}$$

with both the O_2 and $O_2^{\cdot -}$ species located in the organic phase at the time of the electron transfer.

Importantly, whilst a large reduction peak is seen on the forward scan, a much smaller peak is seen on the reverse scan, due to the re-oxidation of $O_2^{\cdot -}$. The size of this peak strongly implies that some $O_2^{\cdot -}$ is lost. Given the higher stability of $O_2^{\cdot -}$ in the oil [25]; this probably results from the following process:

$$O_2^{\cdot -}(\text{oil}) \rightleftharpoons O_2^{\cdot -}(\text{aq}) + H^+(\text{aq}) \rightarrow HO_2^{\cdot}(\text{aq}) \rightarrow \quad \text{products} \tag{4.7}$$

The loss of superoxide was confirmed by simulation (see next section).

From the Randles-Ševčik plot (for the forward peak), shown in Fig. 4.13, the value for the product of ($D^{\frac{1}{2}}$ x c) of 1.5 x 10^{-8} mol cm^{-2} $s^{-\frac{1}{2}}$ was calculated. This value is in good agreement with that previously obtained from the Cottrell fitting of the eight minute pre-concentration time in the O_2 saturated phosphate buffer solution (see section above). For this calculation, the irreversible form of the Randles-Ševčik equation,

$$\text{and} \quad i_p = (2.99 \quad \text{x} \quad 10^5) n (n' + \alpha_{RDS})^{\frac{1}{2}} \nu^{\frac{1}{2}} A C D_i^{\frac{1}{2}} \tag{4.8}$$

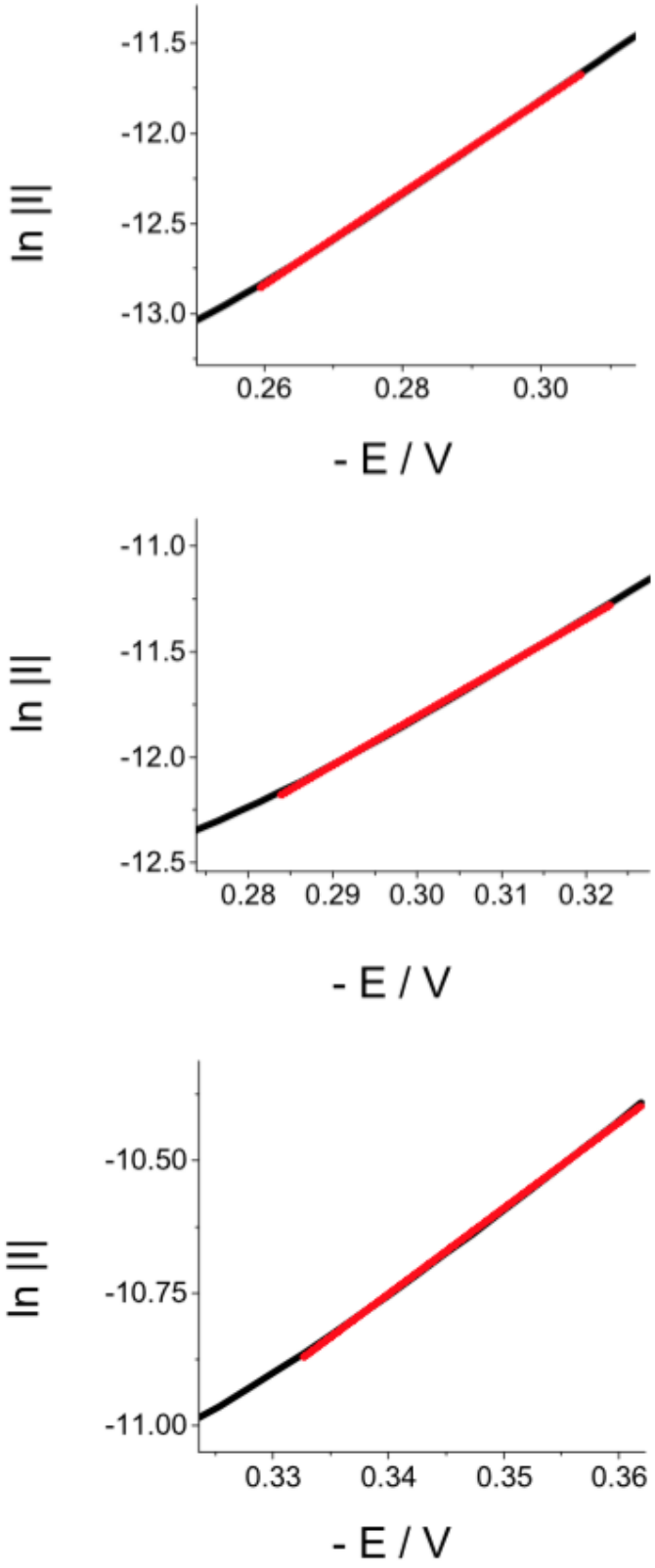

Figure 4.11: Tafel plots for the 25 (top - $\alpha = 0.66$), 100 (middle - $\alpha = 0.42$) and 800 (bottom - $\alpha = 0.59$) mV s^{-1} O_2 reduction responses obtained in a 1.24 mM O_2 phosphate buffer solution of pH = 6.98, containing 0.1 M KCl at 298 K.

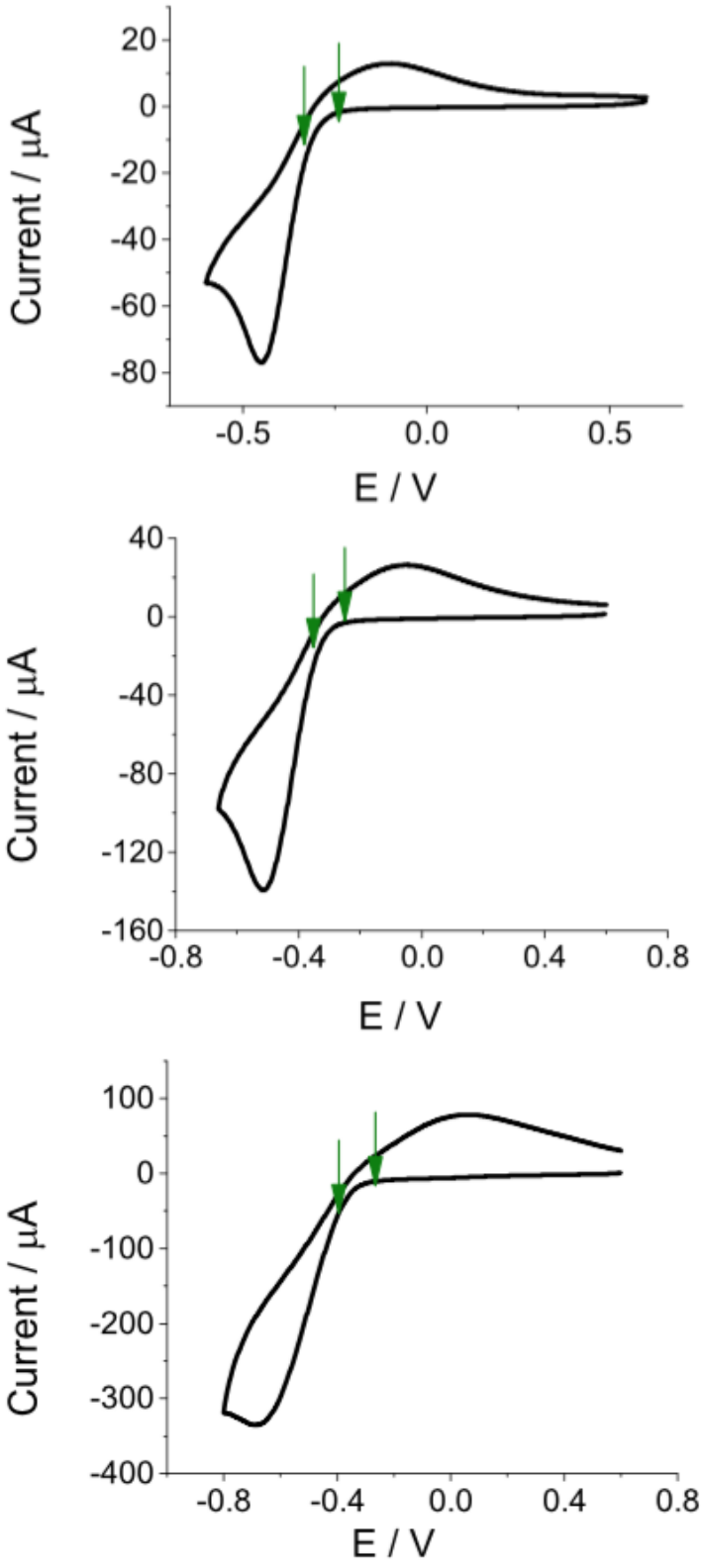

Figure 4.12: The regions of the voltammograms the Tafel analysis above was based on.

α	Electrode	Solvent	Supporting Electrode	Reference
0.50	Graphite	Water	NaOH	[3]
0.53	MDE	Water	NaOH	[25]
0.5	Pt RDE	Water	NaOH	[40]
0.44	GC	Quinoline	TBAP	[41]
0.34	GC	Acetone	TBAP	[42]
0.52	HOPG	Acetonitrile	TEAP	[43]

Table 4.3: Literature α values. MDE: Mercury Drop Electrode, RDE: Rotating Disc Electrode, HOPG: Highly Ordered Pyrolytic Graphite, TBAP: Tetrabutylammonium Perchlorate, TEAP: Tetrabutylammonium Perchlorate.

was used, where n refers to the total number of electrons transferred, n' denotes the number of electrons transferred before the rate determining step, α is the transfer coefficient, ν is the scan rate (mV s^{-1}), A the electrode area (cm^2), C the surface concentration of the analyte of interest (mol cm^{-3}) and D its diffusion coefficient (cm^2 s^{-1}). A one-electron

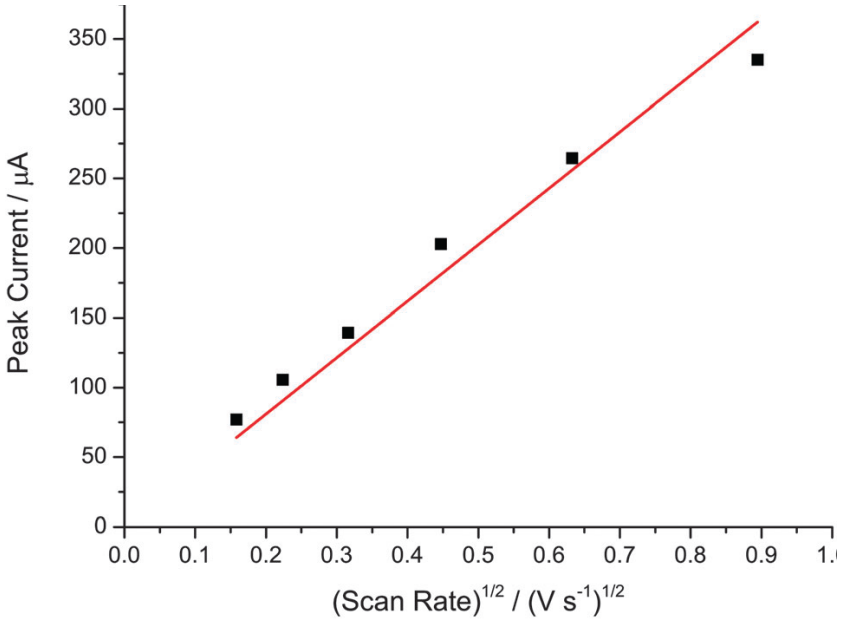

Figure 4.13: The Randles-Ševčik plot for the forward peak of the responses of Fig. 4.10

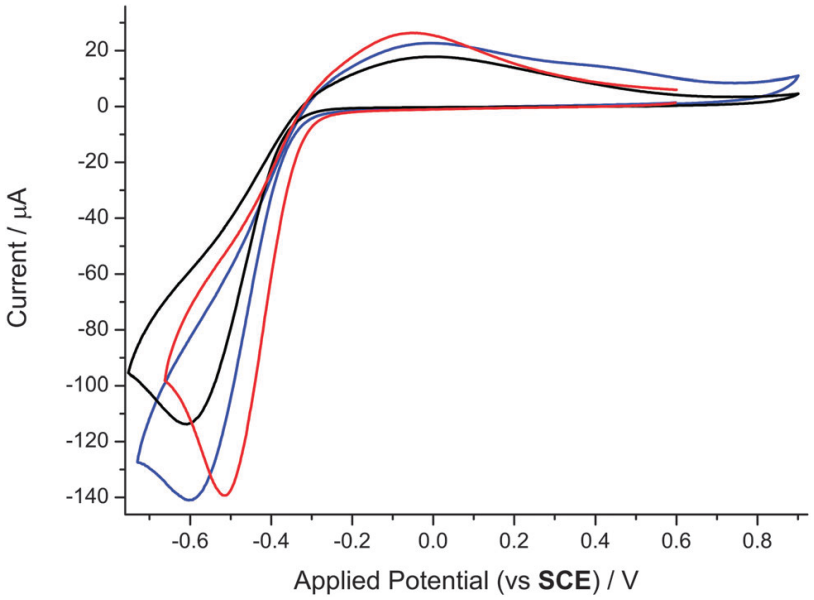

Figure 4.14: Typical 100 mV s^{-1} voltammograms for the reduction of O_2 in a O_2 saturated (1.24 mM) 0.1 M KCl phosphate buffer solution of pH=6.22 (black), pH=6.98 (red) and pH=8.01 (blue), at 298 K.

process ($n = 1$) was assumed to take place, with the first step being the rate determining one, as deduced by the Tafel plots (α_{ave} ca. 0.5). This implied that $n' = 0$, since no electrons are transferred before the rate determining step.

Increasing and decreasing the pH to 8.01 and 6.22, respectively, revealed that the O_2 reduction on the carbon paste electrode surface is essentially pH independent, with the average peak potentials of the forward peak being -0.58 ($\pm$0.08) V (vs. SCE). The pH independence is consistent with the reduction of oxygen to superoxide (reaction 4.6

E^0 ($O_{2(aq)}$ / $O_2^{\cdot-}$) / V (vs. SCE)	Solvent	Reference
-0.358	Water	[25]
-0.355	Water	[32]
-0.399	Water	[44]
-0.424	Water	[45]

Table 4.4: E^0 literature values for the $O_{2(aq)}$)/ $O_2^{\cdot-}$ couple vs. SCE.

above) occurring with no protonation in or before the transition state of the electrode process. Typical voltammograms for the responses observed at each pH, at 100 mV s^{-1}, are overlaid in Fig. 4.14. Variable scan rate studies at each pH showed that α and ($D^{\frac{1}{2}}c$) values were also pH independent. A shoulder on the back peak (at +0.43V vs. SCE) is probably attributable to the oxidation of $O_2^{\cdot-}$ adsorbed on carbon, since it takes place at a more positive potential than that seen for the peak attributed to the oxidation of $O_2^{\cdot-}$ in the oil (0.00 V vs. SCE).

By overlaying the linear parts of the Tafel plots for the forward and reverse peaks of the 100 mV s^{-1} response at pH = 6.98 and extrapolating so the lines intersect, a value for $E_f^{\ominus}$ = -0.293 V (vs. SCE) was found for the O_2(oil) / $O_2^{\cdot-}$(oil) couple. This is in agreement with the value of -0.295 (+ 0.067, - 0.083) V (vs. SCE), determined by averaging the mid-point potentials obtained at all three pHs. Literature values [25, 32, 44, 45], for the E^0 ($O_{2(aq)}$/ $O_2^{\cdot-}$) couple in water, vs. SCE, are summarised in Table 4.4. The variation between the values calculated here and those in the literature can be attributed to the different medium in which the couple is located viz oil, not water [46].

4.5 Simulations

The experimental results of the variable scan rate studies at the three pHs were successfully modelled using the commercially available software package DIGISIM (see Section 3.5 for more information on DIGISIM). This was done by fitting the average peak current of all responses, for all three pHs, as well as their average peak separation (Fig 4.15 and 4.16). All the parameters had been previously determined [$\alpha = 0.54$ (average from measurements all the three pHs), [O_2] = 3 mM, D_{O_2} = 2.50 x 10^{-5} cm^2 s^{-1} and $E_f^{\ominus}$ = -0.295 V], the rate

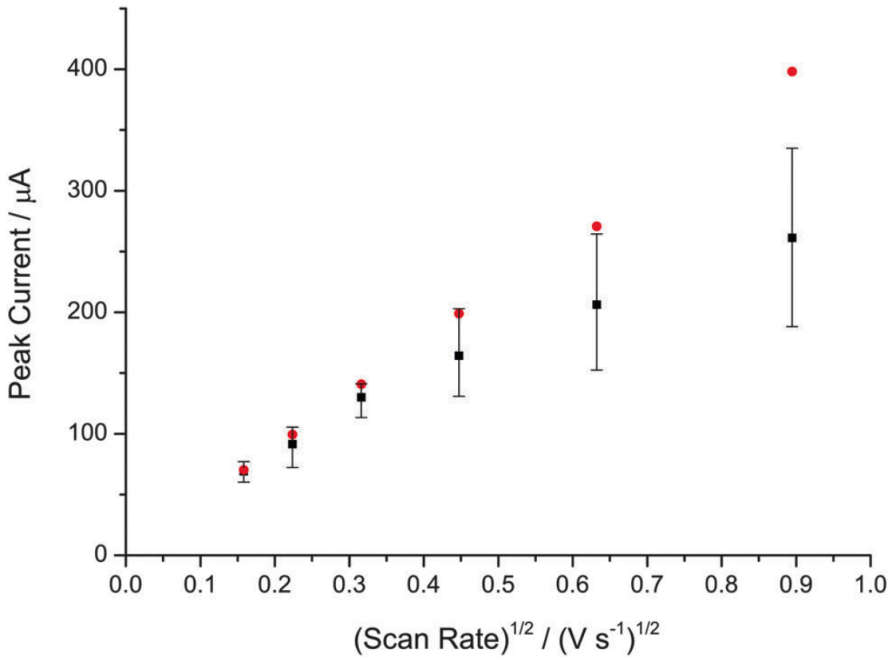

Figure 4.15: Peak current vs. (scan rate)$^{\frac{1}{2}}$ for experimental (black squares) vs. simulated (red circles) O_2 reduction responses.

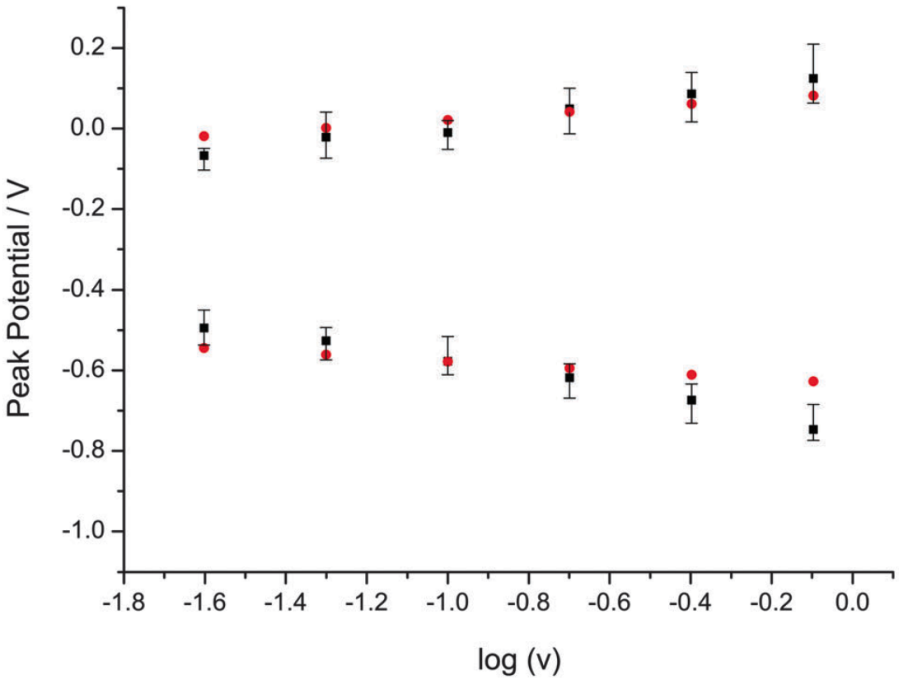

Figure 4.16: Peak potential vs. log of scan rate for experimental (black squares) vs. simulated (red circles) O_2 reduction responses.

of electron transfer, k_s, being the only remaining unknown. The value of k_s was thus varied until the best fit was achieved for k_s ca. 4 x 10^{-5} cm s^{-1}. It was assumed that the diffusion coefficients of the species remained unaltered upon reduction. Simulations confirmed the loss of superoxide since the peak height of the reverse peak was lower compared to the expected value as proposed above.

4.6 Conclusions

Although two two-electron waves were expected to be observed on the carbon paste electrode [16], between -0.30 V and -0.80 V (vs. SCE) [11], three were seen when dioctyl phthalate was used as the pasting liquid, a significant difference compared to other solid carbon substrates [2, 29]. Cyclic voltammetric and single step chronoamperometric experiments have shown that O_2 accumulates in the oil in the paste, in which its diffusion coefficient was measured as 2.50 x 10^{-5} cm^2 s^{-1}. The obtained responses were observed to be pH independent, supporting the inference that superoxide is formed at the graphite/oil/water triple phase boundary. The $E_f^{\ominus}$ value for O_2(oil))/ $O_2^{\cdot -}$(oil) couple was calculated as being -0.295 V (vs. SCE). This study has, thus, shown that the carbon paste electrode provides an additional pathway for the generation of hydrogen peroxide, for which the kinetic and thermodynamic parameters mentioned above have been determined. A superoxide mediated pathway for the reduction of oxygen at the carbon/oil/water triple phase boundary can, hence, now be proposed.

The "new" peak seen on the carbon paste electrode has been shown to be due to

$$O_2(\text{oil}) + e^- \rightleftharpoons O_2^{\cdot -}(\text{oil}) \rightarrow \quad \text{products} \tag{4.9}$$

taking place, while the observed loss of superoxide into the solution is attributed to

$$O_2^{\cdot-}(\text{oil}) \rightleftharpoons O_2^{\cdot-}(\text{aq}) + H^+ \rightarrow HO_2^{\cdot}(\text{aq}) \rightarrow \text{products} \tag{4.10}$$

The two back peaks likely correspond to the re-oxidation of $O_2^{\cdot-}$(oil) and $O_2^{\cdot-}$(ads on carbon). To the best of the authors' knowledge, this is the first time that superoxide has been electrochemically generated using the paste of a carbon paste electrode, certainly as the source of oxygen and to potentially stabilise the $O_2^{\cdot-}$, rather than it being adsorbed on an electrode surface [3–6] or its formation favoured over that of hydrogen peroxide due to the presence of a monolayer [8, 9, 25, 32]. Thus, this study opens up the electrochemical study of superoxide in aqueous media and at the same time gives further insight into the oxygen electrochemical reduction. The latter is of crucial importance to energy transfer technology (e.g. fuel cells) and in bioelectrochemistry.

References

[1] Nissim, R.; Compton, R. G. *Chemical Physics Physical Chemistry* **2013**, *15*, 11918.

[2] Yeager, E. *Electrochimica Acta* **1984**, *29*, 1527.

[3] Morcos, I.; Yeager, E. *Electrochimica Acta* **1979**, *15*, 953.

[4] Zhang, W.; Tryk, D.; Yeager, E. *National Meeting, The Electrochemical Society Extended Abstracts* **1983**, *83*, Abst. 394.

[5] Taylor, R. J.; Humffray, A. A. *Journal of Electroanalytical Chemistry* **1975**, *64*, 63.

[6] Sawyer, D. T.; Seo, I. T. *Inorganic Chemistry* **1977**, *16*.

[7] Hartnig, C.; Koper, M. T. M. *Journal of Electroanalytical Chemistry* **2002**, *532*, 165.

[8] Choi, Y.-k.; Chjo, K.-h.; Park, S.-m. *Journal of the American Chemical Society* **1995**, *142*, 4107.

[9] Yang, H.-h.; Mccreery, R. L. *Journal of the Electrochemical Society* **2000**, *147*, 3420.

[10] Adams, R. N. *Analytical Chemistry* **1958**, *30*, 1576.

[11] Švancara, I.; Vytřas, K.; Kalcher, K.; Walcarius, A.; Wang, J. *Electroanalysis* **2009**, *21*, 7.

[12] Kalcher, K.; Švancara, I.; Metelka, R.; Vytřas, K.; Walcarius, A. *The Encyclopedia for Sensors* **2006**, *4*, 283.

[13] Švancara, I.; Schacl, K. *Chem. Listy* **1999**, *93*, 490.

[14] Kingsley, E. D.; Curran, D. J. *Analytica Chimica Acta* **1988**, *206*, 385.

[15] Březina, M. *Fresenius Zeitschrift fuer Analytiche Chemie* **1967**, *244*, 74.

[16] Schröder, U.; Compton, R. G.; Marken, F.; Bull, S. D. S.; Davies, S. G.; Gilmour, S. *Journal of Physical Chemistry B* **2001**, *105*, 1344.

[17] Rayner, D.; Fietkau, N.; Streeter, I.; Marken, F.; Buckley, B. R.; Page, P. C. B.; Campo, J.; Mas, R.; Mun, F. X.; Compton, R. G. *Journal of Physical Chemistry C* **2007**, *111*, 9992.

[18] Schröder, U.; Wadhawan, J.; Evans, R. G.; Compton, R. G.; Wood, B.; Walton, D. J.; France, R. R.; Marken, F.; Page, P. C. B.; Hayman, C. M. *Journal of Physical Chemistry B* **2002**, *106*, 8697.

[19] Banks, C. E.; Davies, T. J.; Evans, R. G.; Hignett, G.; Wain, A. J.; Lawrence, N. S.; Wadhawan, J. D.; Compton, R. G. *Physical Chemistry Chemical Physics* **2003**, *5*, 4053.

[20] Kachoosangi, R. T.; Xiao, L.; Wildgoose, G. G.; Marken, F.; Page, P. C. B.; Compton, R. G. *Journal of Physical Chemistry C* **2007**, *111*, 18353.

[21] Kachoosangi, R. T.; Musameh, M. M.; Abu-yousef, I.; Yousef, J. M.; Kanan, S. M.; Xiao, L.; Davies, S. G.; Russell, A.; Compton, R. G. *Analytical Chemistry* **2009**, *81*, 435.

[22] Musameh, M. M.; Torabi, R.; Xiao, L.; Russell, A.; Compton, R. G. *Biosensors and Bioelectronics* **2008**, *24*, 87.

[23] Li, Q.; Batchelor-McAuley, C.; Lawrence, N. S.; Hartshorne, R. S.; Compton, R. G. *Journal of Electroanalytical Chemistry* **2013**, *688*, 328.

[24] Švancara, I.; Vytřas, K. *Analytica Chimica Acta* **1993**, *273*, 195.

[25] Divišek, J.; Kastening, E. L. *Journal of Electroanalytical Chemistry* **1975**, *65*, 603.

[26] Rudolph, M. *Journal of Electroanalytical Chemistry* **1991**, *314*, 13.

[27] Rudolph, M. *Journal of Electroanalytical Chemistry* **1992**, *338*, 85.

[28] Achord, J. M.; Hussey, C. L. *Analytical Chemistry* **1980**, *52*, 601.

[29] Šljukić, B.; Banks, C. E.; Compton, R. G. *Journal of the Iranian Chemical Society* **2005**, *2*, 1.

[30] Maricle, D. L.; Hodgson, W. G. *Analytical Chemistry* **1965**, *37*, 1562.

[31] Peover, M. E.; White, B. S. *Electrochimica Acta* **1966**, *11*, 1061.

[32] Chevalet, J.; Rouelle, F.; Gierst, L.; Lambert, J. *Journal of Electroanalytical Chemistry and Interfacial Electrochemistry* **1972**, *39*, 201.

[33] Millero, F. J.; Huang, F.; Graham, T. B. *Journal of Solution Chemistry* **2003**, *32*, 473.

[34] Fischer, K.; Wilken, M. *The Journal of Chemical Thermodynamics* **2001**, *33*, 1285.

[35] Dias, A. M. A.; Bonifácio, R. P.; Marrucho, I. M.; Pádua, A. A. H.; Costa Gomes, M. F. *Physical Chemistry Chemical Physics* **2003**, *5*, 543.

[36] Laoire, C. O.; Mukerjee, S.; Abraham, K. M.; Plichta, E. J.; Hendrickson, M. a. *Journal of Physical Chemistry C* **2010**, *114*, 9178.

[37] Wang, K. K.; Kim, B. J.; Ko, S. H.; Choi, D. H.; Kim, Y. R. *Journal of Nanomaterials* **2012**, *2012*.

[38] Ossowski, T.; Pipka, P.; Liwo, A.; Jeziorek, D. *Electrochimica Acta* **2000**, *45*, 3581.

[39] Vasudevan, D.; Wendt, H. *Journal of Electroanalytical Chemistry* **1995**, *392*, 69.

[40] Sepa, B. D.; Vojnovic, M. V.; Damjanovic, A. *Electrochimica Acta* **1980**, *25*, 1491.

[41] Wu, J. F.; Che, Y.; Okajima, T.; Matsumoto, F.; K.Tokuda,; Ohsaka, T. *Electrochimica Acta* **1999**, *45*, 987.

[42] Wei, Y.; Shao, C.; Hufeng, *Russian Journal of Electrochemistry* **2007**, *43*, 178.

[43] Hossain, M.; Tryk, D.; Yeager, E. *Electrochimica Acta* **1989**, *34*, 1733.

[44] Meisel, D.; Czapski, G. *The Journal of Physical Chemistry* **1975**, *79*, 1503.

[45] Koppenol, W. H.; Stanbury, D. M.; Bounds, P. L. *Free Radical Biology and Medicine* **2010**, *49*, 317.

[46] Sawyer, D. T. *Oxygen Chemistry*; Oxford University Press, London, 1991.

Chapter 5

Measuring the Oxygen Solubility in CTAB Micelles

Due to the low solubility of oxygen in aqueous systems, oil-in-water emulsions and micellar environments can be exploited with the aim of dissolving more oxygen into a studied aqueous system. An added possible advantage is the potential increase of the mass transport of oxygen through the solution. In this chapter, the ability of CTAB micelles to solubilise the species is noted and a simple and generally applicable procedure for the measurement of the solubility of oxygen in CTAB micelles, based on recording the reduced oxygen reduction signals in the presence of the surfactant, is developed. Part of the work here discussed has been accepted for publication in *ChemElectroChem* [1].

5.1 Introduction

Due to it being non-polar and hence having a solvation enthalpy that is close to zero [2], oxygen has a low solubility in aqueous solvents; even in non-aqueous solvents, the solubility is at maximum ca.10 mM [2–5]. Researchers have thus focused on the solubility increase and mass transport enhancement that the use of oxygen carriers such as emulsion droplets or micellar structures can achieve. Careful selection of the organic component of an emulsion for example is important in the development of fuel cells [6], while different

surfactants can have a significant impact on the properties of organic electrochemical transistors [7].

Considering that both micelles and liposomes are involved in the uptake or delivery of a variety of substances in the human body, such as Vitamin K [8, 9], but also that the oxygen transport mechanism in the human body takes place through an analogous mechanism (red blood cells), micelles can also be viewed as a potential biomimetic route through which to increase the oxygen solubility and mass transport in aqueous environments.

It is hence unsurprising that both emulsions as well as systems containing only surfactants have been extensively investigated [10–22]. In the case of emulsions, examples include simpler emulsions where an organic phase has been dispersed into the aqueous solution [10], as well as emulsions where the dispersed droplets contain an electroactive species [23, 24].

As expected, the oxygen solubility in different micelles has also previously been measured [17–22]. This has been done through manometry [17], the use of fluorescent probes [18], spectrophotometry [19], NMR [20] and electrochemically [21, 22]. King et al [17] determined the oxygen solubility in CTAB micelles by measuring the moles of gas released by an aqueous solution of known volume, upon dropping the pressure from an initial 10-15 atm to atmospheric pressure. Turro et al [18] took advantage of the fact that pyrene dissolves in micellar environments and interacts with oxygen. They solubilised pyrene in sodium dodecyl sulfate (SDS) and then measured its decreasing fluorescence response as oxygen also dissolved in SDS and quenched the fluorescence. In their paper, Hunt et al [19] dissolved nitroblue tetrazolium chloride (NBTC) in human low density lipoprotein (LDL), in which they also incorporated superoxide. They then allowed the reduction of NBTC by superoxide to take place and spectrophotometrically monitored the production

of the formazan (the reduced form of NBTC). Given the observed acceleration of the reaction when it is carried out in micellar environments, as well as the lack of any interactions between LDL and NBTC, they concluded that the enhanced NBTC reduction was due to the increased solubility of oxygen in LDL. In the case of the NMR method developed by Inoue et al [20], the oxygen content of perfluorinated cationic surfactants was measured from the NMR longitudinal relaxation time. Lastly, Schlautman et al [21] and Valgmigli et al [22] measured the oxygen uptake of perfluorinated surfactants and SDS micelles, respectively, using a Clark Cell.

However, the method of oxygen saturation of the studied solution used by King [17] is complex and time consuming, while Turro et al [18] only give qualitative conclusions concerning the relative solubilities of oxygen in sodium dodecyl sulfate and water. Moreover, whilst the methods proposed by both Hunt et al [19] and Inoue et al [20] are quantitative, they involve the use of instruments that are complex to use and interpret. Finally, [21] and [22] use a platinum substrate for oxygen uptake measurements which is not generally applicable in systems involving surfactants, as will be discussed later.

At the same time, given the importance of the oxygen reduction reaction in biological processes such as respiration [25] and energy conversion (e.g. fuel cells) [26], the electrochemistry of oxygen has been widely studied [27–30].

$$O_2 + 2H^+ + 2e^- \rightarrow H_2O_2 + 2H^+ + 2e^- \rightarrow 2H_2O \tag{5.1}$$

The different electrochemical pathways that can be followed on different electrode surfaces have been well documented with two two-electron steps generally taking place on carbon surfaces [27–29], as described by Equ. 5.1, and the full four-electron reduction

being possible on platinum substrates [30].

In this chapter, building on the observations that in water CTAB forms micelles [31], and that oxygen can penetrate such micellar structures [18], a simple, novel and general electrochemical method is developed for the determination of the solubility of oxygen in CTAB micelles and validated against a well-known system. The measurement relies on the trapping of different amounts of dissolved oxygen by the CTAB micelles, depending on their concentration. The resulting reduced oxygen levels in the solution are, subsequently, voltammetrically measured and the oxygen solubility inferred.

The electroreduction of oxygen on three different susbtrates - a carbon fibre microdisc electrode, a carbon microwire electrode and a platinum microdisc electrode - is thus first discussed. The same reaction is then carried out in a heptane-in-water emulsion, aiming to observe the increase in the oxygen mass transport through the impact of the heptane droplets, which would contain oxygen at a higher concentration than the aqueous emulsion component, on the electrode surface. However, as spikes due to droplet collisions with the electroactive surface were not seen, these experiments were discontinued. The chapter thus then, and primarily, focuses on the reduction of oxygen in an aqueous CTAB solution and on the monitoring of the oxygen uptake by the CTAB micelles.

5.2 Experimental

Details about the chemical reagents and deoxygenation procedure here utilised can be found in Section 3.1. The heptane-in-water emulsion used was prepared as per [10]; more details can be found in Section 3.1. Cyclic voltammetric measurements were carried out using the equipment and experimental set up described in Section 3.2. A Platinum

microdisc electrode, a Carbon Fibre microdisc electrode (CF) and a Carbon Microwire electrode (CW) were used as working electrodes; their surface was prepared as per Section 3.4. A Saturated Calomel Electrode (SCE) and a platinum mesh acted as the reference and counter electrodes respectively. The carbon wire electrode was fabricated as per [32], as described in Section 3.3.

5.3 The Direct Reduction of Oxygen on Three Surfaces: a Carbon Microwire, a Carbon Fibre Microdisc and a Platinum Microdisc Electrode

In this section, the direct reduction of oxygen is carried out in water, under neutral pH conditions, on two surfaces commonly used in its electroanalysis - a carbon fibre (CF) and a platinum microelectrode. A carbon microwire (CW) is also used. The same reaction is then investigated in two more complex systems; a heptane-in-water emulsion as well as an aqueous CTAB solution.

Starting from the direct reduction of oxygen in a simple aqueous system, the cyclic voltammetric response of an air equilibrated phosphate buffer solution, of pH = 6.97 and which contained 0.1 M KCl as the supporting electrolyte, was recorded at a scan rate of 50 mV s^{-1} on a carbon fibre (r = 3.56 μm), a carbon microwire (r = 3.5 μm, l = 0.80 mm) and a platinum microelectrode (r = 5.06 μm). Scans were carried out from +0.20 V to -1.5 V (vs. SCE) in the case of the carbon fibre electrode, from +0.60 V to -1.15 V (vs SCE) in the case of the microwire electrode and from +0.50 V to -0.40 V (vs. SCE) for the platinum substrate. Typical responses are shown in Fig. 5.1 and 5.2, with higher steady

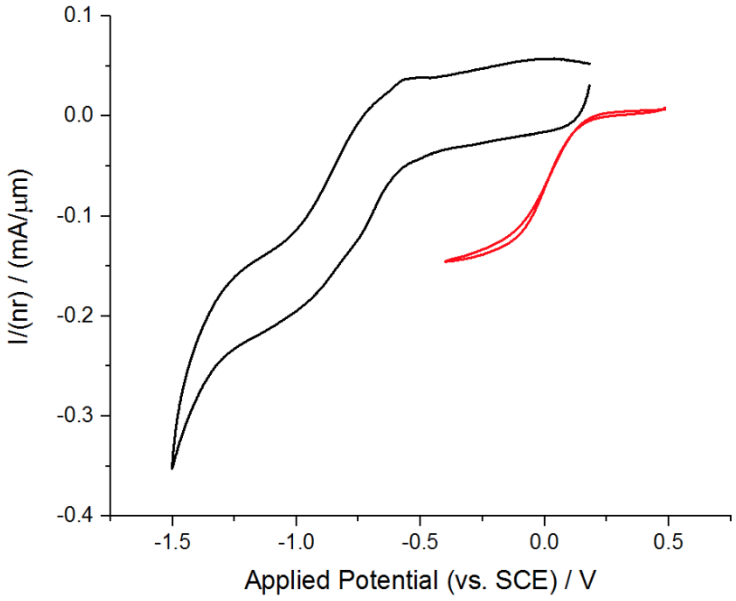

Figure 5.1: Cyclic voltammograms obtained in an air equilibrated (0.25 mM) phosphate buffer solution at pH=6.97 on a CF microdisc electrode of r=3.56 μm (black) and r=5.06 μ (red), at 50 mV s^{-1} and 298 K.

state currents being observed with the wire electrode due to its much larger electroactive surface area, followed by the platinum microdisc. Moreover, the reduction of oxygen can be seen to take place at lower overpotentials on the platinum surface as compared to the two carbon substrates [half wave potentials, $E_{\frac{1}{2}}$: $E_{\frac{1}{2}}$ (CF) = -0.70 V (vs. SCE), $E_{\frac{1}{2}}$ (CW) = -0.56 V (vs. SCE), $E_{\frac{1}{2}}$ (Pt) = 0.0 V (vs. SCE)].

Upon comparing the two microdisc electrodes, while the difference in the radii can partly account for the former observation (r (Pt) = 5.06 μm vs. r (CF) = 3.56 μm), it is also pertinent to consider the differing number of electrons transferred. On the platinum electrode, oxygen can undergo the full four-electron reduction to produce water [30], although there is evidence to suggest that the number of electrons transferred varies as a function of size of the platinum surface [33]; hydrogen peroxide is thus sometimes observed as an intermediate [33–35]. On the carbon fibre electrode, however, even though there is

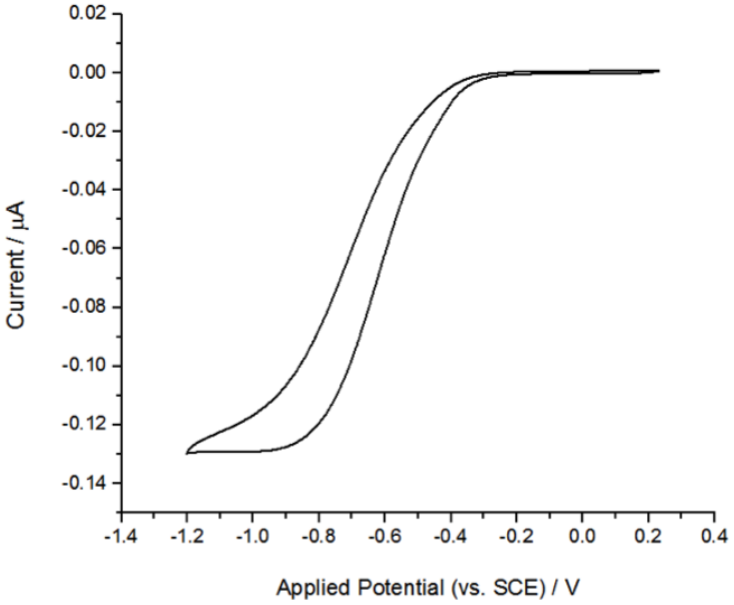

Figure 5.2: Cyclic voltammograms obtained in an air equilibrated (0.25 mM) phosphate buffer solution at pH=6.97 on a CW electrode of r=3.56 μm and l=0.8 mm, at 50 mV s^{-1} and 298 K.

disagreement on the exact steps involved [27–29], two two-electron steps generally take place, which result in two two-electron waves being observed through cyclic voltammetry.

In light of the above, an oxygen concentration of 0.24 mM ± 0.02 mM, which is in agreement with literature values [36], was calculated for the carbon microwire electrode from Equ. 5.2 and 5.3 [32]. For the microdisc electrodes, the concentration of oxygen was calculated from the steady state currents recorded on each microdisc electrode, using Equ. 5.4. Assuming that the number of electrons transferred when the carbon fibre microelectrode is used is two, a value of 0.28 ± 0.04 mM was determined for the oxygen concentration, which again compares well with the literature value of 0.24 mM [36]. Assuming then that four electrons are transferred when using the platinum microelectrode, the concentration of oxygen was calculated as being 0.21 ± 0.04 mM; in all cases, a value of 1.77 x 10^{-9} m^2 s^{-1} was used as the diffusion coefficient of oxygen in water [37].

$$\frac{i_p}{2\pi nFDCl} = 0.446p + 0.335p^{0.15} \tag{5.2}$$

$$\text{with} \quad p = \left(\frac{nFr_0^2\nu}{RTD}\right)^{\frac{1}{2}} \tag{5.3}$$

$$i_{ss} = 4nFDCr_0 \tag{5.4}$$

In Equs. 5.2 - 5.4, n is the total number of electrons transferred, F is the Faraday constant (96.485 C mol^{-1}), D is the diffusion coefficient of the electroactive species (oxygen - cm^2 s^{-1}), C is the concentration of oxygen (mol cm^{-3}), l is the length of the wire (cm), ν is the scan rate (V s^{-1}) and r_0 is the microelectrode radius (cm).

Importantly, the lower overpotentials needed to drive the reaction on the platinum substrate are associated with the high activity of platinum for oxygen reduction and with its alternative mechanism (Equ. 5.4). These lower overpotentials are an important factor in the wide use of platinum in the application of the electroreduction of oxygen, e.g. in the "Clark Cell" [38].

5.4 The Reduction of Oxygen in a Heptane-in-Water Emulsion

Single metal as well as organic nanoparticles are routinely detected through imapct experiments, orignally developed by Heyrovský and Jirovský [39–42]. During such studies, potential step chronoamperometry is usually used with the potential step taking place

from a potential that is not large enough to induce a current flow to a potential at which the nanoparticles undergo oxidation or reduction at a rate controlled by mass transport. The collisions of these "hard" particles with the electrode surface appear as spikes in the current time response (Figs. 5.3 and 5.4). Importantly, impact experiments can also be carried out in emulsions or micelle solutions and there are various examples where collisions of "soft" droplet particles have been been detected [10, 23, 24]; these include both "empty" droplets [10] as well as droplets containing an electroactive species [23, 24]. The latter case is of particular significance as it permits the study of redox species that are sparingly soluble in aqueous systems [43, 44] (Figs. 5.5 and 5.6).

One such example is oxygen, which is known to have a much higher solubility in organic solvents as compared to aqueous environments [2]. Noting this observation and considering a heptane-in-water emulsion, where both components had been saturated with oxygen, it would be expected that oxygen would be present at a higher concentration in the organic component than in the aqueous part. Assuming, in addition, that the heptane droplets would travel fast enough through the solution, in the time frame of the experiment, it would be expected that the mass transport of oxygen through the solution would be enhanced. The impact of the heptane droplets could thus be chronoamperometrically observed through the release of oxygen at the elecctrode surface. Due to the oxygen concentration in the heptane droplet being large compared to its concentration in water, spike-like features would be expected to be overlaid on the background response of the direct reduction of oxygen.

The method used to prepare the heptane-in-water emulsion was based on previous research carried out by Compton et al [10], where importantly the emulsion was acousti-

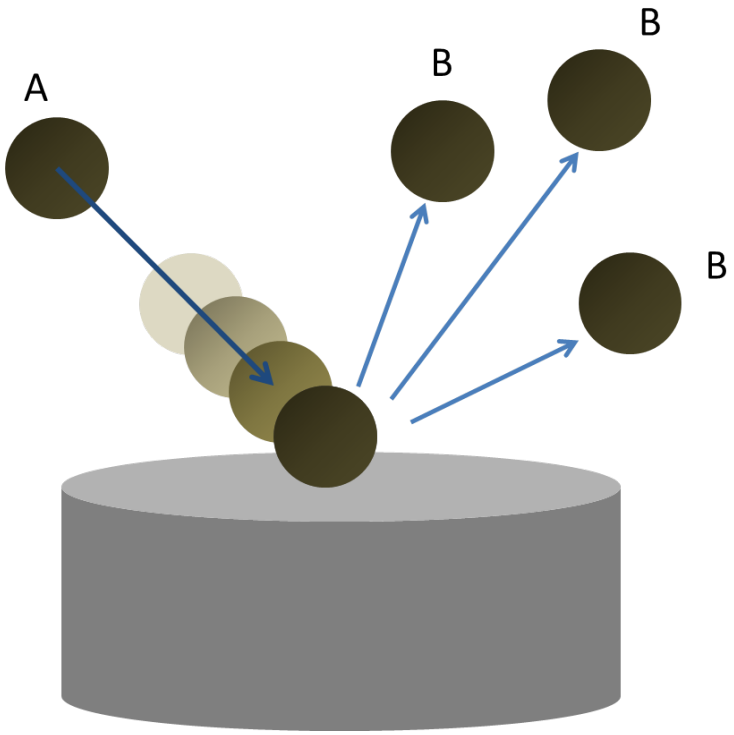

Figure 5.3: Schematic representation of an oxidative impact of a solid nanoparticle, where B is the oxidised form of A.

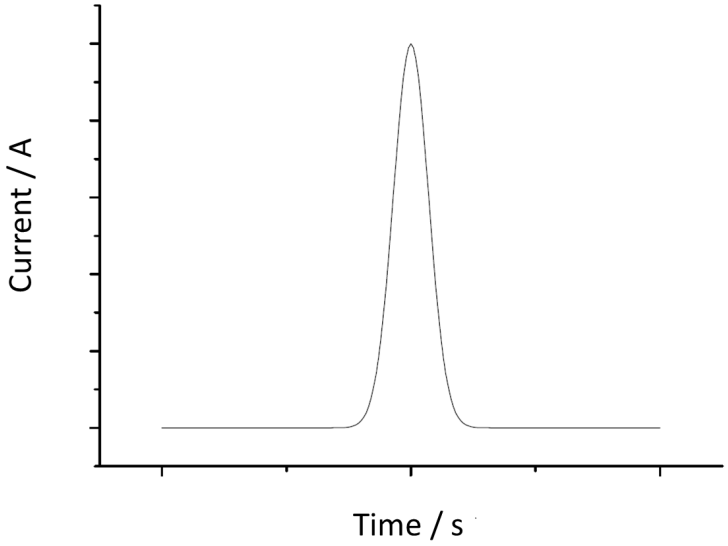

Figure 5.4: The spike observed in the current time response when particle A collides with the electrode and is oxidatively destroyed.

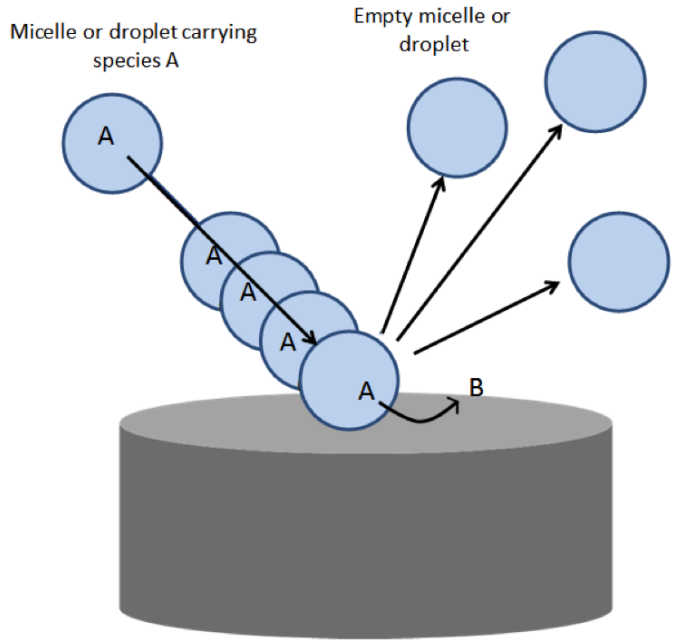

Figure 5.5: Schematic representation of a reductive micelle or droplet impact, where B is the reduced form of A.

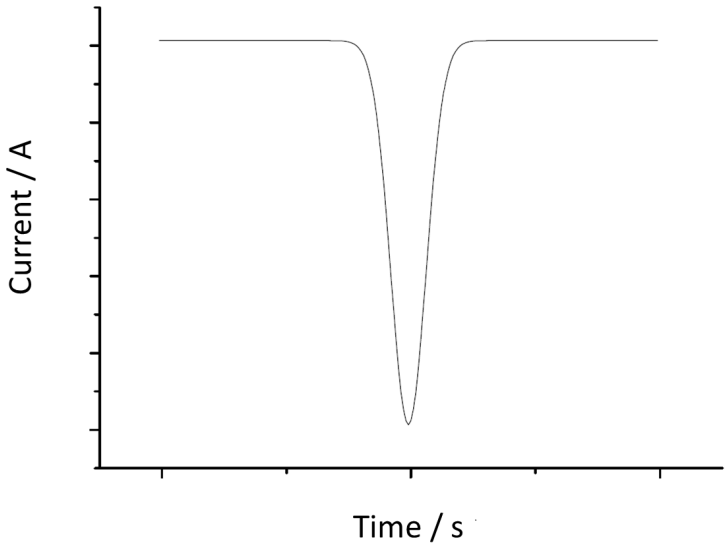

Figure 5.6: The spike observed in the current time response when micelle/droplet A collides with the electrode and is reductively destroyed.

cally emulsified; acoustic emulsifcation has become a topic of interest [10–15] as it eliminates the need for surfactants [16] and emulsification can instead be achieved through acoustic sonication [10]. Here, however, the heptane was dispersed in an aqueous phosphate buffer solution, rather than an acid component. The amount of heptane was also adjusted to 3% v/v, to ensure the emulsion was stable for the longest possible amount of time (Section 3.1). The two components were separately saturated with oxygen before emulsification.

Before any experiments were completed in the emulsion the diffusion coefficient of heptane in water was calculated as being 1.63 x 10^{-13} m^{-2} s^{-1}, using the Stokes-Einstein Equation [45]:

$$D = \frac{k_B T}{6\pi\eta_w r_h} \tag{5.5}$$

where k_B is the Boltzman constant (1.38 x 10^{-23} J K^{-1}), η_w is the viscosity of water (8.9 x 10^{-4} Pa s^{-1}) and r_h is the average radius of a heptane droplet (ca. 1.5 μm [10]) and where the rest of the terms have been previously defined.

The diffusion coefficient, along with the droplet concentration of 3.5 pM, determined by assuming that the droplets are spherical, was then substituted in the following equation which describes the number of droplets expected to impact the electrode surface as a function of time, t (s).

$$N = 4N_A D C_p r_0 t \tag{5.6}$$

In Equ. 5.6, C_p is the droplet concentration (mol cm^{-3}) and the rest of the terms have been previously defined.

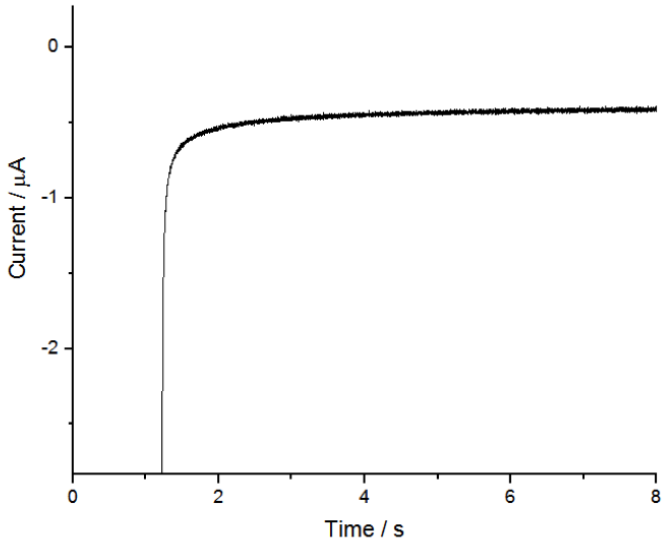

Figure 5.7: Potential step chronoamperogram obtained in a heptane-in-water emulsion, where both components had been saturated with oxygen, on a CW electrode of r=3.56 μm and l = 0.4 mm. Measurements we recorded at 298 K.

However, the calculated N value was less than unity in the case of both substrates, meaning that it would not be likely for a droplet to impact the carbon fibre or platinum surface. Potential step chronoamperometric measurements were thus completed in a stable heptane-in-water emulsion prepared as above, where both components had been saturated with oxygen, only on a carbon microwire electrode (r = 3.50 μm, l = 0.4 mm). This was because its larger electroactive surface area would increase the probability of a droplet coming into contact with the electrode; the results are shown in Fig. 5.7. However, despite the long duration of the measurement, as can be concluded by the lack of spike features on the recorded responses, no droplets impacted the electrode surface, implying that the mass transport of oxygen had not been increased through the addition of heptane.

Moreover, reductive cyclic voltammograms were also run, from from +0.60 V to -1.15 V (vs SCE), in the above emulsion. A scan rate of 50 mV s^{-1} was selected in order to allow the droplets to travel through the emulsion and come into contact with the wire.

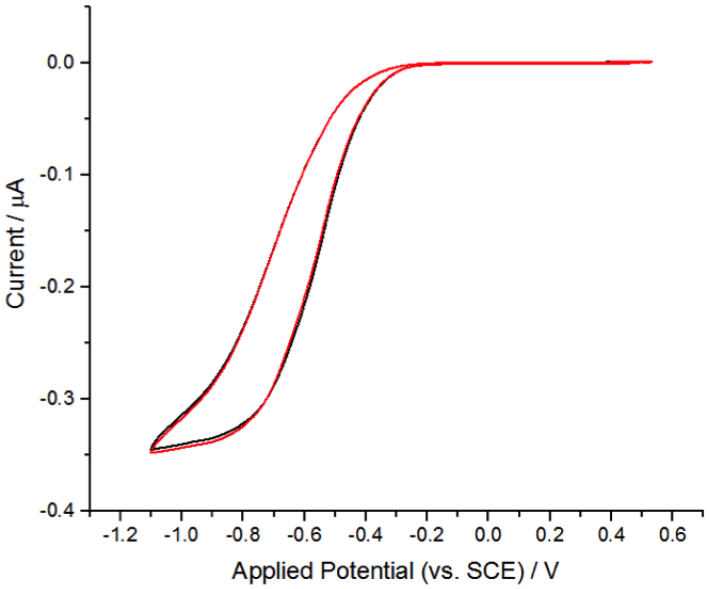

Figure 5.8: Cyclic voltammograms obtained in an oxygen saturated phosphate buffer solution of pH = 6.97 (black) and a heptane-in-water emulsion, where both components had been saturated with oxygen (red), on a CW electrode of r=3.56 μm and l = 0.4 mm, at 50 mV s^{-1}. Measurements were recorded at 298 K.

Typical responses are depicted in Fig. 5.8 where the cyclic voltammogram previously obtained in an oxygen saturated phosphate buffer solution of pH = 6.97 that contained 0.1 M KCl as the supporting electrolyte is also overlaid. Neither an appreciable difference between the steady state currents obtained in the presence and absence of heptane nor spike like features were seen. This again implies that the mass transport of oxygen in the emulsion was not higher than in the simple aqueous solution, though it is possible that the heptane droplets are reaching the electrode surface but not releasing the trapped oxygen. Given previous investigations in a similar emulsion however where the explosion of heptane droplets has been observed to take place [10] the latter is unlikely.

The investigation thus subsequenlty focused on an alternative system - namely an aqueous solution containing CTAB at concentrations above its critical micelle concentration. CTAB micelles are known to be able to trap oxygen and the oxygen solubility

within them has previously been measured [17–22]. The next section thus studies the uptake of oxygen by CTAB micelles, aiming to develop a simple and quantitative electrochemical method for the determination of the solubility of the gas in the micelles. Given the biological significance of such structures, discussed in Section 5.1, the development of a generally applicable procedure is envisioned to advance the study of micellar media.

5.5 The Trapping of Oxygen in CTAB Micelles

Proceeding to the study of CTAB in an aqueous phosphate buffer solution, the behaviour of the carbon fibre and the platinum microelectrodes towards the reduction of oxygen was investigated in the presence of CTAB. This step was necessary to identify the most reliable electrochemical set up with which to validate the method developed for the measurement of the oxygen solubility in the CTAB micelles.

It was also of particular importance since studies have shown that the presence of ionic and non-ionic surfactants can alter the electrochemical reduction of oxygen when adsorbed on the electrode surface [46–48]. For example, several surfactants have been reported to be able to suppress the two-electron reduction of oxygen to hydrogen peroxide, even at low surface coverages [46]. Cationic surfactants such as Aliquat 336 have also been seen to increase the standard rate constant of the reaction under alkaline conditions, with anionic and non-ionic surfactants (e.g. sodium dodecyl sulphate and Triton X-100 respectively) have been shown to have the opposite effect and slow down the process. It has been suggested that the former effect is due to changes on the pH near the electrode surface while the latter is possibly the result of the surface films that are formed blocking access to the electroactive sites [47]. It has also been observed that certain surfactants are able

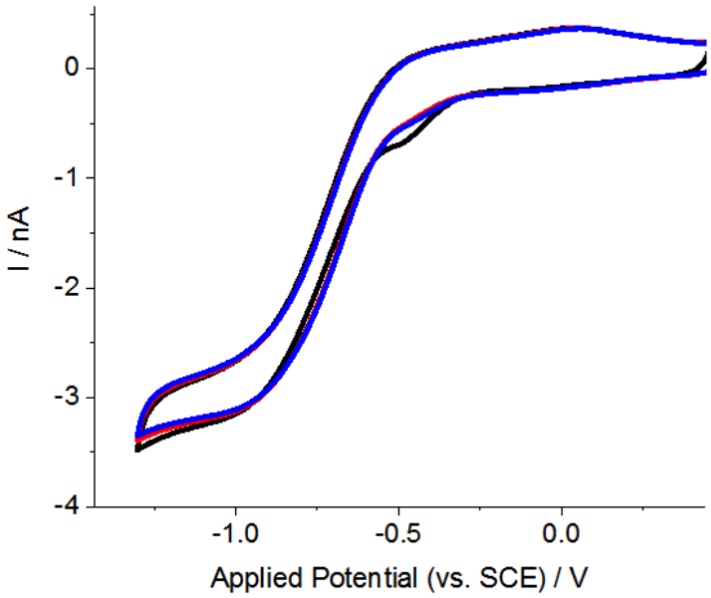

Figure 5.9: Successive 50 mV s^{-1} cyclic voltammograms obtained on the CF microdisc electrode, in an oxygen saturated (1.24 mM) phosphate buffer solution containing 200 mM CTAB, at pH=6.97 and 298 K.

to drive the electrochemical decomposition of hydrogen peroxide, thus altering the route followed [48].

Since oxygen has previously been shown to dissolve in CTAB micelles [18], it was inferred that upon addition of CTAB to a solution pre-saturated with oxygen, at concentrations above its critical micelle concentration (cmc) of ca. 1.0 mM [49], a proportion of the oxygen would dissolve in the formed CTAB micelles. A reduction in the oxygen signal would then be observed that would be expected to become larger with increasing CTAB concentration, as larger amounts of oxygen would be trapped in the CTAB micelles.

The reduction of oxygen was thus investigated in an oxygen pre-saturated phosphate buffer solution, of pH = 6.97, which contained 0.1 M KCl and 200 mM CTAB. Both a carbon fibre microelectrode and a platinum microelectrode were used and cyclic voltammetric scans were carried out at a scan rate of 50 mV s^{-1}, in the same potential ranges

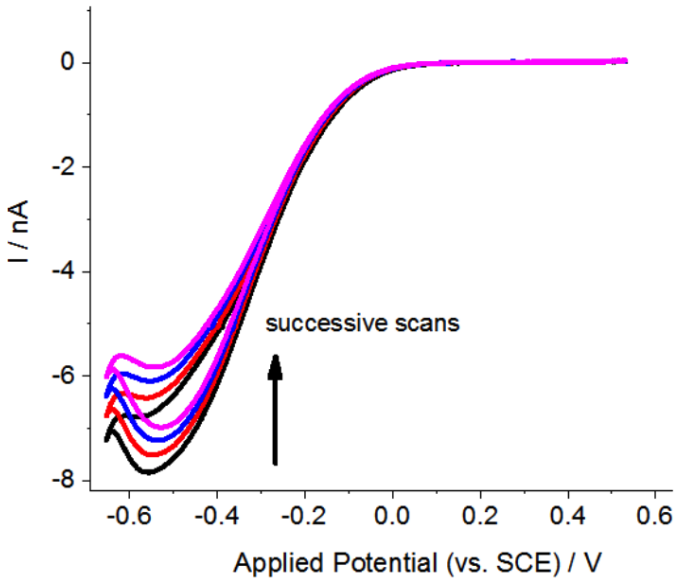

Figure 5.10: Successive 50 mV s^{-1} cyclic voltammograms obtained on the Pt microdisc electrode, in an oxygen saturated (1.24 mM) phosphate buffer solution containing 200 mM CTAB, at pH=6.97 and 298 K.

as in Section 5.3. Fig. 5.9 and 5.10 depict the results obtained on each electrode; the current was seen to decrease upon successive scans on the platinum electrode, while this was not the case with the carbon fibre surface. CTAB has previously been shown to adsorb on a single crystal platinum electrode with the adsorption of the CTA^+ cation having been shown to be irreversible [50]. Since surfactant adsorption on the electrode surface is known to change the voltammetric responses of studied species [47], the altered cyclic voltammetric responses in the presence of the surfactant were attributed to CTAB "fouling", i.e. adsorbing onto, the electrode surface of platinum.

Further experiments were thus completed only with the carbon fibre microelectrode to ensure greater reproducibility of results; the same experiment as above was repeated on the carbon fibre surface, varying the concentration of CTAB between 0 and 200 mM. The obtained 50 mV s^{-1} cyclic voltammetric scans are shown in Fig. 5.11, with Fig. 5.12

depicting the decrease of the current due to the reduction of oxygen with increasing CTAB concentration. This is consistent with increasing quantities of oxygen being trapped in the CTAB micelles, as their concentration is increased, which in turn results in a decrease in the concentration of oxygen in the bulk solution and hence a decrease in the recorded peak current.

It is then assumed that the total volume occupied by the CTAB micelles can, at each CTAB concentration, be calculated using $d = \frac{m}{V}$, where d is the CTAB density (g/mL), m is the mass of CTAB dissolved in solution (g) and V is the occupied volume (mL). In the concentration range used, CTAB is known to form spherical micelles [51], with the transition to rod-like structures having been observed to take place at the higher end of

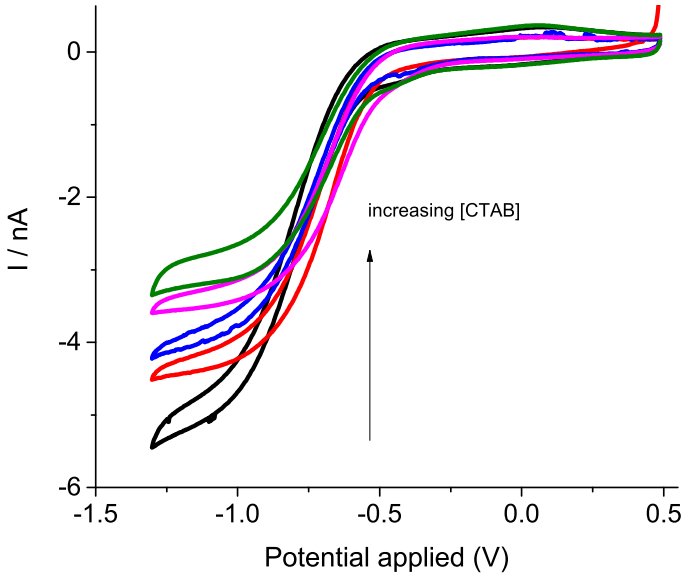

Figure 5.11: 50 mV s^{-1} cyclic voltammograms obtained in an oxygen saturated (1.24 mM) phosphate buffer solution , pH = 6.97, on the CF microelectrode. The scans were run in the absence of CTAB (black) and in the presence of 50 mM CTAB (red), 100 mM CTAB (blue), 150 mM CTAB (magenta) and 200 mM CTAB (green), at 298 K.

the range at ca. 250 mM [52, 53]. The ability of micelles to solubilise analytes, however, is not compromised by their preferred geometry; SDS for example cannot form perfect spheres but can still solubilise oxygen [18], while liposomes whose most stable structure is a bilayer have been shown to be able to solubilise Vitamin C [8]. It is thus important to note that this technique relies on the calculation of the total volume occupied by the micelles. It is hence not sensitive to the shape of the micelles, leading to assumptions regarding the geometry of the formed micelles not being necessary.

Equ. 5.4 could then be used to calculate the concentration of "free" oxygen in the solution at each CTAB concentration ($i_{ss}(2)$). Knowing the amount of oxygen available in the solution in the absence of CTAB ($i_{ss}(1)$), the amount of oxygen dissolved in the CTAB micelles could be determined by subtracting $i_{ss}(2)$ from $i_{ss}(1)$, for each CTAB concentration. However, the concentration of oxygen in the CTAB micelles is seen to

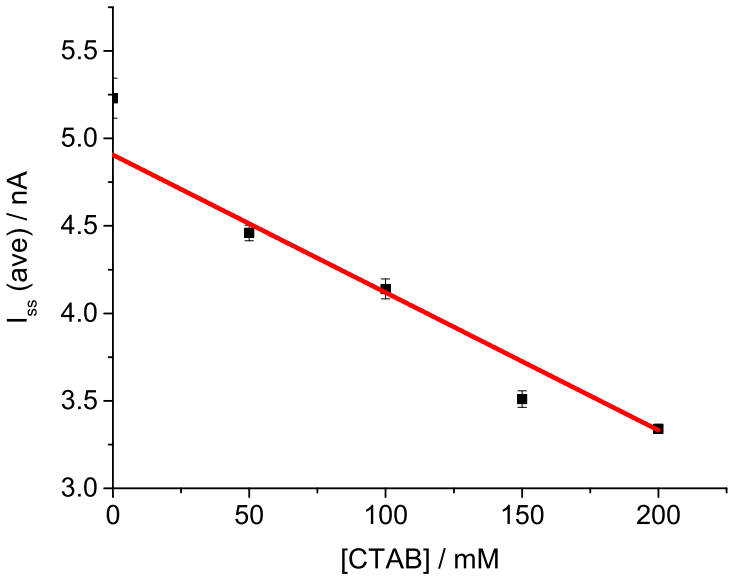

Figure 5.12: The decrease in the peak current with increasing CTAB concentration.

remain constant at an average value of 6.7 ± 0.72 mM. Since no more oxygen can transfer into the micelles, it is concluded that this is because the solubility limit has been reached. The value of 6.7 ± 0.72 mM thus provides a measure of the solubility of oxygen in CTAB micelles. This is summarised in Table 5.1.

Importantly, this solubility value agrees with previously reported values of the oxygen solubility in CTAB micelles [17], determined using a manometric technique where a vessel containing a known concentration of CTAB dissolved in water is first equilibrated with oxygen over a period of five hours, under high pressures of 10-15 atm. The pressure is subsequently decreased to atmospheric pressure at which point the oxygen is allowed to escape the supersaturated solution and the oxygen evolution is measured. It is the agreement between the two values that indicates that the method here presented can accurately and reliably measure the concentration of oxygen in CTAB micelles. At the same time, given that the time frames of the manometric method span hours, the decreased time

[CTAB] / mM	$i_{ss}(ave)$ / nA	$i_{ss}(1) - i_{ss}(2)$ / nA	Moles of O_2 in CTAB micelles	CTAB volume / mL	$[O_2]$ in CTAB micelles / mM	Errors / %
0	$i_{ss}(1)$	0.00	-	-	-	-
50	$i_{ss}(2)$	0.77	7.91×10^{-7}	0.091	8.69	1.41
100		1.1	1.12×10^{-6}	0.182	6.32	0.71
150		1.7	1.76×10^{-6}	0.273	6.59	0.45
200		1.9	1.95×10^{-6}	0.364	5.36	0.32

Table 5.1: The calculation of the concentration of oxygen in CTAB micelles, at each CTAB concentration.

needed for the electrochemical method here presented offers a significant advantage.

5.6 Conclusions

A simple, quantitative electrochemical method for the measurement of the oxygen solubility in CTAB micelles has been developed. Contrary to direct oxygen reduction measurements, for this micellar titration procedure, the carbon substrate is found to be preferable over the platinum substrate. This is because CTAB is seen to severely block platinum surfaces. The solubility of oxygen in CTAB micelles is determined to be 6.7 ± 0.72 mM. The method proposed is generally applicable and because of its simplicity and quantitative nature is likely to greatly facilitate the study of oxygen dissolved in micellar media.

References

[1] Nissim, R.; Batchelor-McAuley, C.; Compton, R. G. *ChemElectroChem* **2015**, *DOI: 10.1002/celc.201500380*.

[2] Li, Q.; Batchelor-McAuley, C.; Lawrence, N. S.; Hartshorne, R. S.; Compton, R. G. *Journal of Electroanalytical Chemistry* **2013**, *688*, 328–335.

[3] Achord, J. M.; Hussey, C. L. *Anal. Chem.* **1980**, *52*, 601–602.

[4] Fischer, K.; Wilken, M. *The Journal of Chemical Thermodynamics* **2001**, *33*, 1285.

[5] Dias, A. M. A.; Bonifácio, R. P.; Marrucho, I. M.; Pádua, A. A. H.; Costa Gomes, M. F. *Physical Chemistry Chemical Physics* **2003**, *5*, 543.

[6] Kronberger, H.; Bruckner, K.; Fabjan, C. *Journal of Power Sources* **2000**, *86*, 562.

[7] Kumar, P.; Yi, Z.; Zhang, S.; Sekar, A.; Soavi, F.; Cicoira, F. *Appl., Phys. Lett.* **2015**, *106*, 053303.

[8] Cheng, W.; Compton, R. G. *Angewandte Chemie, International Edition* **2014**, *53*, 13928.

[9] Thompson, G. R. *J. Clin. Pathol.* **1971**, *5*, 85.

[10] Banks, C. E.; Rees, N. V.; Compton, R. G. *Journal of Physical Chemistry B* **2002**, *106*, 5810.

[11] Blythe, A. N.; Akkermans, R. P.; Compton, R. G. *Electroanalysis* **2000**, *12*, 16.

[12] Beckett, E. L.; Lawrence, N. S.; Evans, R. G.; Davis, J.; Compton, R. G. *Talanta* **2001**, *54*, 871.

[13] Hardcastle, J. L.; Compton, R. G. *Analyst* **2001**, *126*, 2075.

[14] Hardcastle, J. L.; Paterson, C. J.; Compton, R. G. *Electroanalysis* **2001**, *13*, 899.

[15] Davis, J.; Cardosi, M. F.; Brown, I.; Hetheridge, M. J.; Compton, R. G. *Analytical Letters* **2001**, *34*, 2375.

[16] Gao, J.; Rusliing, J. F.; Zhou, D. L. *Journal of Organic Chemistry* **1996**, *61*, 5972.

[17] Matheson, I. B.; King, A. *J. Colloid Interf. Sci.* **1978**, *66*, 464.

[18] Geiger, M. W.; Turro, N. J. *Photochem Photobiol* **1975**, *22*, 273.

[19] Petyaeo, I.; Hunt, J. *Biochim. Biophys. Acta* **1997**, *1345*, 293.

[20] Kameo, Y.; Takahashi, S.; Krieg-Kowald, M.; Ohmachi, T.; Takagi, S.; Inoue, H. *J. Phys. Chem. B* **1999**, *103*, 9562.

[21] An, Y.-J.; Carraway, E. J.; Schlautman, M. A. *Water Res.* **2002**, *36*, 300.

[22] Barillari, J.; Iori, R.; Papi, A.; Orlandi, M.; Bartolini, G.; Gabbanini, S.; Pedulli, G. F.; Valgmigli, L. *J. Agric. Food Chem.* **2008**, *56*, 7823.

[23] Banks, C. E.; Rees, N. V.; Compton, R. G. *Journal of Electroanalytical Chemistry* **2002**, *535*, 41.

[24] Kim, B.-K.; Boika, A.; Kim, J.; Dick, J. E.; Bard, A. J. *Journal of the American Chemical Society* **2014**, *136*, 4849.

[25] Kaya, A.; Gerashchenko, M. V.; Seim, I.; Labarre, J.; Toledano, M. B.; Gladyshev, V. N. *Proc. Natl. Acad. Sci. USA* **2015**, *DOI: 10.1073/pnas.1505315112*.

[26] Wu, Z.-Y.; Xu, X.-X.; Hu, B.-C.; Liang, H.-W.; Lin, Y.; Cheng, L.-F.; Yu, S.-H. *Angew. Chem. Int.* **2015**, *54*, 8179.

[27] Šljukić, B.; Banks, C. E.; Compton, R. G. *Journal of the Iranian Chemical Society* **2005**, *2*, 1.

[28] Morcos, I.; Yeager, E. *Electrochimica Acta* **1970**, *15*, 953.

[29] Zhang, W.; Tryk, D.; Yeager, E. *National Meeting, The Electrochemical Society Extended Abstracts* **1983**, *83*, Abst. 394.

[30] Yeager, E. *Electrochimica Acta* **1984**, *29*, 1527.

[31] Svenson, S. *Reactions and Synthesis*; Marcel Dekker, Inc., New York, US, 2001.

[32] Ellison, J.; Batchelor-McAuley, C.; Tschulik, K.; Compton, R. G. *Sensors and Actuators B* **2014**, *200*, 47.

[33] Garra, M.; Laborda, E.; Holdway, P.; Crossley, A.; Jones, C. J. V.; Compton, R. G. *Phys. Chem. Chem. Phys.* **2013**, *15*, 19487.

[34] Song, C.; Zhang, J. *PEM Fuel Cell Electrocatalyst and Catalyst Layers Fundamentals and Applications*; Springer, Berlin, Germany, 2007.

[35] Kishi, A.; Fukasawa, T.; Umeda, M. *J. Power Res.* **2010**, *95*, 5996.

[36] Battino, R.; Rettich, T. R.; Tominaga, T. *Journal of Physical Chemistry Reference Date* **1983**, *12*, 164.

[37] Laoire, C. O.; Mukerjee, S.; Abraham, K. M.; Plichta, E. J.; Hendrickson, M. a. *Journal of Physical Chemistry C* **2010**, *114*, 9178.

[38] Clark, L. C.; Wolf, R.; Granger, D.; Taylor, Z. *J. Appl. Physiol.* **1953**, *6*, 189.

[39] Heyrovský, M.; Jirovský, J. *Langmuir* **1995**, *11*, 4288.

[40] Heyrovský, M.; Jirovský, J. *Langmuir* **1995**, *11*, 4293.

[41] Heyrovský, M.; Jirovský, J. *Langmuir* **1995**, *11*, 4300.

[42] Heyrovský, M.; Jirovský, J. *Langmuir* **1995**, *11*, 4309.

[43] Akkermans, R. P.; Roberts, S. L.; Compton, R. G. *J. Chem. Soc. Chem. Commun.* **1999**, *1115*.

[44] Akkermans, R. P.; Roberts, S. L.; Marken, F.; Coles, B. A.; Wilkins, S. J.; Cooper, J. A.; Woodhouse, K. E.; Compton, R. G. *J. Phys. Chem. Sect. B* **1999**, *103*, 9987.

[45] Bard, A. J. A. J.; Faulkner, R. L. *Electrochemical Methods: Fundamentals and Application*; John Willey and Sons: New York, 2001.

[46] Kolthoff, I. M.; Lingane, J. J. *Polarography*, 2nd ed.; Interscience Publishers, 1952.

[47] Gyenge, E. L.; Oloman, C. W. *J. Appl. Electrochem.* **2001**, *31*, 233.

[48] Chaenko, N. V.; Kornienko, G. V.; Vasileva, I. S.; Kornienko, V. L. *Russ. J. Appl. Chem.* **1996**, *69*, 706.

[49] Kuperkar, K.; Abezgauz, L.; Prasad, K.; Bahadur, P. *J. Surfact. Deterg.* **2010**, *13*, 293.

[50] Xu, C.-D.; Ye, J.-Y.; Chen, L.; Chen, D.-H.; Li, J.-T.; Zhen, C.-H.; Sun, S.-G. *Electrochim. Acta* **2015**, *162*, 129.

[51] Patel, V.; Dharaiya, N.; Ray, D.; Aswal, V. K.; Bahadur, P. *Colloids and Surfaces A: Physicochem. Eng. Aspects* **2014**, *455*, 67.

[52] Goyal, P. S.; Dasannacharya, B. A.; Kelkar, V. K.; Manohar, C.; Rao, K. S.; Valaulikar, B. S. *Physica B* **1991**, *174*, 196.

[53] Kuperkar, K.; Abezgauz, L.; Danino, D.; Verma, G.; Hassan, P. A.; Aswal, V. K.; Varade, D.; Bahadur, P. *Colloid Interface Sci.* **2008**, *323*, 403.

Chapter 6

Non-Enzymatic Electrochemical Superoxide Sensor

In this chapter, a new, simple and rapid method for the detection of superoxide is presented and discussed. It is based on the widely used colorimetric test developed by Baehner for the diagnosis of chronic granulomatous disorder [1–3] and thus also takes advantage of the selective reaction between superoxide and nitroblue tetrazolium chloride for the reliable detection of the free radical. The work herein presented has been published in *ChemElectroChem* [4] and patented by *Isis Innovation*, on behalf of the University of Oxford; *Isis Innovation* is the technology transfer company of the University.

6.1 Introduction

Reactive oxygen species such as superoxide have a variety of roles in the human body, including and most importantly in immune defence [5]. They are produced during the oxidative burst response of activated neutrophils [6–8], through the one-electron reduction of oxygen that is catalysed by NADPH oxidase [9, 10]; this in turn takes place during phagocytosis. In addition, superoxide has been found to be involved in processes such as the inactivation of iron-sulphur containing proteins [11] as well as DNA damage [12] and signal

transduction. Numerous methods exist for sensing this anion radical, the most commonly used ones being flow cytometry [13–15], polarography [16], the use of N-halopiperidines [17] and spin traps [18]. Superoxide detection can thus be achieved for example through the increase of the fluorescence intensity of an acridinium ion-linked porphyrin triad upon addition of the radical in the porphyrin solution [14], through the synthesis of spin traps such as 5-(diethoxyphosphoryl)-5-methyl-pyrroline N-oxide (DEPMPO) which, upon reaction with superoxide form stable products that can be detected through Electron Paramagnetic Resonance (EPR) [18].

One of the most widely used detection methods for superoxide in biological samples is colorimetric, through the reduction of the pale yellow nitroblue tetrazolium chloride (NBTC) to its pale blue formazan. Such nitroblue tetrazolium salts were first synthesised by von Pechmann and Ruge [19] and their reversible potentials were measured potentiometrically soon after [20, 21]. Given their striking colour when reduced, they were quickly exploited in the detection of reducing substances and particularly superoxide [22].

The so-called NBT test was developed by Baehner, during his investigation into chronic granulomatous disorder [1–3]. His experiments were a practical demonstration of a phagocytic cell being able to reduce the salt to its pale blue formazan only if it is able to produce the superoxide radicals needed to fight off infections. In contrast, neutrophils isolated from patients suffering from chronic granulomatous disorder were unable to reduce the compound due to the absence of NADPH oxidase, i.e. due to the absence of superoxide.

In recent years, electrochemical sensing methods have received a lot of attention, due to their speed of response and high sensitivity and reliability. Other advantages of some electrochemical sensors include their low detection limit, low cost and compatibility for miniaturisation [23]. Concerning the detection of superoxide, most electrochemical sen-

sors that have been developed are enzymatic and use cytochrome c [24–26] or superoxide dismutase [27–29] because of the high selectivity that these enzymes ensure. Both are usually immobilised on the electrode surface, either through binding on thiol groups [24] or the utilisation of sono-gels [29, 30]. Between the two, superoxide dismutase is often preferred [31, 32], mainly due to the structure of the heme group in cytochrome c resembling that of peroxidase, which is not specific for superoxide [31, 32]. However, these enzyme-based devices have an important limitation; their inherent lack of stability, which results in the responses being a function of variables such as temperature and pH [23] and in the sensor being destroyed by non-standard conditions.

Researchers have addressed this issue through alternative modification procedures [23, 32, 33]. Kim et al [23] modified a glassy carbon electrode with a Pt-MWCNT film while Lin et al [33] used Au nanoparticles in their film instead. Yuasa et al [34] synthesised a Fe-porphyrin polymerised film. Even though these results are both important and encouraging, the syntheses and characterisation assays involved are complicated and time-consuming.

In this chapter we propose the first electrochemical analogue of the NBT test, which relies on the equilibration of a carbon paste electrode with NBTC. As has been previously

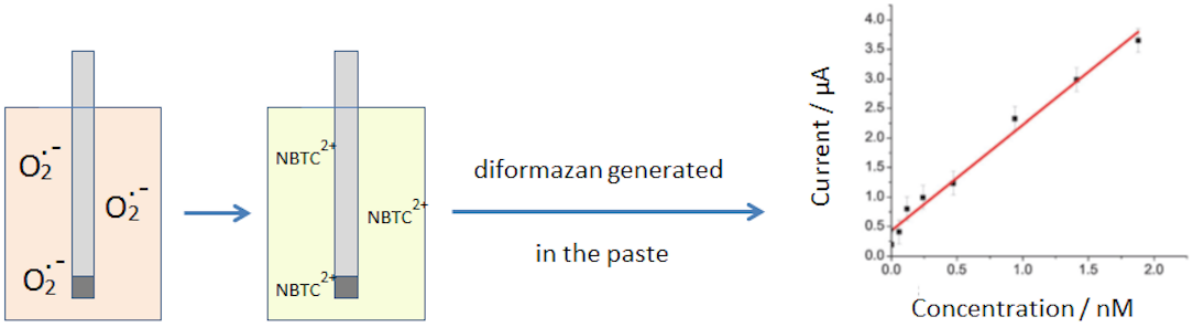

Figure 6.1: The sequence of steps involved in the detection of the superoxide anion.

observed with oxygen [35], by immersing the paste electrode in aqueous superoxide solutions of varying concentrations, different amounts of superoxide can be pre-concentrated in the pasting liquid dioctyl phthalate. Similarly, dioctyl phthalate can be pre-concentrated with NBTC by immersing the paste electrode in an aqueous NBTC solution, which acts as the source of NBTC. NBTC can thus be reduced by superoxide in the liquid binder. The oxidation of the produced diformazan is then observed at ca. +0.69 V (vs. SCE) and this peak is used as the superoxide detection signal. The sequence of steps involved in this procedure are summarised in Fig. 6.1.

The device gives immediate quantitative results, as opposed to the traditional qualitative NBT test, and is easy to use. Importantly, given for example its widespread use in medicine as a diagnostic test for chronic granulomatous disorder, NBTC is a compound with proven high, albeit not perfect [36], selectivity for superoxide. Practically useful values for the limit of detection and the sensitivity of the sensor are obtained.

6.2 Experimental

Details about the chemical reagents and deoxygenation procedure here utilised can be found in Section 3.1; Section 3.1 also includes details regarding the method followed for the synthesis of superoxide. Cyclic voltammetric measurements were carried out using the equipment and experimental set up described in Section 3.2. A glassy carbon macroelectrode (GC), a carbon fibre microdisc electrode (CF) as well as a carbon paste electrode (CPE), fabricated as described in Section 3.3, were used as working electrodes. A Saturated Calomel Electrode (SCE) and a platinum mesh acted as the reference and counter electrodes respectively. The graphite/dioctyl phthalate paste used was fabricated as per

Section 3.3, while the surface of each working electrode was prepared as per Section 3.4. The cyclic voltammetric responses obtained on the carbon fibre microdisc electrode were simulated using in-house programmes [37, 38].

6.3 The Electrochemical Behaviour of Nitroblue Tetrazolium Chloride

Prior to exploiting the reaction between NBTC and superoxide, the electrochemical behaviour of NBTC in water was investigated on three carbon substrates - a glassy carbon macroelectrode, a carbon fibre microelectrode and a carbon paste electrode. In order for the electrochemical system to be fully characterised, the presence of oxygen as well as the adsorptive properties of the diformazan (reduced NBTC) was also studied.

6.3.1 The Reduction of NBTC on a Glassy Carbon Macroelectrode

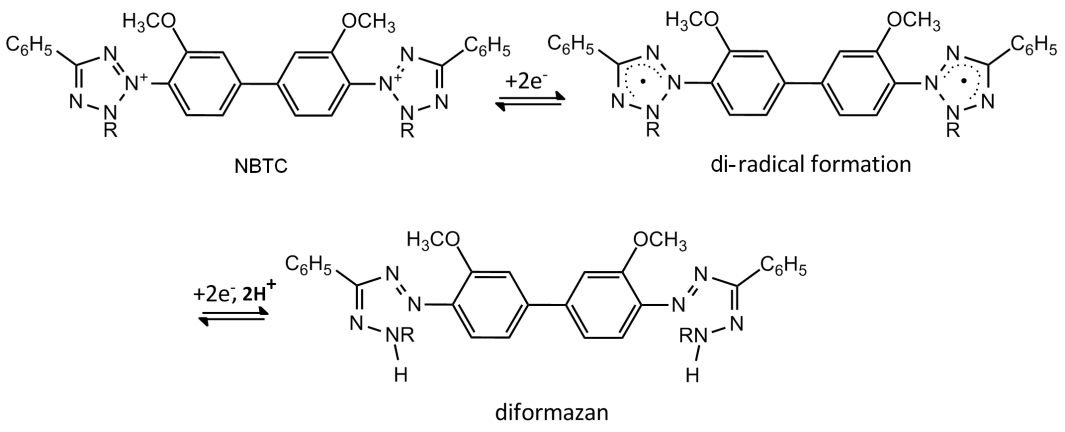

Figure 6.2: The sequence of steps involved in the reduction NBTC.

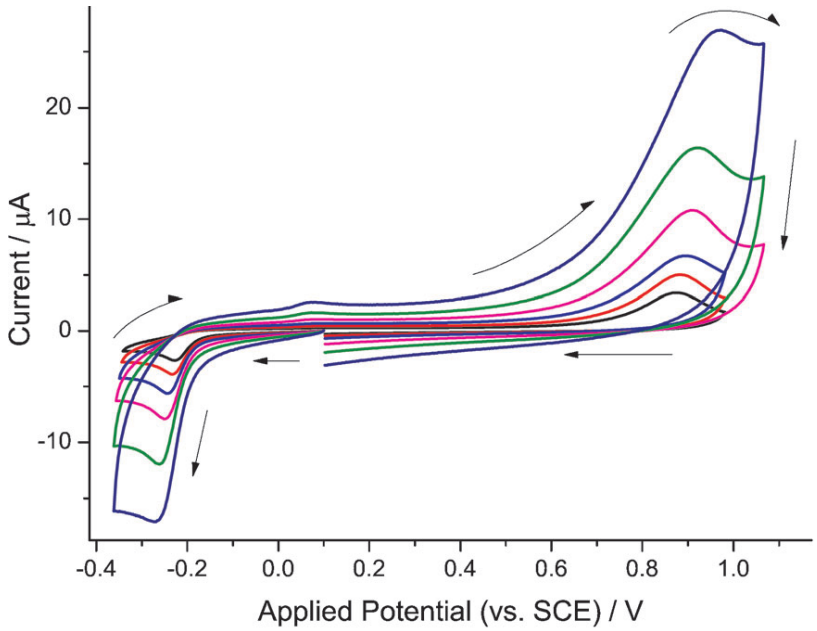

Figure 6.3: The reduction of NBTC on a GC macroelectrode (0.095 mM NBTC) in a deoxygenated phosphate buffer solution, containing 0.1 M KCl, at pH = 6.97, variable scan rates (25 - 800 mV s^{-1}) and 298 K.

Nitroblue tetrazolium chloride (NBTC - structure shown in Fig. 6.2) is an organic dye that is electrochemically active due to the presence of two tetrazole moieties and two nitro substituents; each tetrazole ring needs two electrons and a proton to become fully reduced (Fig. 6.2), while each nitro group requires four electrons and four protons for a full reduction [39]. Importantly, the reduction of the tetrazole rings can also be brought about by superoxide acting as a reducing agent, a reaction that finds application in the NBT test [2]. Aiming to use the latter reaction for the detection of superoxide, it was the electrochemistry of the tetrazole rings that was important. Cyclic voltammetric scans were thus, unless otherwise stated, carried out between +1.2 and -0.40 V (vs. SCE), which is outside of the potential window required for the reduction of the nitro groups but sufficient to reduce the tetrazole rings.

To study the electrochemical reduction of NBTC, a cyclic voltammetry variable scan rate study (25-800 mV s^{-1}) was thus completed on a glassy carbon macroelectrode, in a

deoxygenated aqueous phosphate buffer solution, containing 0.095 mM NBTC and 0.1 M KCl, at pH = 6.97. Typical responses obtained at each scan rate are shown in Fig. 6.3, where a clear reduction peak can be seen at around -0.25 V (vs. SCE). The oxidation of the produced formazan was also voltammetrically observed at around +0.93 V (vs. SCE) during the reverse scan.

Tafel analysis (Figs. 6.4 and 6.5) was then performed to obtain an average value of the transfer coefficient for the reduction process, α_{ave}. An average value of 0.98 ± 0.05 was generated, indicating that the first electron transfer was electrochemically reversible. Given the observed transfer coefficient and the likely stoichiometry of the electrode process (Fig. 6.2), the following mechanism (Eq. 6.1 and 6.2) was considered, in which a reversible one-electron process is followed by a total of $(m-1)$ fully driven one-electron transfers, giving an m-electron process overall:

$$\text{NBTC}^{2+} + \text{e}^- \rightleftharpoons \text{NBT}^{\cdot+} \tag{6.1}$$

$$\text{NBT}^{\cdot+} + (m-1)\text{e}^- \rightarrow \text{products} \tag{6.2}$$

The data in Fig. 6.3 was thus analysed assuming the following form of the Randles-Ševčik equation [40] (Fig. 6.6 - Eq. 6.3)

$$I_p = m(2.69 \quad \text{x} \quad 10^5)\nu^{\frac{1}{2}}ACD^{\frac{1}{2}} \tag{6.3}$$

where m is the total number of electron transfer reactions in the process giving rise to the voltammetric peak of interest, ν is the scan rate (V s^{-1}), A is the electrode area (cm^2), C the surface concentration of the analyte (mol cm^{-3}) and where D is the diffusion coefficient (cm^2 s^{-1}). Depending on the value of m (=1, 2, 3 or 4), different values of D could be

obtained.

In order to identify the correct choice, cyclic voltammetric experiments were next conducted in a deoxygenated aqueous phosphate buffer solution, containing 0.078 mM

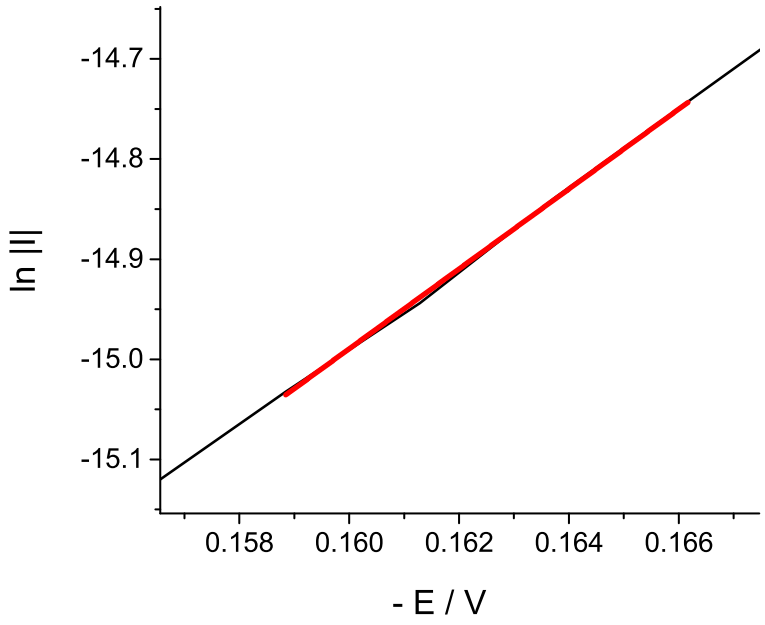

Figure 6.4: Tafel plot for the forward peak of the 100 mV s^{-1} NBTC reduction peak on the GC macroelectrode. Calculated $\alpha = 1.03$. Average $\alpha = 0.98 \pm 0.05$.

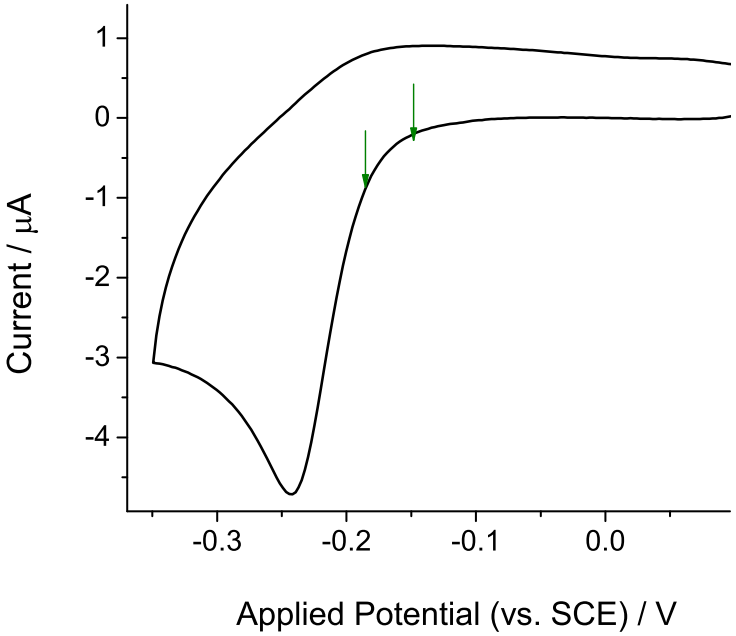

Figure 6.5: The region of the voltammogram the Tafel analysis above was based on.

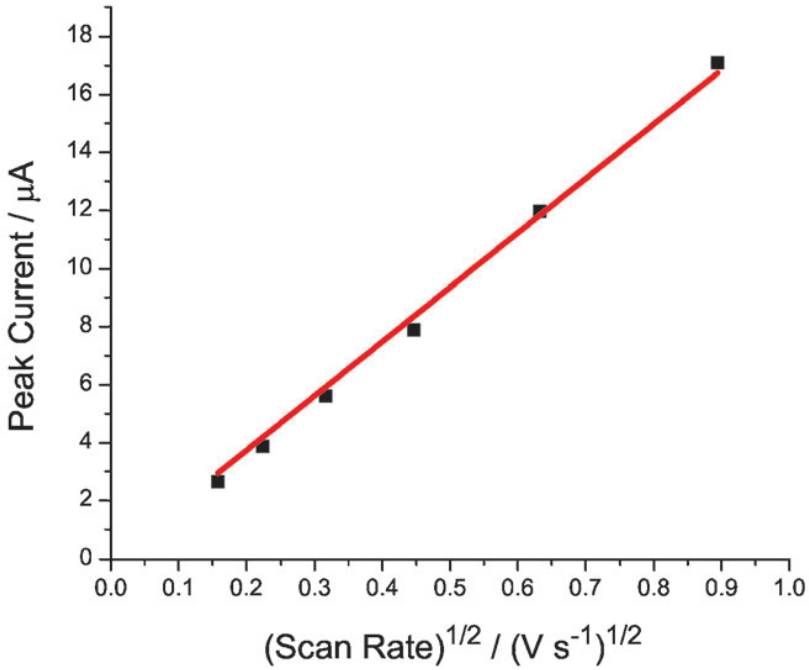

Figure 6.6: The Randles-Ševčik plot for the results depicted in Fig. 6.3.

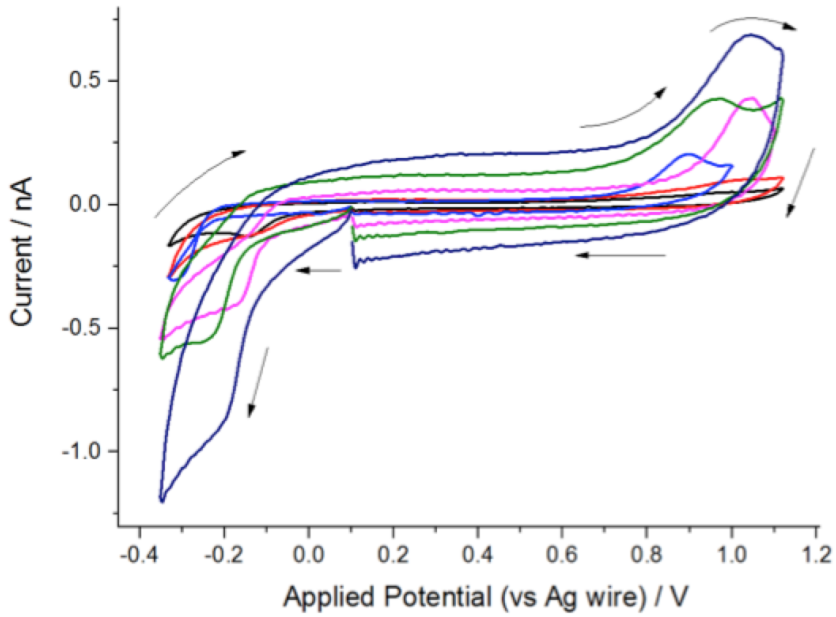

Figure 6.7: The reduction of NBTC on a CF microdisc electrode (0.078 mM NBTC) in a deoxygenated phosphate buffer solution, containing 0.1 M KCl, at pH=6.97, variable scan rates (100-800 mV s^{-1}) and 298 K.

NBTC and 0.1 M KCl, at pH = 6.97, on a carbon fibre *microelectrode* (Fig. 6.7), at four scan rates between 100 and 800 mV s^{-1}. Since the steady state current was seen to increase greatly with scan rate, as illustrated in Fig. 6.7, in-house simulation programmes [37, 38] were used to simulate the results for the microdisc voltammograms; these simulated the mechanism described by Eq. 6.1 and 6.2.

Through Fig. 6.8, it is demonstrated that the best agreement between the theoretical and experimentally obtained current values was achieved by using the diffusion coefficient obtained for m=4, D = 7.2 x 10^{-6} cm^2 s^{-1}. Thus the process likely corresponds to a four one-electron step process, where all steps after the first are indeed fully driven:

$$NBTC^{2+} + e^- \rightleftharpoons NBT^{\cdot+} \tag{6.4}$$

$$NBT^{\cdot+} + e^- \rightarrow NBT^{\cdot} \tag{6.5}$$

$$NBT^{\cdot} + e^- \rightarrow NBT^{-} \tag{6.6}$$

$$NBT^{-} + e^- \rightarrow NBT^{2-} \tag{6.7}$$

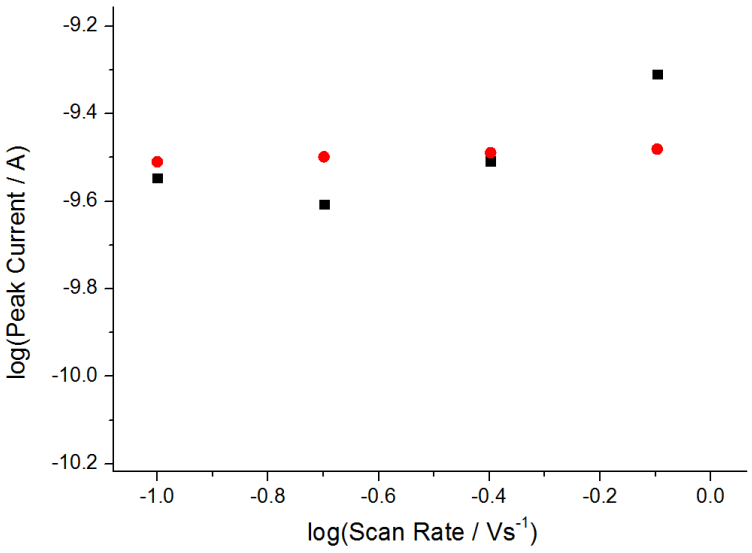

Figure 6.8: The steady state current values obtained through the simulation of the microdisc electrode depicted in Fig. 6.7 for m = 4 and D = 7.2 x 10^{-6} cm^2 s^{-1}, for each scan rate (red circles), overlaid with the experimentally obtained ones (black squares).

Protonation steps are here neglected; the reader is referred to Fig.6.2 for a mechanism that includes those steps.

To complete the characterisation of the electrochemical behaviour of NBTC in this system, a 100 mV s^{-1} oxidative scan was first carried out on the glassy carbon macroelectrode, from +0.15 to +0.95 V (vs. SCE). Since the large back peak seen at ca. +0.93 V (vs. SCE) in Fig. 6.3 was not observed, it was concluded that the peak was in fact a consequence of the oxidation of the diformazan as opposed to the oxidation of the starting material.

6.3.2 The Adsorption of Diformazan on the Glassy Carbon Macroelectrode

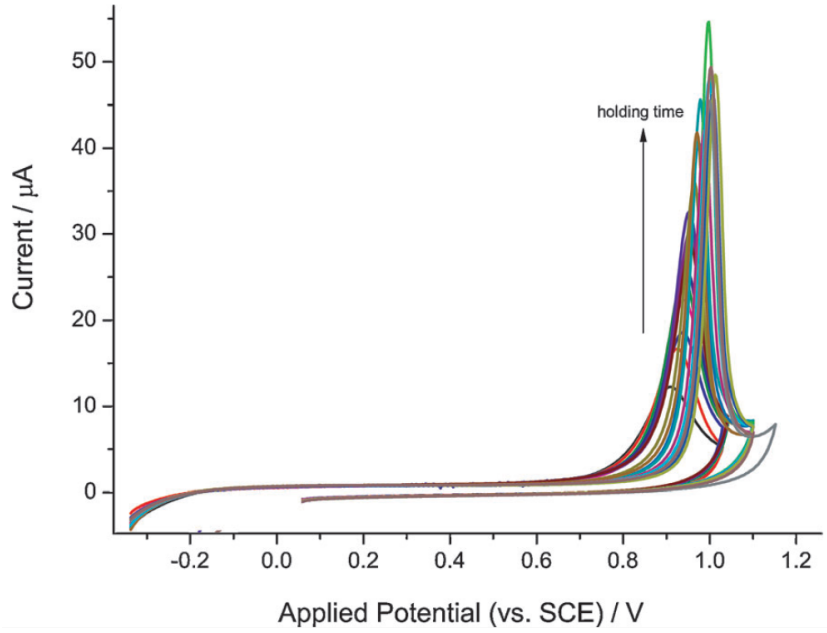

Figure 6.9: 100 mV s^{-1} cyclic voltammetric responses for the oxidation of diformazan adsorbed on the GC surface. The scans were obtained at 298 K in a deoxygenated phosphate buffer solution, containing 0.1 M KCl, at pH=6.97, after holding the potential at -0.35 V (vs. SCE), for increasing holding times, in an identical solution that also contained 0.1 mM NBTC.

The adsorptive properties of the diformazan were next investigated, on the glassy carbon macroelectrode, through a cyclic voltammetric transfer-holding experiment. For this, first a negative scan, from +0.20 V to -0.35 V (vs. SCE), was carried out in a deoxygenated aqueous phosphate buffer solution, containing 0.1 mM NBTC and 0.1 M KCl, at pH = 6.97. The potential was then held at -0.35 V (vs. SCE), for increasing holding times, after which the reverse scan was completed in a fresh deoxygenated aqueous phosphate buffer solution, which was of the same pH but, importantly, only contained 0.1 M KCl and no NBTC (Fig. 6.9).

As can be seen in Fig. 6.10, the observed peak area increased with increasing holding time, consistent with increasing amounts of the diformazan being adsorbed and with the material being bound to the electrode surface when oxidised. The plateau seen in the inlay at 40 s indicates, on the basis of the charge passed, that an apparent monolayer is formed. These observations are consistent with:

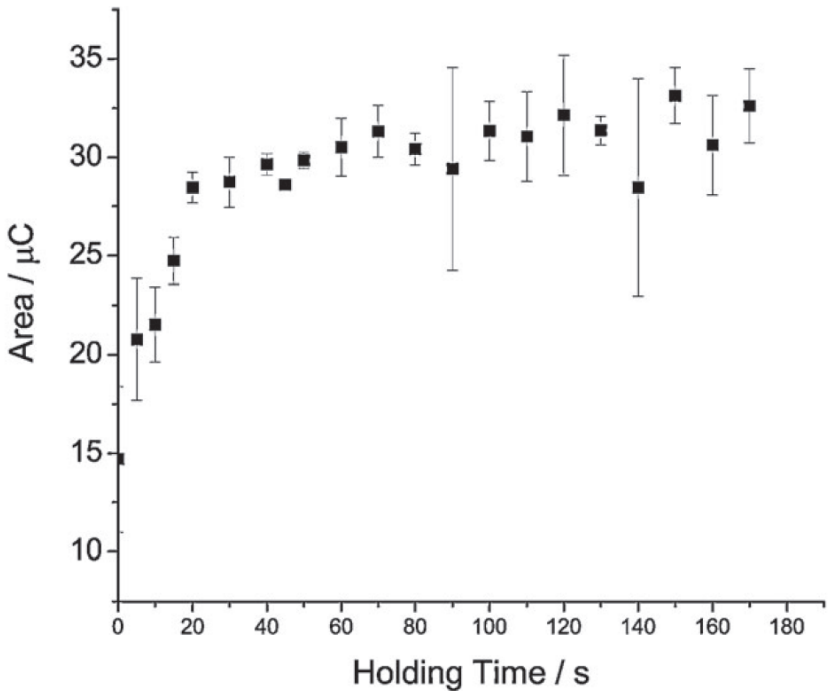

Figure 6.10: The increase in the peak area with increasing holding times, until a plateau is reached at holding times of 40 s.

$$\mathrm{NBTC}^{2+} + 4\mathrm{e}^- \rightleftharpoons \mathrm{NBTDF} \qquad \text{Reduction Scan} \tag{6.8}$$

$$\mathrm{NBTDF} \rightarrow \mathrm{NBTDF}_{(ads)} \tag{6.9}$$

$$\mathrm{NBTDF}_{(ads)} + n\mathrm{e}^- \rightarrow \text{products} \qquad \text{Oxidation Scan} \tag{6.10}$$

where NBTDF is the protonated form of the produced diformazan.

6.3.3 The Effect of Oxygen

The reduction of O_2 in an oxygen saturated (pure O_2 - 1.24 mM [41]) phosphate buffer solution, containing 0.1 M KCl at pH = 6.97, was next investigated, on the glassy carbon substrate, by cyclic voltammetry (Fig. 6.11). As expected, one two-electron peak was seen in the reductive scan at around -0.81 V (vs. SCE), while no peak was observed in the reverse sweep, according to $O_2 + 2e^- \rightarrow H_2O_2$.

$$I_p = (2.99 \quad \text{x} \quad 10^5) n(n^{'} + \alpha)^{\frac{1}{2}} AcD^{\frac{1}{2}} \tag{6.11}$$

The average α value calculated through Tafel analysis (Fig. 6.12 and 6.13) was $\alpha_{ave} = 0.24 \quad \pm 0.06$, showing that the first step was rate determining, and that hence $n^{'} = 0$, where $n^{'}$ is the number of electrons transferred before the rate determining step (RDS); n is the total number of electrons transferred (two) and the rest of the terms have been perviously defined (Equ. 6.3). Utilising the irreversible Randles-Ševčik equation (Eq. 6.11), where n is the number of electrons transferred and where the rest of the terms have been previously defined, D_{O_2} was found to be equal to 1.8 x 10^{-5} cm^2 s^{-1} (Fig. 6.14); both α and D are in agreement with literature [42–46].

By then recording the cyclic voltammetric responses, on the glassy carbon macroelectrode, of systems in which both NBTC and O_2 were present in solution, it was established that the presence of O_2 did not cause a significant interference with the electrochemistry of NBTC. This is illustrated in Fig. 6.15, where the voltammograms obtained in the presence and absence of oxygen overlay well with each other. The solutions used were once again aqueous phosphate buffer solutions, containing 0.1 M KCl, at pH = 6.97, though they contained both NBTC (0.095 mM) and O_2 (1.24 mM).

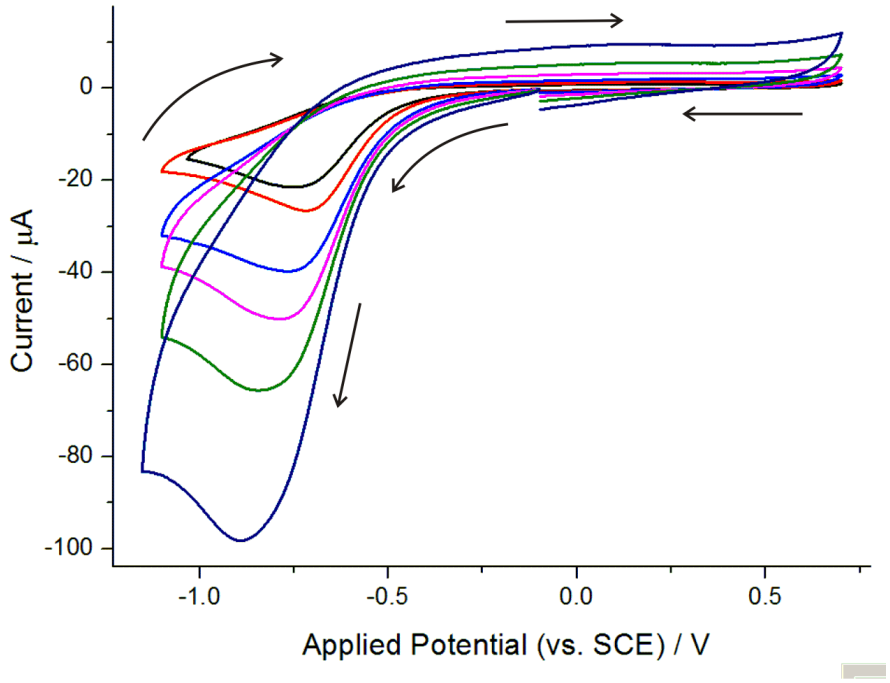

Figure 6.11: The reduction of O_2 on the GC macroelectrode in an oxygen saturated (1.24 mM) phosphate buffer solution, containing 0.1 M KCl, at pH = 6.97, variable scan rates (25-800 mV s^{-1}) and 298 K.

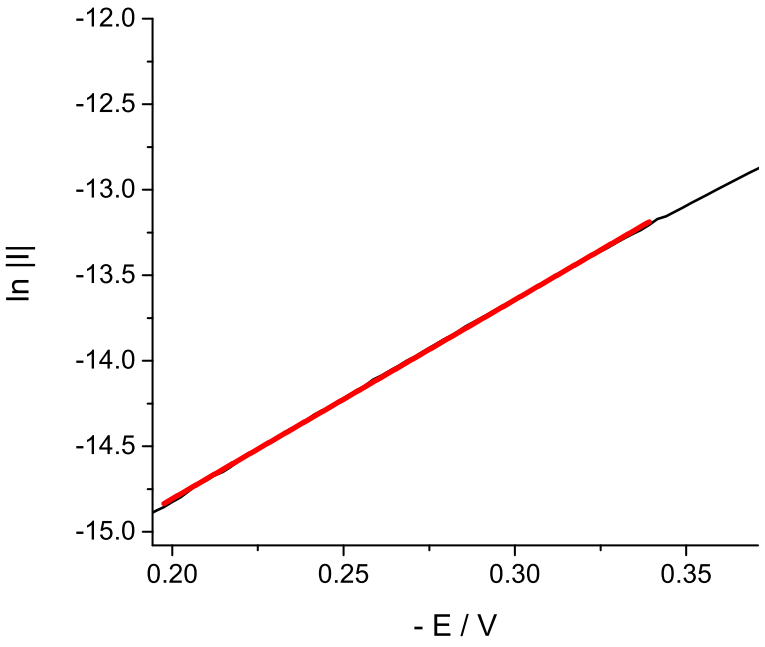

Figure 6.12: Tafel plot for the forward peak of the 100 mV s^{-1} O_2 reduction peak on the GC macroelectrode. Calculated $\alpha = 0.30$. Average $\alpha = 0.26 \pm 0.06$.

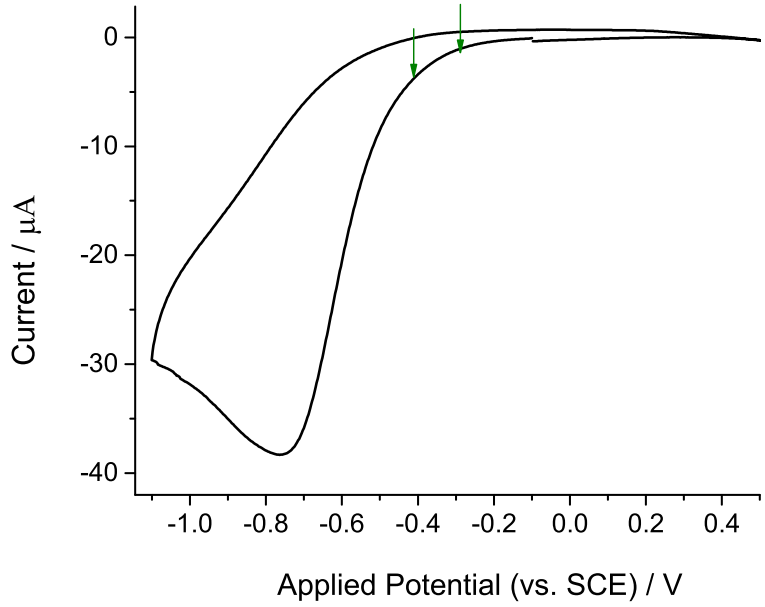

Figure 6.13: The region of the voltammogram the Tafel analysis above was based on.

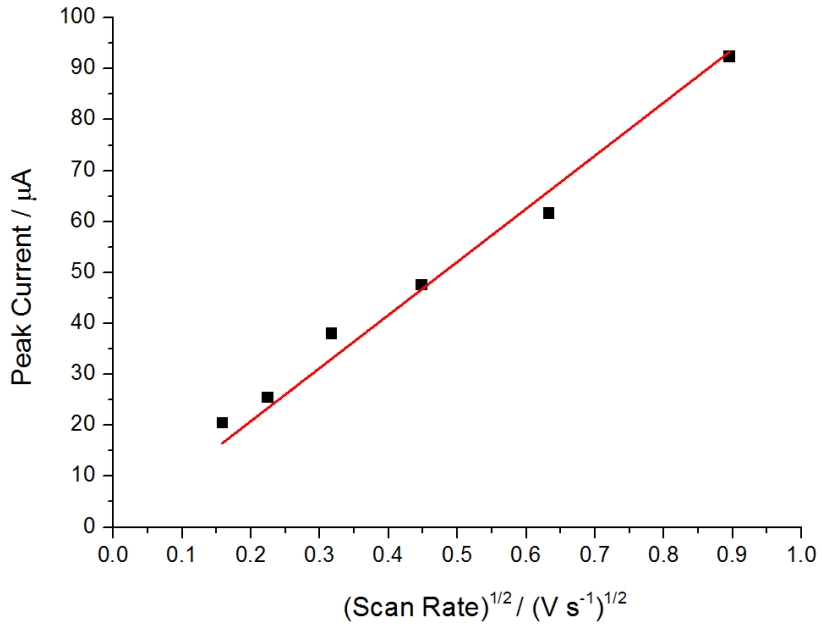

Figure 6.14: The Randles-Ševčik plot for the results presented in Fig. 6.11, which gives D = 1.8 x 10^{-5} cm^2 s^{-1}.

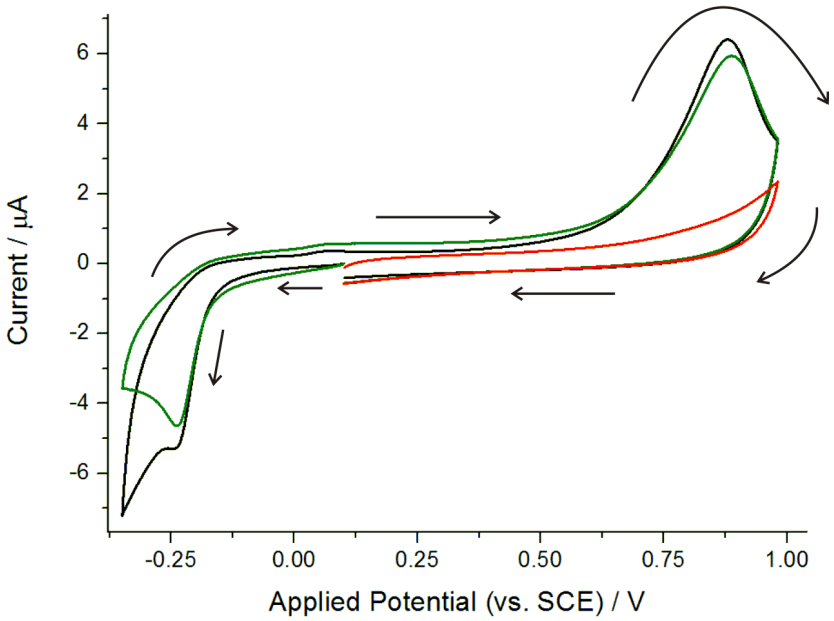

Figure 6.15: 100 mV s^{-1} cyclic voltammetric responses for the reduction of NBTC (0.095 mM) in a deoxygenated phosphate buffer solution, containing 0.1 M KCl, at pH = 6.97 (green) and an identical solution that had previously been saturated with O_2 (black). An oxidative scan (red) was carried out in the first solution indicating that the peak observed at +0.80 V (vs. SCE) is due to the oxidation of the diformazan and not the oxidation of the starting material. Responses were recorded on the GC macroelectrode at 298 K.

6.3.4 The Electrochemical Behaviour of NBTC on a Carbon Paste Electrode

A carbon paste electrode was also used in the study of the reduction of NBTC in water. This was done by taking advantage of an interesting feature of such surfaces; the fact that analyte species can dissolve and accumulate in the liquid binder if they have a high solubility and stability in it. This has been previously observed to happen with oxygen when the oil dioctyl phthalate is, as in this case, used as the pasting liquid [35], and with ferrocene when mineral oil is used as the binder [47]. In such studies, in order for any results obtained to be meaningful, it is vital to ensure that the amount of relative materials present in the paste does not vary. A cyclic voltammetry transfer experiment was hence carried out to determine the necessary pre-concentration time of the paste

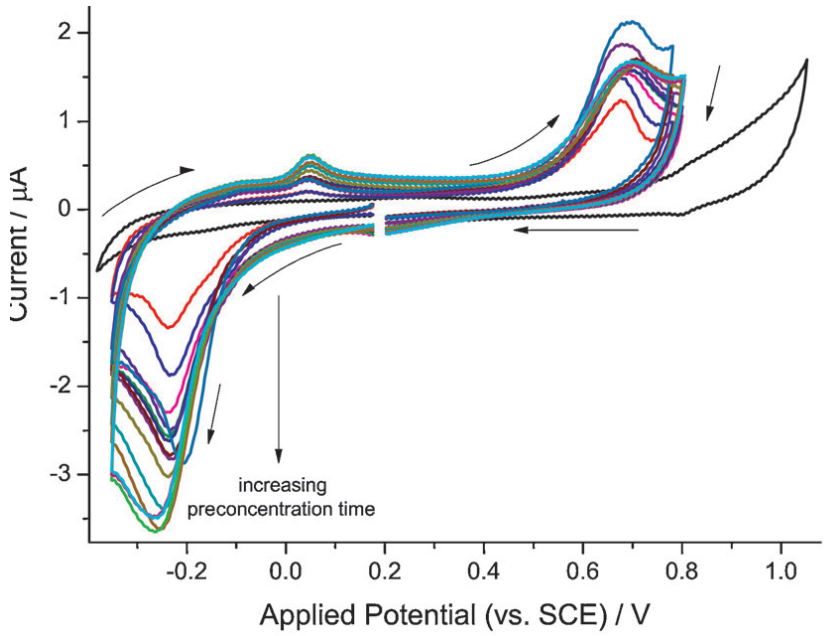

Figure 6.16: 100 mV s^{-1} cyclic voltammetric responses for the reduction of NBTC on a CPE. The scans were obtained in a deoxygenated phosphate buffer solution, containing 0.1 M KCl, at pH = 6.97, after immersing the CPE in an identical solution that also contained 0.147 mM NBTC for increasing pre-concentration times, at 298 K.

electrode with NBTC.

The paste electrode was thus immersed in a deoxygenated aqueous phosphate buffer solution, containing 0.147 mM NBTC and 0.1 M KCl, at pH = 6.97, for different pre-concentration times, under open-circuit conditions. A potential cycle between +0.85 and -0.35 V (vs. SCE) was then conducted in a fresh deoxygenated aqueous phosphate buffer solution, of the same pH and which only contained 0.1 M KCl. The peak corresponding to the reduction of NBTC was seen at around -0.23 V (vs. SCE), while the peak due to the oxidation of the generated diformazan was observed at around +0.68 V (vs. SCE).

The results of this experiment are presented in Fig. 6.16, where a clear increase of the peak current with pre-concentration time can be observed. As is depicted in Fig.6.17, the peak current reaches a plateau at 90 s. It was thus concluded that NBTC does in fact dissolve and accumulate in dioctyl phthalate and that the paste is equilibrated with NBTC after 90 s.

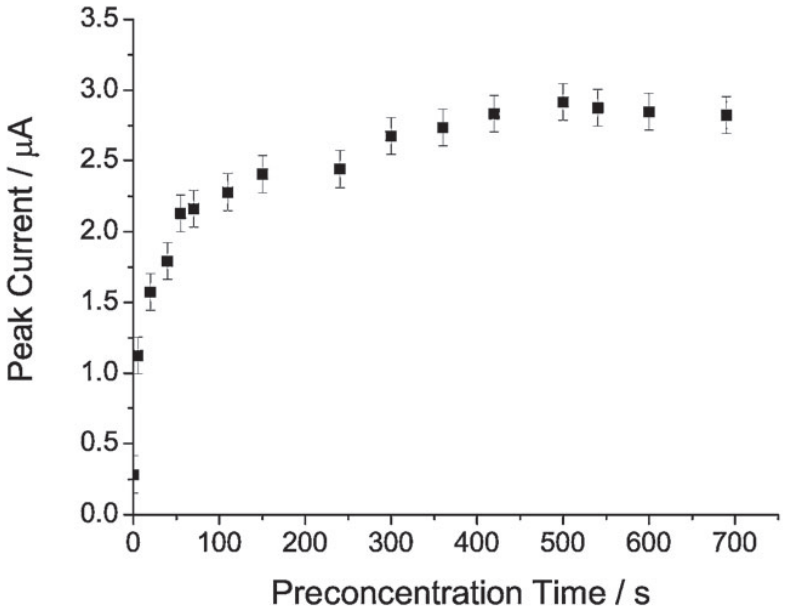

Figure 6.17: The increase of the peak current with increasing pre-concentration time.

6.4 Detecting Superoxide

Having shown that NBTC can build up in dioctyl phthalate, it was surmised that this would also be the case with superoxide and that hence the reduction of NBTC by superoxide might take place *in* the paste. Superoxide was thus synthesised using the method proposed by Hyland et al [48], whereby NaOH and H_2O are added to an air-saturated DMSO solution. The carbon paste electrode was first immersed in the produced 0.22 mM superoxide solution for 40 s, under open-circuit conditions. Next, it was immersed in a deoxygenated aqueous phosphate buffer solution, containing 0.147 mM NBTC and 0.1 M KCl, at pH = 6.97, for different pre-concentration times, again under open-circuit conditions. For each NBTC pre-concentration time, a 100 mV s^{-1} oxidative scan was

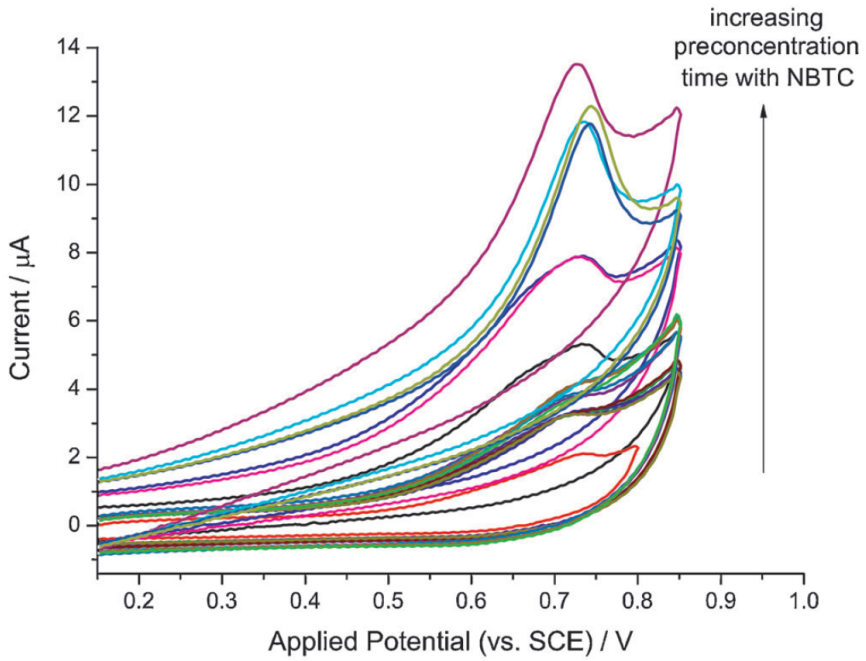

Figure 6.18: 100 mV s^{-1} cyclic voltammetric responses for the oxidation of diformazan generated in the pasting liquid. The CPE was first immersed in a 0.22 mM superoxide solution for 40 s and was then pre-concentrated with NBTC for increasing pre-concentration times. The scans were recorded at 298 K in a deoxygenated phosphate buffer solution of pH = 6.97, which contained 0.1 M KCl.

carried out, from 0.15 V up to +0.85 V (vs. SCE), in a deoxygenated phosphate buffer solution, of the same pH and which contained only 0.1 M KCl (no NBTC). The results are presented in Fig. 6.18 where the peak observed at around +0.74 V (vs. SCE) corresponds to the oxidation of the now chemically produced diformazan.

Through the presence of the diformazan oxidation peak, it was concluded that the reduction of NBTC was indeed occurring in the paste. It was thus inferred that the superoxide radical can transfer into the paste, noting its high stability in organic media [49, 50] such as dioctyl phthalate. Importantly, this interpretation is consistent with the increasing size of the diformazan oxidation peak with increasing NBTC pre-concentration time (Fig. 6.18). The trend reflects the increasing amount of NBTC accumulating in the liquid binder and being reduced by superoxide, which results in increasing amounts of diformazan being oxidised. At pre-concentration times longer than 90 s, as was previously observed, the paste is equilibrated with NBTC. The maximum possible amount of

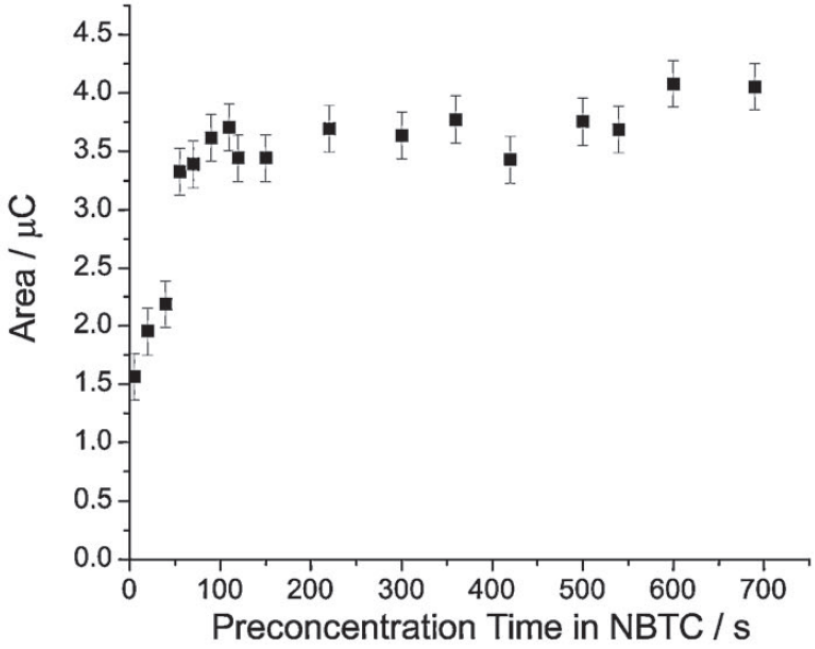

Figure 6.19: The increase in the peak area with increasing pre-concentration time with NBTC, reaching a plateau at the optimum NBTC pre-concentration time of 90 s.

diformazan is then produced and it is this that leads to the plateau shown in Fig. 6.19. The optimum pre-concentration time with NBTC was thus identified as being 90 s.

Lastly, the original 0.22 mM superoxide solution was diluted in water in order to test the sensor in aqueous 0.059 - 1.88 nM superoxide solutions. The above optimised method was used and, for each superoxide concentration, the paste electrode was thus immersed first in the superoxide solution for the fixed time of 40 s, under open-circuit conditions, and next equilibrated with NBTC, again under open-circuit conditions. A 100 mV s^{-1} oxidative scan was then carried out from +0.15 V to 0.85 V (vs. SCE), in a deoxygenated phosphate buffer solution containing only 0.1 M KCl (no NBTC), at pH = 6.97. The cyclic voltammetric responses obtained are shown in Fig. 6.20, with a signal having been observed at ca. +0.69 V (vs. SCE) for concentrations as low as 0.059 nM.

As expected, the obtained peak current increases with increasing superoxide concentration (Fig. 6.20) since increasing amounts of diformazan are formed and then oxidised. Importantly, the fact that the lowest concentration for which a signal was seen was 0.059 nM determined the *practical* limit of detection as being 0.059 nM. The slope of the calibration curve (Fig. 6.21) gave a value of 1.79 μA nM^{-1} for the sensor sensitivity.

It is worth noting that the obtained practical limit of detection is much lower compared to (calculated) theoretical values [Table 6.1]. These values are usually determined by extrapolating the calibration curve and using the equation $LOD = \frac{3\sigma}{s}$, where σ is the measured standard deviation of the signal in the absence of the target and s is the sensitivity of the sensor [51]. They hence may not represent the lowest superoxide concentration that can be practically detected. The sensitivity of the method results from the accumulation of superoxide over 40 s and as such mimics stripping voltammetry where nanomolar concentrations are routinely observed.

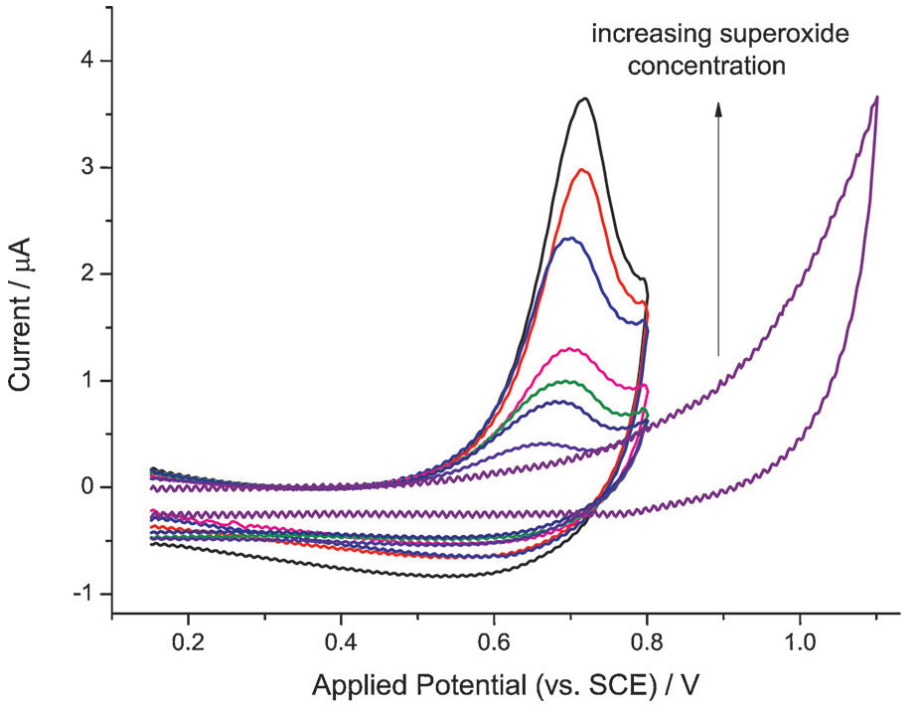

Figure 6.20: 100 mV s^{-1} cyclic voltammetric responses for the oxidation of diformazan generated in the pasting liquid for varying superoxide concentrations. The CPE was first immersed in a 0.22 mM superoxide solution for 40 s and then equilibrated with NBTC. The scans were recorded at 298 K in a deoxygenated phosphate buffer solution of pH = 6.97, which contained 0.1 M KCl.

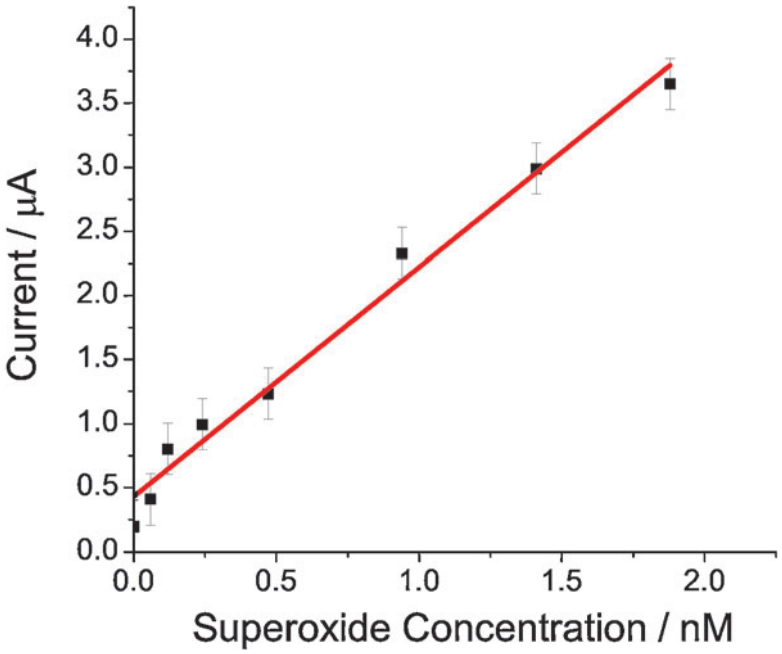

Figure 6.21: The increase in the peak current with increasing superoxide concentration.

Electrode	Calculated LOD / nM	Sensitivity / μA nM^{-1}	Reference
PTTCA-CytC/GC	50	-	[28]
DTSP-CytC/Au	73	2.8 x 10^{-9}	[26]
MWCNTs-Pt/GC	100	6.1 x 10^{-5}	[25]
Au-NS/SOD	100	5.9 x 10^{-7}	[30]
SOD/Pt SPE	190	3.5 x 10^{-6}	[29]

Table 6.1: Limit of detection (LOD) and sensitivity literature values for other superoxide sensors, where PTTCA for poly- 5,2':5'2"-terthiophene-3'-carboxylic acid, CytC for Cytochrome c, DTSP for dithiobis(succinimidyl)propionate, MWCNTs stands for multi-walled carbon nano-tubes, Au-NS for Au nanospherical electrode, SOD for superoxide dismutase and SPE for screen printed electrode. The reader's attention is drawn to the fact that the LOD values are calculated and hence may not represent the lowest superoxide concentration that can be practically detected.

6.5 Conclusions

This work has focused on the electrochemistry of NBTC on two carbon-based electrodes - a glassy carbon macroelectrode and a carbon fibre microelectrode. Through cyclic voltammetric experiments, the electrochemical behaviour of the material on the above substrates, in aqueous solutions, has been characterised and it has been shown that, neglecting protonation, the following mechanism is likely operating.

$$\mathrm{NBTC}^{2+} + \mathrm{e}^- \rightleftharpoons \mathrm{NBT}^{\cdot +} \tag{6.12}$$

$$\mathrm{NBT}^{\cdot +} + \mathrm{e}^- \rightarrow \mathrm{NBT}^{\cdot} \tag{6.13}$$

$$\mathrm{NBT}^{\cdot} + \mathrm{e}^- \rightarrow \mathrm{NBT}^- \tag{6.14}$$

$$\mathrm{NBT}^- + \mathrm{e}^- \rightarrow \mathrm{NBT}^{2-} \tag{6.15}$$

With the overall mechanism likely being

$$\mathrm{NBTC}^{2+} + 4\mathrm{e}^- \rightleftharpoons \mathrm{NBTDF} \tag{6.16}$$

$$\mathrm{NBTDF} \rightarrow \mathrm{NBTDF}_{ads} \tag{6.17}$$

$$\mathrm{NBTDF}_{ads} + n\mathrm{e}^- \rightarrow \text{products} \tag{6.18}$$

The reduction of oxygen on the glassy carbon macroelectrode yielded results that agreed with literature and it was also confirmed that the presence of oxygen in the system did not significantly affect the electrochemical behaviour of NBTC.

Importantly, NBTC was observed to build up in the pasting liquid dioctyl phthalate as has previously been seen with oxygen [35] and ferrocene [47]. Transfer cyclic voltammetric experiments determined that the paste became equilibrated with NBTC after 90 s. By fixing the immersion time of the paste electrode to a 0.22 mM superoxide solution at 40 s, while varying the NBTC pre-concentration time, the hypothesis that NBTC would get reduced by superoxide *in* the paste was confirmed. Oxidative scans were carried out from +0.15 V to +0.85 V (vs. SCE), for each NBTC pre-concentration time, during which the diformazan oxidation signal was voltammetrically visible at + 0.74 V (vs. SCE). It was thus inferred that superoxide can also accumulate in the liquid binder. An optimum NBTC pre-concentration time of 90 s was established.

The sensor was finally calibrated in aqueous superoxide solutions of increasing concentrations. Concentrations between 0.059 and 1.88 nM were used, obtaining a practical limit of detection of 0.059 nM, along with a sensor sensitivity of 1.79 μA nM^{-1}.

To the best of the authors' knowledge, this is the first electrochemical analogue of the NBT test and one of the first examples of a non-enzymatic electrochemical superoxide

sensor. This device is easy to use, in contrast to the NBT test which requires trained personnel for the interpretation of a patient's blood test results. This study also gives further insight into the properties of carbon paste electrodes.

References

[1] Baehner, R. L.; Nathan, D. G. *New England Journal of Medicine* **1968**, *278*, 971.

[2] Baehner, R. L. R. L.; Boxer, L. A.; Davis, J. *Blood* **1976**, *48*, 309.

[3] Baehner, R. L. R. L.; Jr., R. B. J. *Blood* **1972**, *40*, 31.

[4] Nissim, R.; Compton, R. G. *ChemElectroChem* **2014**, *1*, 763.

[5] Wan, C. P.; Myung, E.; Lau, B. H. S. *J. Immunol. Methods* **1993**, *159*, 131.

[6] Konorev, E. A.; Kennedy, M. C.; Kalyanaraman, B. *Arch. Biochem. Biophys.* **1999**, *368*, 421.

[7] Wallace, D. C. *Science* **1999**, *283*, 1482.

[8] Beckman, J. S.; Beckman, T. W. *Proceedings of the National Academy of Sciences of the United States of America* **1990**, *87*, 1620.

[9] Djaldetti, M.; Salman, H.; Bergman, M.; Djaldetti, R.; Bessler, H. *MIcrosc. Res. Tech* **2002**, *57*, 421.

[10] Babior, M. *New England Journal of Medicine* **1978**, *298*, 659.

[11] Flint, D. H.; Tuminello, J. F.; Emptage, M. *J. Biol. Chem.* **1993**, *268*, 22369.

[12] Keyer, K.; Imlay, J. A. *Proceedings of the National Academy of Sciences of the United States of America* **1996**, *93*, 13635.

[13] Back, P.; Matthijssens, F.; Vanfleteren, J. R.; Braeckman, B. P. *Anal. Biochem.* **2012**, *423*, 147.

[14] Kotani, H.; Ohkubo, K.; Crossley, M. J.; Fukuzimi, S. *Journal of the American Chemical Society* **2011**, *133*, 11092.

[15] Luo, J.; Li, N.; Robinson, J. P.; Shi, R. *J. Neurosci. Methods* **2002**, *120*, 105.

[16] Jurisnic, P. A. *FEBS Letters* **1978**, *90*, 15.

[17] Rico, A.; Argese, E.; Orsega, E. F.; Viglino, P. *Inorg. Chim. Acta* **1979**, *35*, 161.

[18] Vásquez-Vivar, J.; Joseph, J.; Karoui, H.; Zhang, H.; Miller, J.; Mart'asek, P. *Dossier* **2000**, *28*, 487.

[19] von Pechmann, H.; Runge, P. *Ber. Dtsch. Chem. Ges.* **1894**, *27*, 2920.

[20] Kuhn, R.; Jerchel, D. *Ber. Dtsch. Chem. Ges.* **1941**, *74*, 941.

[21] Kuhn, R.; Jerchel, D. *Ber. Dtsch. Chem. Ges.* **1941**, *74*, 949.

[22] Windhorst, D. B.; Holmes, B.; Good, R. A. *The Lancet* **1967**, *289*, 737.

[23] Kim, S. K.; Kim, D.; You, J.-M.; Han, H. S.; Jeon, S. *Electrochimica Acta* **2012**, *81*, 31.

[24] Chen, X. J.; West, A. C.; Cropek, D. M.; Banta, S. *Anal. Chem.* **2008**, *80*, 9622.

[25] Ge, B.; Lisdat, F. *Anal. Chim. Acta* **2002**, *454*, 53.

[26] Daraina, F.; Park, J.-S.; Akutsu, H.; Shima, Y.-B. *Biosensors and Bioelectronics* **2007**, *23*, 161.

[27] Hiatt, L. A.; McKenzie, J. R.; Deravi, L. F.; Harry, R. S.; Wright, D. W.; Cliffel, D. E. *Biosensors and Bioelectronics* **2012**, *33*, 128.

[28] Liu, H.; Tian, Y. *Langmuir* **2008**, *24*, 6359.

[29] Pastor, I.; Esquembre, R.; Micol, V.; Mallavia, R.; Matero, C. R. *Anal. Biochem.* **2004**, *334*, 335.

[30] Di, J.; Bi, S.; Zhang, M. *Biosensors and Bioelectronics* **2004**, *19*, 1479.

[31] Gobi, K. V.; Mituzani, F. *Journal of Electroanalytical Chemistry* **2000**, *484*, 172.

[32] Krylov, A.; Beissenhirtz, M.; Adamzig, H.; Scheller, F. W.; Lisdat, F. *Anal. Bioanal. Chem.* **2004**, *378*, 1327.

[33] Lin, Z.; Huang, L.; Liu, Y.; Lin, J.-M.; Chi, Y.; Chen, G. *Elecrochemical Communications* **2008**, *10*, 1708.

[34] Yuasa, M.; Oyaizu, K.; Yamaguchi, A.; Ishikawa, M.; Eguchi, E.; Kobayasi, T.; Toyoda, Y.; Tsutsui, S. *Polym. Adv. Technol.* **2005**, *16*, 616.

[35] Nissim, R.; Compton, R. G. *Physical Chemistry Chemical Physics* **2013**, *15*, 11918.

[36] Hope, B. T.; Michael, G. J.; Kingge, K. M.; Vincent, S. R. *Proceedings of the National Academy of Sciences of the United States of America* **1991**, *88*, 2811.

[37] Alden, J. A.; Hutchinson, F.; Compton, R. G. *J. Phys. Chem. B* **1997**, *101*, 949.

[38] Alden, J. A.; Compton, R. G. *J. Phys. Chem. B* **1997**, *101*, 8941.

[39] Wildgoose, G. G.; Wilkins, S. J.; Williams, G. R.; France, R. R.; Carnahan, D. L.; Jiang, L.; Jones, T. G. J.; Compton, R. G. *ChemPhysChem* **2005**, *6*, 352.

[40] Compton, R. G.; Banks, C. E. *Understanding Voltammetry*; World Scientific Publishing Co. Pte. Ltd.: London, 2007.

[41] Achord, J. M.; Hussey, C. L. *Anal. Chem.* **1980**, *52*, 601.

[42] Vazquez, M. V.; de Sanchez, S. R.; Calvo, E. J.; Schiffrin, D. J. *Journal of Electroanalytical Chemistry* **1994**, *374*, 189.

[43] St-Denis, C. E.; Fell, C. J. D. *Canadian Journal of Chemical Engineering* **1971**, *49*, 885.

[44] Divišek, J.; Kastening, B. *Journal of Electroanalytical Chemistry* **1975**, *65*, 603.

[45] Yano, T.; Tryk, D. A.; Hashimoto, K.; Fujushima, A. *J. Electrochem. Soc.* **1998**, *145*, 1870.

[46] Li, Q.; Batchelor-McAuley, C.; Lawrence, N. S.; Hartshorne, R. S.; Compton, R. G. *Journal of Electroanalytical Chemistry* **2013**, *688*, 328.

[47] Lowinsohn, D.; Gan, P.; Tschulik, K.; Foord, J. S.; Compton, R. G. *Electroanalysis* **2013**, *25*, 2435.

[48] Hyland, K.; Auclair, C. *Biochemical and Biophysical Research Communications* **1981**, *102*, 531.

[49] Maricle, D. L.; Hodgson, W. G. *Anal. Chem.* **1965**, *37*, 1562.

[50] Peover, M. E.; White, B. S. *Electrochimica Acta* **1966**, *11*, 1061.

[51] Analytical Methods Committee, E., Recommendations for the Definition; of the Detection Limit, U. *Analyst* **1987**, *112*, 119.

Chapter 7

Absorptive Stripping Voltammetry and its Application to the Detection of Phenolic Compounds

This chapter introduces a new, simple yet powerful electroanalytical approach - "absorptive stripping voltammetry". Its power lies in the pre-concentration of the target analyte in the bulk of the paste, which allows very low analyte concentrations to be detected during the determination step, when the target is "stripped" off back into the bulk solution. As is discussed below, absorptive stripping voltammetry is applicable not only for the sensitive detection of redox species but also in the detection of high analyte concentrations, where the commonly encountered issue of solid electrode surface "fouling" is overcome; the novel approach is illustrated through its application to the detection of both substituted and unsubstituted phenols. The work herein presented on wide range phenol detection has been published in the *Analyst* [1], while the work on the detection of cannabis has been published in the *Chemistry Central Journal* [2].

7.1 Introduction

The term "phenol" refers to a family of organic compounds whose characterising feature is the presence of at least one hydroxyl group that is attached directly onto an aromatic

ring. Its simplest member, itself commonly referred to as "phenol", is a starting material in the production of herbicides, paints and lubricants [3]. It is also a precursor in the synthesis of drugs such as aspirin, though it is mainly used in the manufacturing of plastics and phenolic resins [3]. Both substituted and unsubstituted phenols, known for the high toxicity and relatively long-term persistence in ground water - depending on temperature and pH [4] - are also common by-products of numerous industrial processes [4] and thus frequent contaminants in both waste and fresh water [4, 5]. They have in addition been found in several food matrices [6].

Importantly, Δ^9-tetrahydrocannabinol (THC), the active constituent of cannabis, is also a phenolic compound. It is known to reduce psychomotor function and cognition thus greatly impairing driving ability [7, 8], with reports indicating that the degree of impairment is related to the amount of THC present in the body; as low as 0.95 μM of THC in blood has been found to cause equivalent driving impairment to an alcohol blood concentration of 11.5 mM, the legal limit in most European countries [7]. At the same time, studies have also shown that cannabis is not only one of the most commonly used illegal drugs [9, 10] but that it is also associated with many drug driving motor vehicle accidents [11].

The development of appropriate analytical techniques for the sensitive detection and accurate quantification of phenols is hence extremely important for the assessment of their environmental impact [5]. There is also great for accurate, low-concentration detection for the development of methodologies suitable for road-side detection. Unsurprisingly, various sensing methods for phenolic compounds are used, including electrochemical techniques [12–14], gas chromatography [15–17], high performance liquid chromatography [4, 18–20], which is sometimes used in conjunction with electrochemical techniques [4, 18, 20–22],

and spectrophotometry [15–17].

However, electrochemical sensors are known for their high reliability and speed of response, their low cost and their compatibility for miniaturisation [23]; they thus offer an attractive portable alternative [24–26]. The substrates that are often selected for phenol sensing are carbon paste, glassy carbon as well as platinum electrodes. In the case of carbon paste electrodes (CPEs), extensive work has been completed using tyrosinase as the paste modifier [6, 27–31], with some of those investigations having also examined the effect of the pasting liquid on the stability of these biosensors [28, 29]. With regards to glassy carbon electrodes, they are also usually modified, for example with surfactants in which the phenols can be accumulated [32]. In the case of THC, preferred sensing molecules include Gibbs Reagent [24] and 4-aminophenol [25]. Although phenolic compounds are readily oxidised on platinum, these surfaces are quickly fouled and are hence not ideal for electrochemical studies [33–35].

Electrode surface fouling, however, can constitute a major issue with the use of electrochemical oxidation to detect phenols even when electrodes other than platinum are selected. This is because the reaction leads to radical cations and radicals that can further rapidly polymerise. Thus, for all but very dilute samples, the phenol oxidation is intrinsically "self-passivating" [33–35] and electrodes are often constrained to "single-shot" usage before either renewal or disposal. Overcoming this problem is key to the development of practical electrochemical sensors for phenols.

The aim of this investigation was to develop an electrochemical method that is both sensitive but also applicable to high concentration phenol quantification, and to illustrate its practical applicability. In contrast to earlier work with CPEs, rather than using direct electroanalysis at the CPE-solution interface, we use the bulk phase of an optimised paste

to pre-concentrate four target phenols: phenol, 4-phenoxyphenol, 4-methoxyphenol and cannabis. Each target is subsequently "stripped off" back into the bulk solution during an electrochemical measurement that is carried out in a blank supporting electrolyte solution and the peaks due to the oxidation of each phenol are used as the detection signal. We thus take analytical advantage of previous studies that have shown that that carbon paste electrodes may, under open circuit conditions, be "loaded" with an analyte of interest by being immersed in a solution containing that analyte [32–36].

We term this new electroanalytical approach "*absorptive* stripping voltammetry", with concentration in the electrode bulk, as opposed to "*adsorptive* stripping voltammetry" where the target is allowed to adsorb on the electrode surface. Importantly, the use of "absorptive stripping voltammetry" both helps overcome the effect of fouling in the less dilute samples but also ensures low limits of detection.

7.2 Experimental

Details about the chemical reagents and deoxygenation procedure here utilised can be found in Section 3.1. Cyclic voltammetric and square wave voltammetric measurements were carried out using the equipment and experimental set up described in Section 3.2. A carbon paste electrode, fabricated as described in Section 3.3, was used as the working electrode, with a Saturated Calomel Electrode (SCE) and a platinum mesh acting as the reference and counter electrodes respectively. The pastes used were fabricated as per Section 3.3, while the surface of the paste electrodes was renewed as per Section 3.4. Section 3.6 includes details about the method used to deconvolute square wave voltammetric responses.

7.3 Absorptive Stripping Voltammetry for Wide Range Phenol Detection

As has been previously mentioned, when analytes of interest have a higher solubility in the liquid binder of the paste of a carbon paste electrode than in the solution they are dissolved in, they can diffuse into and accumulate in the binder, under open circuit conditions. This can be done by simply immersing the carbon paste electrode in a solution containing the analyte. By then transferring the electrode to a fully supported blank solution and carrying out the appropriate measurement, the accumulation of the analyte can be confirmed and its electrochemistry can be studied. Unlike solid electrode substrates however where the electrode/solution interface consists of a two-phase boundary, in this case the electrochemical process likely takes place at the carbon-oil (binder)-water triple boundary as the analyte is released from the paste into the bulk solution [37]. This is because only at that point are electrons from the carbon powder, electrons from the analyte and charge balancing ions from the supporting electrolyte all available for the reaction to occur. This concept of reaction at the triple phase boundary has been successfully studied for a variety of redox active species, including oxygen [36], nitroblue tetrazolium chloride [38], ferrocene [37] and Vitamin K1 [39].

Importantly, variation of the immersion time of the carbon paste electrode in the analyte solution, i.e. variation of the pre-concentration time of the paste with the analyte, allows the quantification of the accumulation of the species in the paste. The minimum pre-concentration time needed for the paste to be equilibrated with the analyte can thus be identified and further experiments can then be carried out by pre-concentrating known

amounts of the species. At the same time, however, the composition of the paste used can also greatly affect the observed uptake, leading to the additional need of optimising the paste "recipe" to achieve as high an accumulation of an analyte as possible. This means that pastes can be tailored to match the exact needs of the studied analyte, i.e. that very sensitive detection strategies can be developed.

What should be highlighted is that the sequence of pre-concentration and determination steps involved when carbon paste electrodes are used to "store" a species is reminiscent of adsorptive stripping voltammetry (see Section 1.5.4.2), where an analyte is allowed to adsorb onto the electrode surface before being "stripped" off into the solution during a measurement. In the present case, the analyte is absorbed in the bulk of the paste, rather than accumulate through adsorption onto the surface. By analogy to "adsorptive stripping voltammetry" the new approach that is here introduced might thus be termed "absorptive stripping voltammetry".

The ability of four carbon pastes - fabricated by mixing graphite powder with dioctyl phthalate, graphite powder with mineral oil, nanocarbon with dioctyl phthalate and nanocarbon with mineral oil - to accumulate phenol and 4-phenoxyphenol in their paste component was here first explored. Given that the recorded background currents were not seen to vary with immersion time, an optimum paste, made from graphite powder and dioctyl phthalate, was chosen based on the observed analyte uptake. It was then used with different phenol, 4-phenoxyphenol and 4-methoxyphenol concentrations, with the aim of determining analytical limits of detection for each compound in aqueous solutions of pH 10. The oxidation peaks of phenol, 4-phenoxyphenol and 4-methoxyphenol, observed at peak potentials of ca. +0.60, +0.40 and +0.30 V [vs. saturated calomel electrode (SCE)] respectively, were used as the detection signals. The use of square wave voltammetry

to address the issue of simultaneous detection of the three phenols is also presented and discussed.

It will be shown in this chapter that practically useful analytical limits of detection in the low micromolar range can be obtained and, in the case of phenol, concentrations as high as 10 mM can be detected before the detection becoming limited by the uptake ability of the paste. Importantly, for concentrations up to 1.0 mM, the electrode surface did not need to be renewed; this indicates that surface fouling becomes an issue much later than is observed with other electrode surfaces, which are conventionally used [33–35]. The reduced fouling also explains why concentrations of phenol at the mM level can be assessed.

7.3.1 The Electrochemistry of 4-Phenoxyphenol and Phenol on the Four Carbon Paste Electrodes

7.3.1.1 Determining the Oxidation Products of 4-Phenoxyphenol

To determine the products of the 4-phenoxyphenol oxidation, each paste electrode was immersed in a deoxygenated aqueous borate buffer solution of pH 10.01 that contained 35 μM benzoquinone and 0.1 M KCl. This was done under open circuit conditions, for 30 s. The electrode was then transferred to a deoxygenated aqueous borate buffer solution of pH 10.01 that only contained 0.1 M KCl. 100 mV s^{-1} reductive scans were then run between +0.80 V and -0.40 V (vs. SCE). Peaks attributed to the reduction of benzoquinone (see below) were observed at peak potentials of -0.16 V, -0.15 V and -0.30 V (vs. SCE) on the graphite/dioctyl phthalate, graphite/mineral oil and nanocarbon/mineral oil pastes respectively; no peaks were observed with the nanocarbon/dioctyl phthalate paste.

The graphite/dioctyl phthalate, graphite/mineral oil and nanocarbon/mineral oil paste electrodes were each then immersed in a deoxygenated aqueous borate buffer solution of pH 10.01 that contained 7.0 μM 4-phenoxyphenol and 0.1 M KCl. This was done under open circuit conditions, for 60 s. They were each then transferred to a deoxygenated aqueous borate buffer solution of pH 10.01 that only contained 0.1 M KCl, in which oxidative 100 mV s^{-1} scans were run between -0.40 V and +0.80 V (vs. SCE). Peaks corresponding to the reduction of the 4-phenoxyphenol oxidation product were again seen at peak potentials of -0.16 V, -0.15 V and -0.30 V (vs. SCE) on the graphite/dioctyl phthalate, graphite/mineral oil and nanocarbon/mineral oil pastes respectively.

Typical responses obtained for the reduction of benzoquinone and the oxidation of 4-phenoxyphenol, on the graphite/dioctyl phthalate paste, are overlaid in Fig. 7.1. Since the peaks due to the reduction of benzoquinone were observed at the same peak potentials

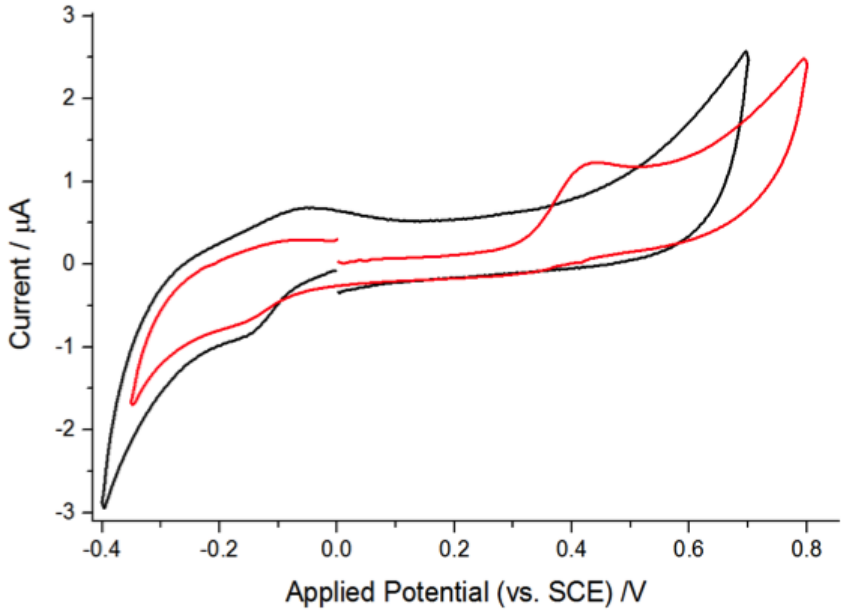

Figure 7.1: 100 mV s^{-1} cyclic voltammetric responses of the reduction of benzoquinone (red) and the oxidation of 4-phenoxyphenol (black) on the graphite/dioctyl phthalate CPE, obtained at 298 K in a deoxygenated borate buffer solution, containing 0.1 M KCl, of pH = 10.01, after the CPE had been immersed in identical solutions containing 35 μM benzoquinone (for 30 s) or 7.0 μM 4-phenoxyphenol (for 60 s), respectively.

as those due to the reduction of the 4-phenoxyphenol oxidation product, on each of the three pastes used, it was concluded that the mechanism followed in the 4-phenoxyphenol oxidation reaction was likely:

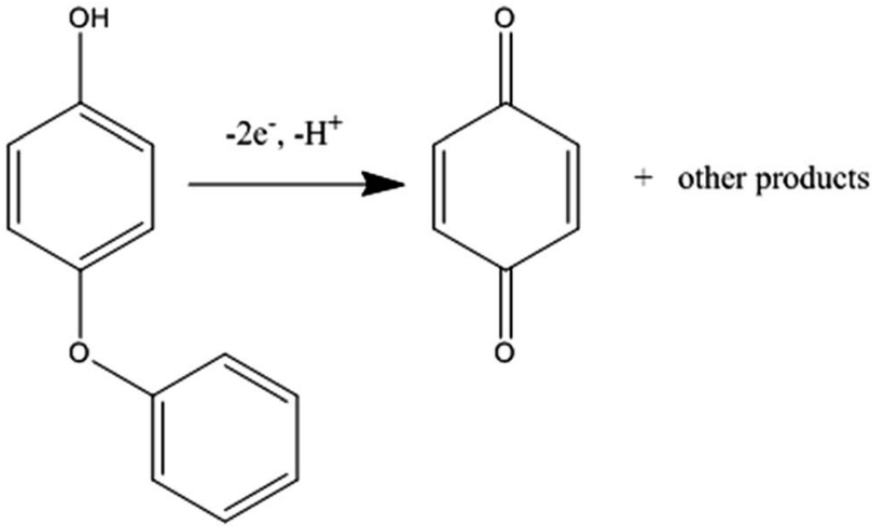

Figure 7.2: The oxidation of 4-phenoxyphenol.

7.3.1.2 Determining the Oxidation Products of Phenol

The products of the phenol oxidation were next investigated. Given that known soluble products of the oxidation of phenol are oxidised 1,2-dihydroxybenzene (oxidised catechol) and oxidised 1,4-dihydroxybenzene [34], their electrochemistry was fingerprinted on the four paste electrodes. Each paste electrode was thus first immersed in a deoxygenated aqueous borate buffer solution of pH 10.01 that contained 1.0 mM catechol and 0.1 M KCl. This was done under open circuit conditions, for 60 s. The electrode was then transferred to a deoxygenated aqueous borate buffer solution of pH 10.01 that only contained 0.1 M KCl. 100 mV s^{-1} reductive scans were then run, between +0.80 V and -0.10 V (vs. SCE). Peaks due to the reduction of oxidised catechol (orthoquinone [40]) were seen at peak potentials of -0.010 V on all four pastes. An analogous experiment was then carried

out with 1,4-dihydroxybenzene. Each paste electrode was immersed in a deoxygenated aqueous borate buffer solution of pH 10.01 that contained 1.0 mM 1,4-dihydroxybenzene and 0.1 M KCl. This was again done under open circuit conditions, for 60 s. Each electrode was then transferred to a deoxygenated aqueous borate buffer solution of pH 10.01 that only contained 0.1 M KCl, in which reductive 100 mV s^{-1} scans were run between +0.80 V and -0.35 V (vs. SCE). Peaks due to the reduction of oxidised 1,4-dihydroxybenzene (benzoquinone [40]) were seen at peak potentials of -0.15 V, -0.14 V, -0.20 V and -0.21 V (vs. SCE) on the graphite/dioctyl phthalate, graphite/mineral oil, nanocarbon/mineral oil and nanocarbon/dioctyl phthalate pastes respectively.

Each paste electrode was finally immersed in a deoxygenated aqueous borate buffer solution of pH 10.01 that contained 40 μM phenol and 0.1 M KCl. This was once again

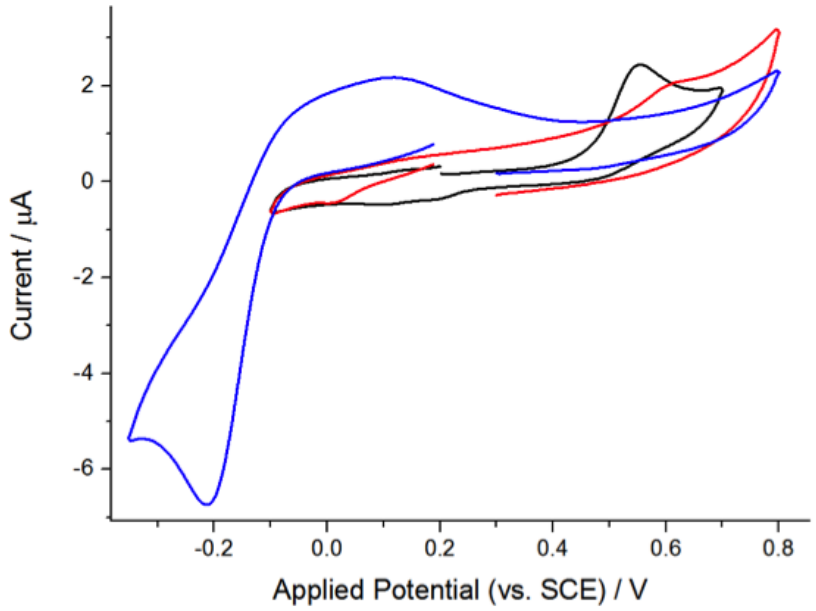

Figure 7.3: 100 mV s^{-1} cyclic voltammetric responses of the reduction of 1,2-dihydroxybenzene (catechol - red), the reduction of 1,4-dihydroxybenzene (hydroquinone - blue) and the oxidation of phenol (black) on the graphite/dioctyl phthalate CPE, obtained at 298 K in a deoxygenated borate buffer solution, containing 0.1 M KCl, of pH = 10.01, after the CPE had been immersed in identical solutions containing 1.0 mM catechol (for 60 s), 1.0 mM hydroquinone (for 60 s) or 40 μM phenol (for 60 s), respectively.

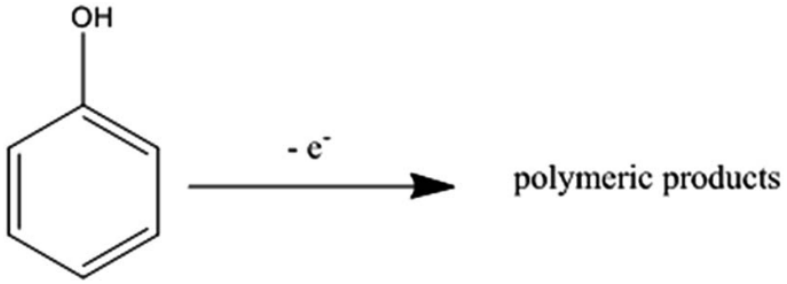

Figure 7.4: The oxidation of 4-phenoxyphenol.

done under open circuit conditions, for 90 s. The electrode was then transferred to a deoxygenated aqueous borate buffer solution of pH 10.01 that only contained 0.1 M KCl. 100 mV s^{-1} oxidative scans were run, between -0.10 V and +0.80 V (vs. SCE). Two peaks that can be attributed to the reduction of the phenol oxidation products were observed at peak potentials of +0.20 V and +0.11 V (vs. SCE), with the graphite/dioctyl phthalate and graphite/mineral oil pastes. Only one back peak is seen with the nanocarbon/dioctyl phthalate paste, at a peak potential of +0.11 V (vs. SCE), while no peaks are seen with the nanocarbon/mineral oil paste.

Typical responses, obtained on the graphite/dioctyl phthalate paste, are overlaid in Fig. 7.3. Since the peaks due to the reduction of both orthoquinone and benzoquinone were observed at more negative peak potentials than the phenol oxidation products, it was concluded that the mechanism followed in the phenol oxidation reaction was the one summarised in Fig. 7.4, where polymeric products are assumed to be formed upon the oxidation of phenol, under the conditions identified.

7.3.2 Selection of the Optimum Paste Composition

Having studied the mechanism followed in the oxidation of both 4-phenoxyphenol as well phenol, the equilibration of the four pastes with these two analytes was quantified with the

aim of selecting the most appropriate paste composition for further experiments. A study on the possible variation of the background current with immersion time in a supporting electrolyte solution was also conducted in order to confirm the paste remained stable during the electrochemical measurements.

7.3.2.1 Equilibrating the Four Carbon Pastes with 4-Phenoxyphenol

Starting from the quantification of the accumulation of 4-phenoxyphenol, each carbon paste electrode was immersed in a deoxygenated aqueous borate buffer solution of pH 10.01 that contained 2.5 - 20 μM 4-phenoxyphenol and 0.1 M KCl as the supporting electrolyte. This was done under open circuit conditions, for progressively increasing pre-concentration times. The paste electrode was then transferred to a deoxygenated

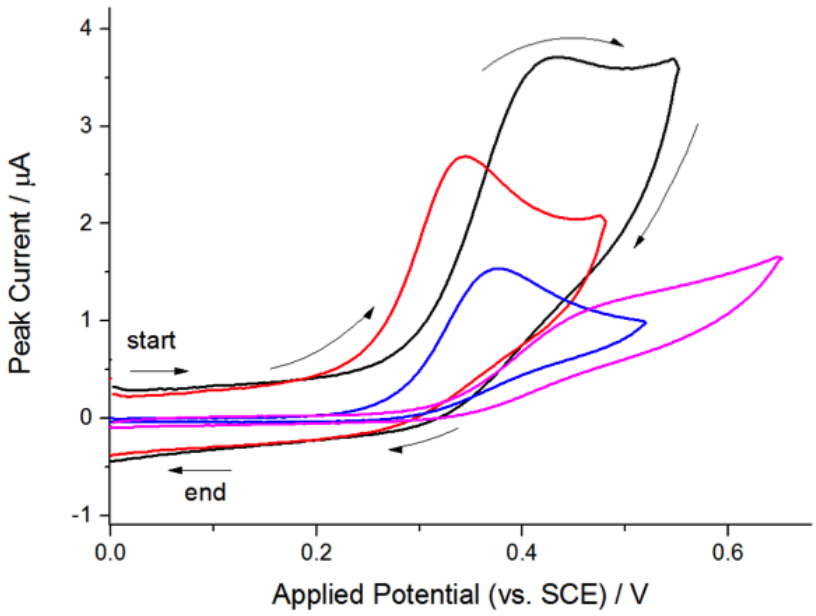

Figure 7.5: Comparison of typical 100 mV s^{-1} oxidative voltammetric responses for the oxidation of 4-phenoxyphenol on the graphite/dioctyl phthalate (black), graphite/mineral oil (red), nanocarbon/mineral oil (blue) and nanocarbon/dioctyl phthalate paste (magenta) CPE, respectively. These were obtained at 298 K in a deoxygenated borate buffer solution of pH 10.01, containing 0.1 M KCl, after the CPEs had been immersed in an identical solution that also contained 20 μM 4-phenoxyphenol for 60s.

aqueous borate buffer solution of pH 10.01, which only contained 0.1 M KCl, and in which oxidative 100 mV s^{-1} cyclic voltammetric scans were run, between 0.0 V and + 0.60 V (vs. SCE). Peaks due to the oxidation of 4-phenoxyphenol were seen at peak potentials of +0.43 V, +0.35 V, +0.38 V and +0.51 V (vs. SCE) on the graphite/dioctyl phthalate, graphite/mineral oil, nanocarbon/mineral oil and nanocarbon/dioctyl phthalate pastes respectively (Fig. 7.5).

The results obtained with the 20 μM 4-phenoxyphenol solution can be seen in Figs. 7.6 - 7.9 where, for all four pastes used, the peak current increased with increasing pre-concentration time and a plateau was reached at ca. 60 s (Figs. 7.10 - 7.13 and 7.14 - 7.17). Figs. 7.10 to 7.13, as well as Figs. 7.14 to 7.17, also demonstrate the similar trends that were seen to be followed with the 2.5, 7.0 and 11 μM 4-phenoxyphenol solutions, again with all four pastes. The expected effect of higher peak areas and peak currents being seen with increasing target concentration is also shown.

Considering Fig. 7.5, the observation that higher peak currents were seen with the graphite/ dioctyl phthalate paste indicates a greater ability to uptake the target phenol. Examining Figs. 7.6 to 7.17, the increase in peak area and peak current with increasing pre-concentration time, observed for each set of measurements at a given 4-phenoxyphenol concentration, for all four pastes, is consistent with increasing amounts of 4-phenoxyphenol being accumulated in each paste with increasing pre-concentration times. This is observed until the pastes are equilibrated with the analyte of interest, at which point the plateau is reached. Upon comparing the results obtained at different target concentrations for each paste, the increase in the peak areas (and peak currents) with 4-phenoxyphenol concentration is again reasonable as more and more 4-phenoxyphenol is present in solution and able to transfer into the paste.

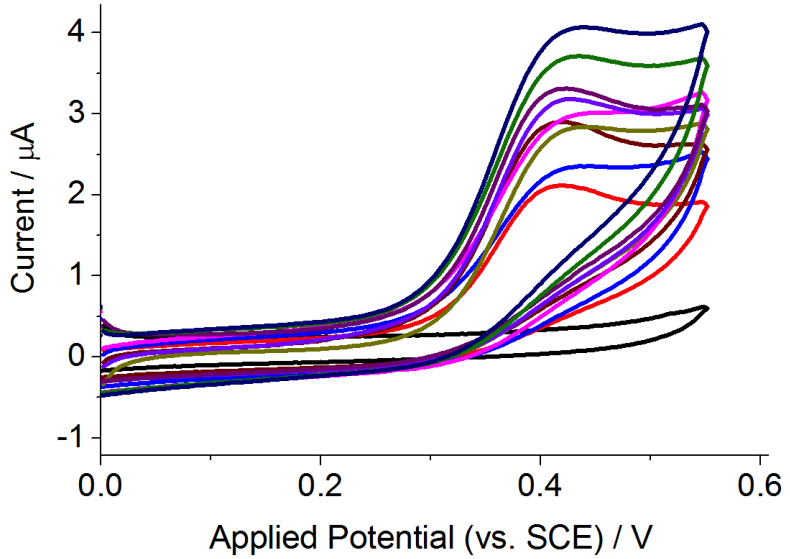

Figure 7.6: 100 mV s^{-1} cyclic voltammetric responses for the oxidation of 4-phenoxyphenol to benzoquinone on the graphite/dioctyl phthalate CPE, obtained at 298 K in a deoxygenated borate buffer solution of pH 10.01, containing 0.1 M KCl, after pre-concentration from an identical solution that also contained 20 μM 4-phenoxyphenol, for increasing pre-concentration times between 0 and 210 s.

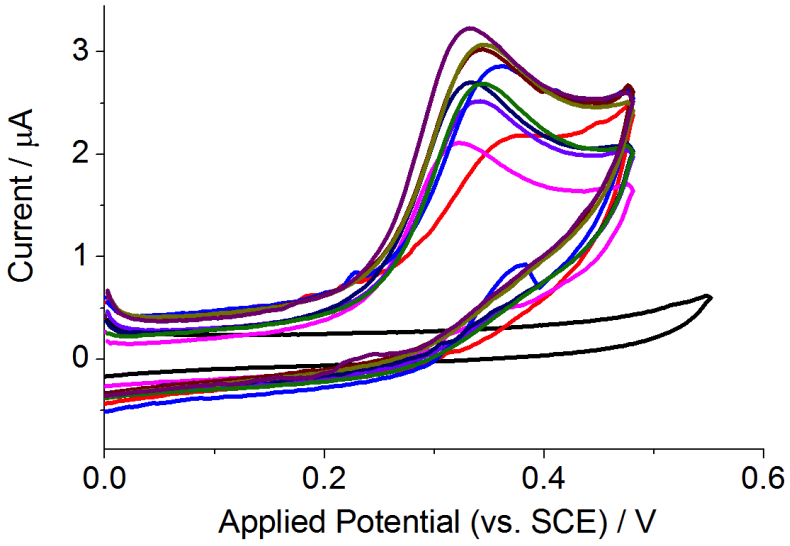

Figure 7.7: 100 mV s^{-1} cyclic voltammetric responses for the oxidation of 4-phenoxyphenol to benzoquinone on the graphite/mineral oil CPE, obtained at 298 K in a deoxygenated borate buffer solution of pH 10.01, containing 0.1 M KCl, after pre-concentration from an identical solution that also contained 20 μM 4-phenoxyphenol for increasing pre-concentration times between 0 and 210 s.

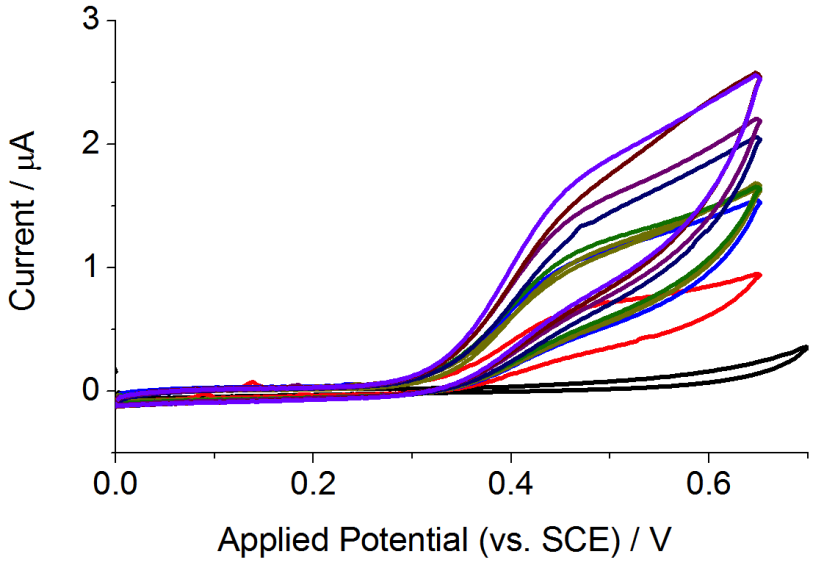

Figure 7.8: 100 mV s^{-1} cyclic voltammetric responses for the oxidation of 4-phenoxyphenol to benzoquinone on the nanocarbon/mineral oil CPE, obtained at 298 K in a deoxygenated borate buffer solution of pH 10.01, containing 0.1 M KCl, after pre-concentration from an identical solution that also contained 20 μM 4-phenoxyphenol for increasing pre-concentration times between 0 and 210 s.

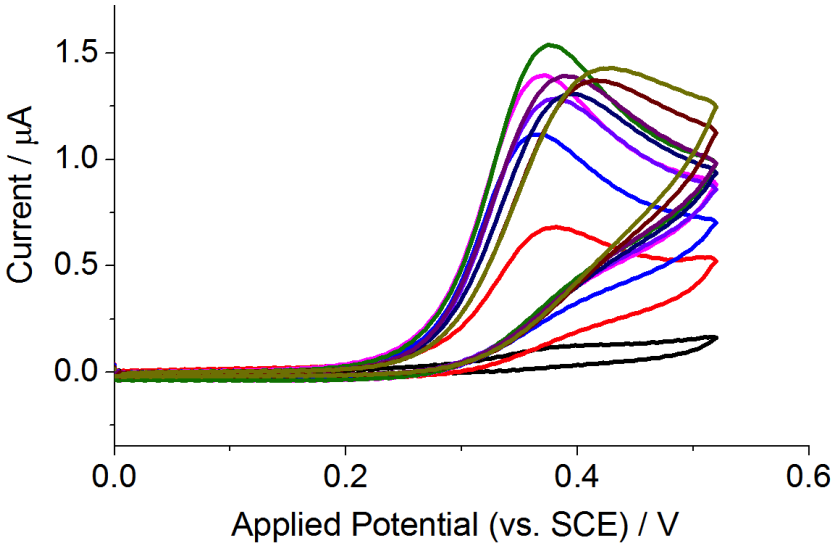

Figure 7.9: 100 mV s^{-1} cyclic voltammetric responses for the oxidation of 4-phenoxyphenol to benzoquinone on the nanocarbon/dioctyl phthalate CPE, obtained at 298 K in a deoxygenated borate buffer solution of pH 10.01, containing 0.1 M KCl, after pre-concentration from an identical solution that also contained 20 μM 4-phenoxyphenol for increasing pre-concentration times between 0 and 210 s.

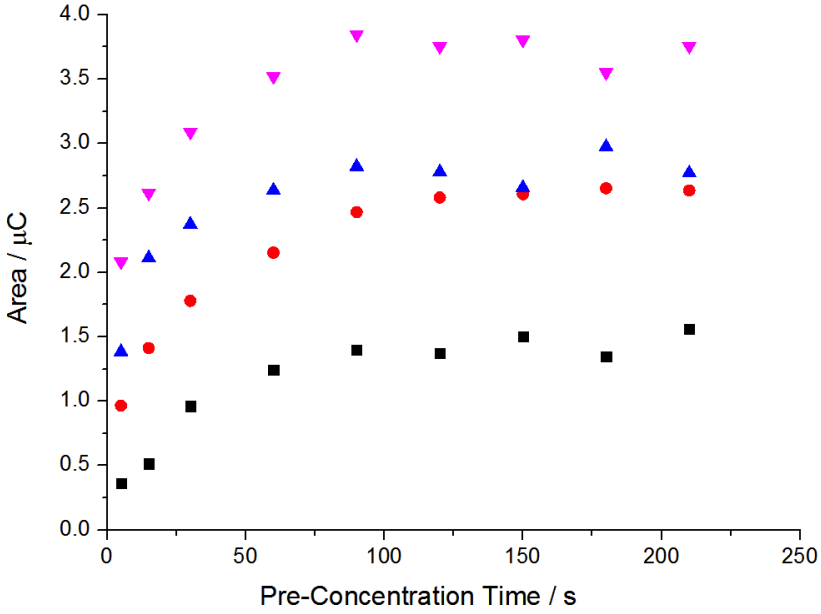

Figure 7.10: The variation of the peak area with pre-concentration time of the responses obtained at different 4-phenoxyphenol concentrations on the graphite/dioctyl phthalate CPE, where black: 2.5 μM, red: 7.0 μM, blue: 11 μM and magenta: 20 μM.

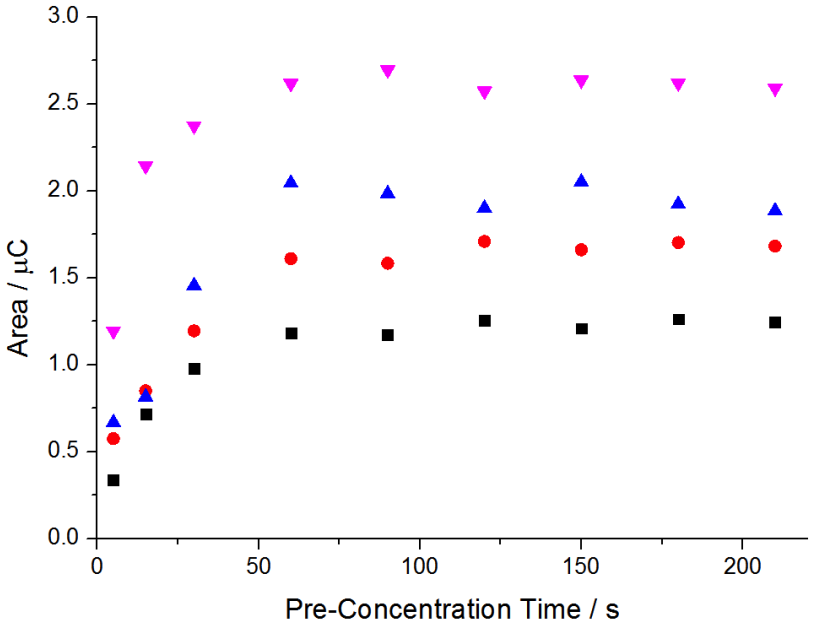

Figure 7.11: The variation of the peak area with pre-concentration time of the responses obtained at different 4-phenoxyphenol concentrations on the graphite/ mineral oil CPE, where black: 2.5 μM, red: 7.0 μM, blue: 11 μM and magenta: 20 μM.

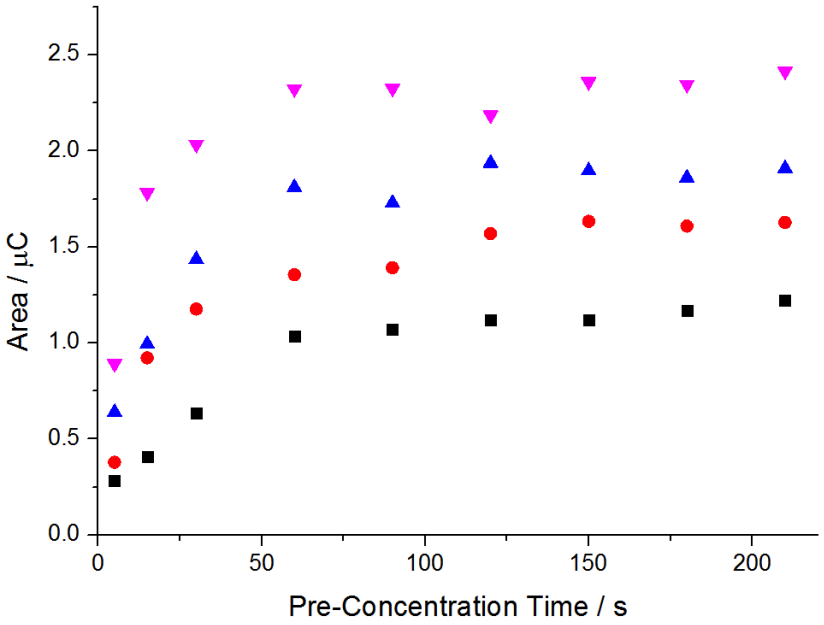

Figure 7.12: The variation of the peak area with pre-concentration time of the responses obtained at different 4-phenoxyphenol concentrations on the nanocarbon/mineral oil CPE, where black: 2.5 μM, red: 7.0 μM, blue: 11 μM and magenta: 20 μM.

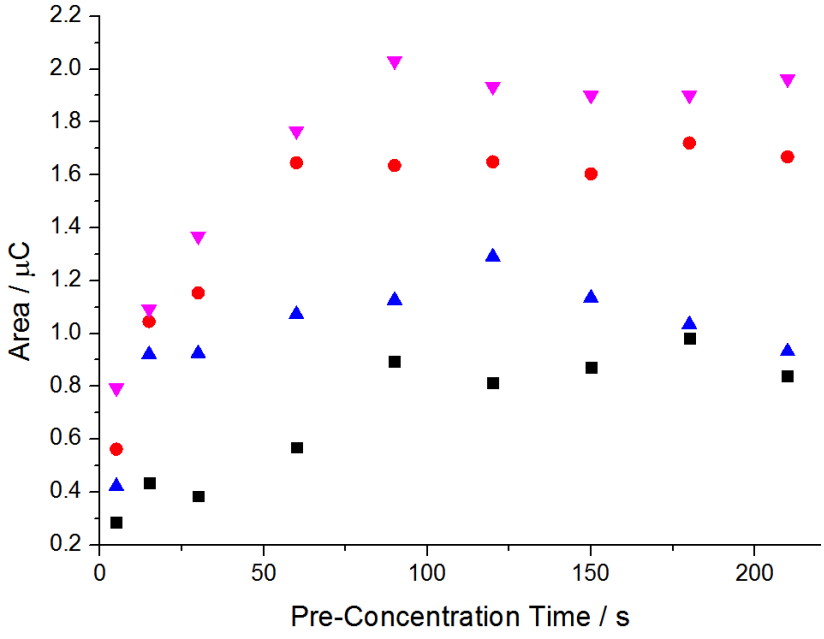

Figure 7.13: The variation of the peak area with pre-concentration time of the responses obtained at different 4-phenoxyphenol concentrations on the nanocarbon/dioctyl phthalate CPE, where black: 2.5 μM, red: 7.0 μM, blue: 11 μM and magenta: 20 μM.

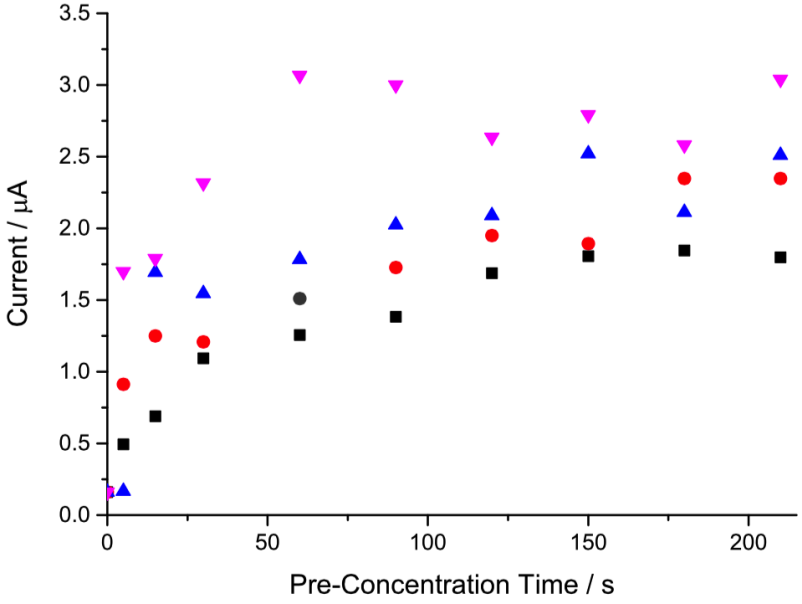

Figure 7.14: The variation of the peak current with pre-concentration time of the responses obtained at different 4-phenoxyphenol concentrations on the graphite/dioctyl phthalate CPE, where black: 2.5 μM, red: 7.0 μM, blue: 11 μM and magenta: 20 μM.

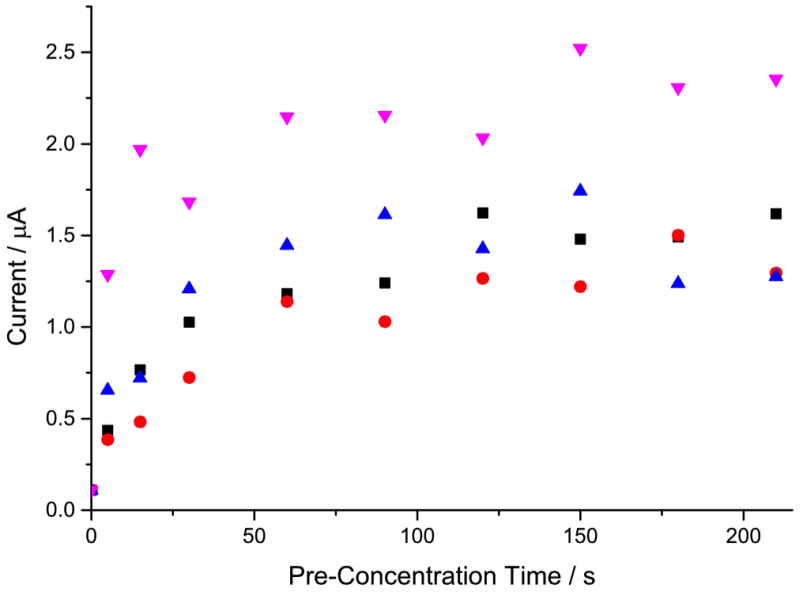

Figure 7.15: The variation of the peak current with pre-concentration time of the responses obtained at different 4-phenoxyphenol concentrations on the graphite/ mineral oil CPE, where black: 2.5 μM, red: 7.0 μM, blue: 11 μM and magenta: 20 μM.

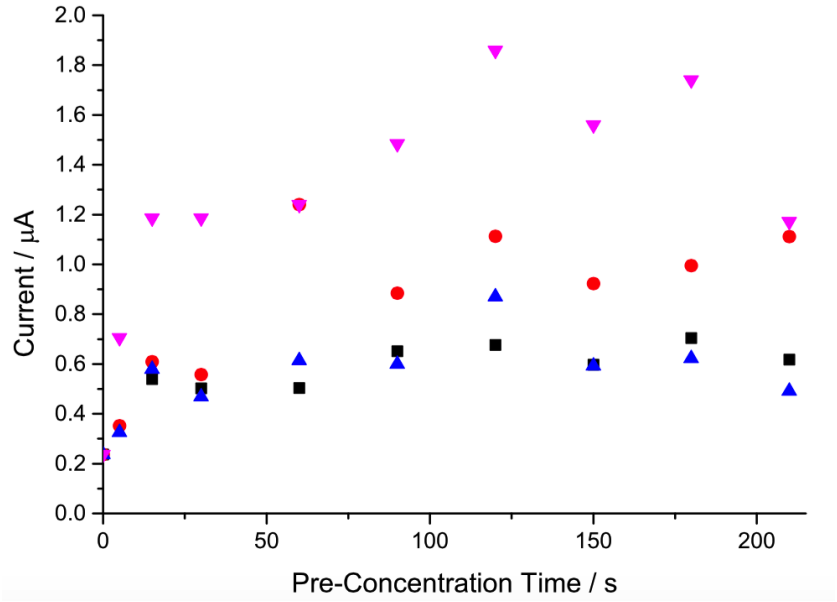

Figure 7.16: The variation of the peak current with pre-concentration time of the responses obtained at different 4-phenoxyphenol concentrations on the nanocarbon/mineral oil CPE, where black: 2.5 μM, red: 7.0 μM, blue: 11 μM and magenta: 20 μM.

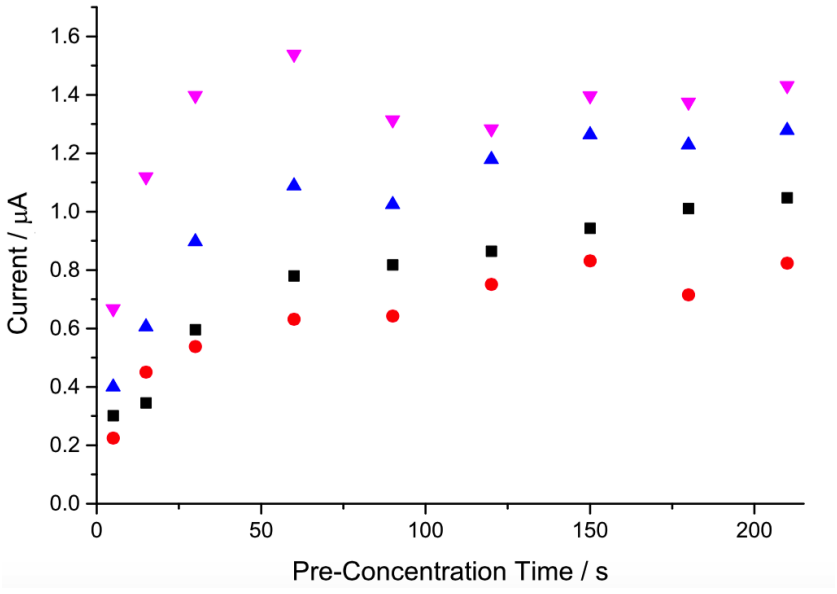

Figure 7.17: The variation of the peak current with pre-concentration time of the responses obtained at different 4-phenoxyphenol concentrations on the nanocarbon/dioctyl phthalate CPE, where black: 2.5 μM, red: 7.0 μM, blue: 11 μM and magenta: 20 μM.

Importantly, the similar equilibration times of ca. 60 s that were observed for all pastes combined with the greater 4-phenoxyphenol uptake of the graphite/dioctyl phthalate paste, clearly indicated that the graphite/dioctyl phthalate combination was the optimum one for further experiments with 4-phenoxyphenol. Given that the same information can be obtained from peak area vs. pre-concentration time plots and peak current vs. pre-concentration time plots, the latter are used in the remaining text as they are analytically easier to obtain.

7.3.2.2 Equilibrating the Four Carbon Pastes with Phenol

The four pastes were next used to explore the uptake of phenol. Each carbon paste electrode was first immersed in a deoxygenated aqueous borate buffer solution of pH 10.01 that contained 7.0 - 40 μM phenol and 0.1 M KCl as the supporting electrolyte. This

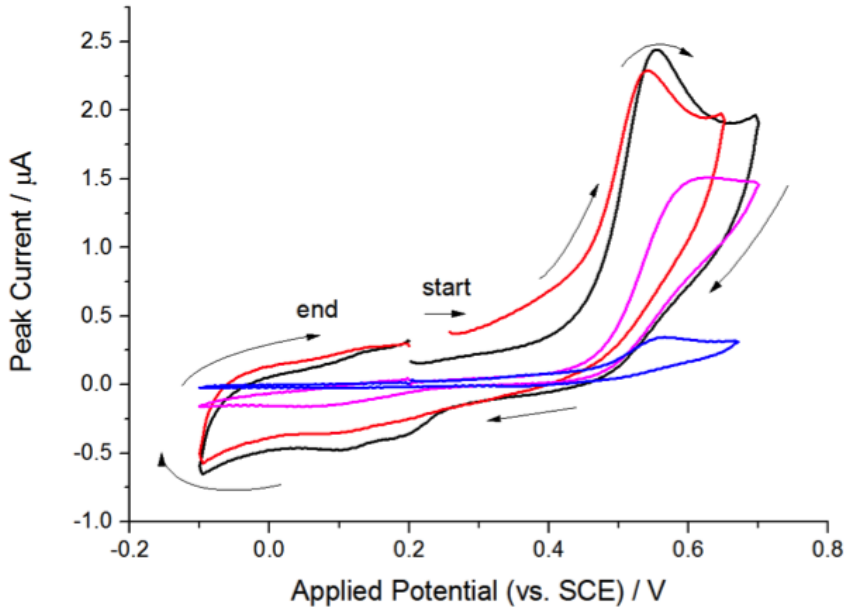

Figure 7.18: Typical 100 mV s^{-1} cyclic voltammetric responses for the oxidation of phenol on the four carbon paste electrodes used (black: graphite/dioctyl phthalate, red: graphite/ mineral oil, blue: nanocarbon/mineral oil, magenta: nanocarbon/dioctyl phthalate), obained at 298 K in a deoxygenated borate buffer solution, containing 0.1 M KCl, of pH = 10.01, after pre-concentration from an identical solution that also contained 40 μM phenol for 90 s.

was again done under open circuit conditions, for increasing pre-concentration times. Oxidative 100 mV s^{-1} cyclic voltammetric scans were then run, between -0.10 V and +0.70 V (vs. SCE), in a deoxygenated aqueous borate buffer solution of pH 10.01, which only contained 0.1 M KCl. Peaks corresponding to the oxidation of phenol were seen at peak potentials of +0.55 V, +0.54 V, 0.56 V and +0.62 V (vs. SCE), on the graphite/dioctyl phthalate, graphite/mineral oil, nanocarbon/mineral oil and nanocarbon/dioctyl phthalate pastes respectively (Fig. 7.18).

The results obtained with the 40 μM phenol solutions, on the graphite/dioctyl phthalate paste, are shown in Fig. 7.19. As in the case of 4-phenoxyphenol, the peak currents were again seen to increase with increasing pre-concentration time, though this time the plateau was reached after ca. 90 s. Higher currents were also again seen with

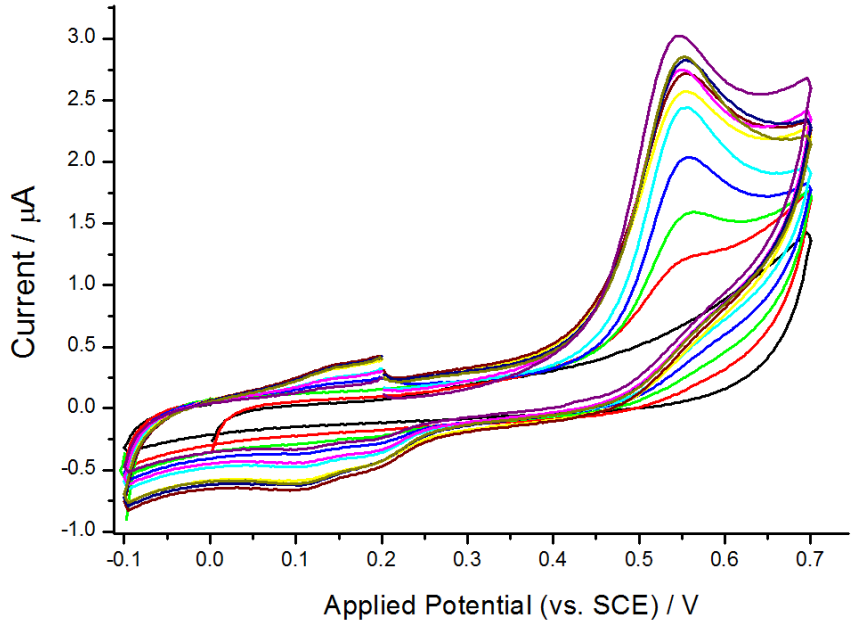

Figure 7.19: 100 mV s^{-1} cyclic voltammetric responses for the oxidation of phenol on the graphite/dioctyl phthalate paste, obtained at 298 K in a deoxygenated borate buffer solution, containing 0.1 M KCl, after pre-concentration from an identical solution that also contained 40 μM phenol for increasing pre-concentration times between 0 s and 240 s.

the graphite/dioctyl phthalate paste and the four pastes were again equilibrated with the analyte at similar equilibration times, here of ca. 90 s (Fig. 7.20). These results were

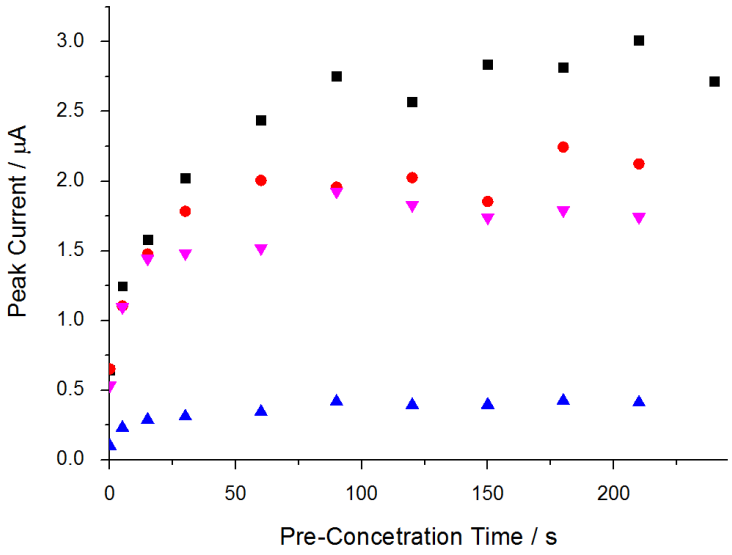

Figure 7.20: The variation of the peak current of the responses on each CPE with pre-concentration time (black: graphite/dioctyl phthalate, red: graphite/ mineral oil, blue: nanocarbon/mineral oil, magenta: nanocarbon/dioctyl phthalate), after pre-concentration from a 40 μM phenol solution for 90 s.

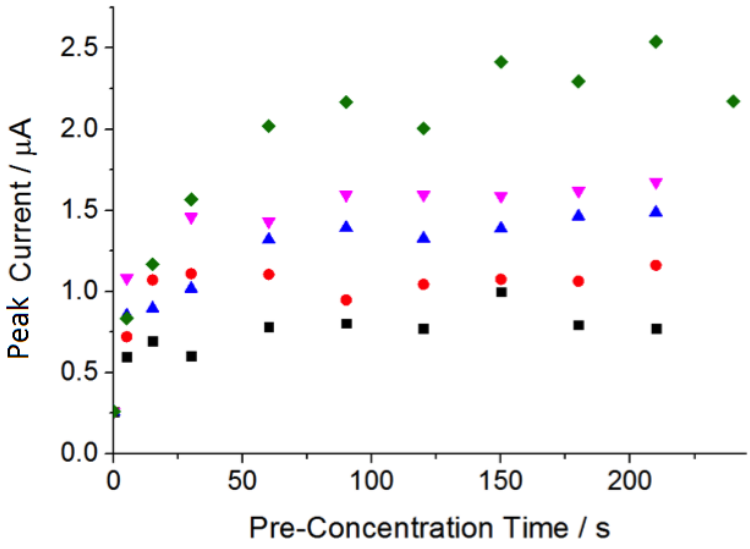

Figure 7.21: The variation of the peak current with pre-concentration time of the responses obtained after pre-concentration of the graphite/ dioctyl phthalate paste with phenol from source solutions of 7.0 μM (black), 9.5 μM (red), 13 μM (blue), 20 μM (magenta) and 40 μM (olive).

not only consistent with more and more phenol being accumulated in the paste and then oxidised, up to the point at which the paste was equilibrated with phenol, but also confirmed the choice of the graphite/dioctyl phthalate paste as the optimum paste with which to carry out analogous phenol pre-concentration experiments with phenol solutions of concentrations 7.0 - 20 μM (Fig. 7.21).

As expected, the peak current increased with increasing pre-concentration time, as illustrated in Fig. 7.21, where the plateau is seen to be reached at ca. 90 s, once the paste had been equilibrated with phenol. Again as anticipated, higher currents were observed when solutions of higher phenol concentrations were used as the source of phenol.

7.3.2.3 The Possible Variation of the Background Current with Immersion Time

Having studied the uptake of phenol and 4-phenoxyphenol on the four paste electrodes and chosen one substrate to focus on, a short investigation was done into the effect of the immersion time of the paste electrodes in a deoxygenated aqueous borate buffer solution of pH 10.01 that contained 0.1 M KCl as the supporting electrolyte. Such experiments were needed given the shape of the voltammograms in Figs. 7.6 - 7.9 and 7.19, where the diffusion tail of the measurements can be seen to change with increasing pre-concentration time with each analyte.

Each carbon paste electrode was thus left, under open circuit conditions, in a deoxygenated aqueous borate buffer solution of pH 10.01, which contained 0.1 M KCl as the supporting electrolyte, for increasing times, after which oxidative scans were run between -0.20 V and +0.60 V (vs. SCE). Typical scans obtained with the graphite/doctyl phthalate carbon paste electrode are shown in Fig. 7.22, where the background current

is seen to remain effectively constant throughout the experiment, leading to the conclusion that it was the organic analyte that was responsible for any changes previously observed. In light of this conclusion, the concentration of phenol, 4-phenoxyphenol and 4-methoxyphenol were next varied, fixing the pre-concentration times at the previously determined equilibration times.

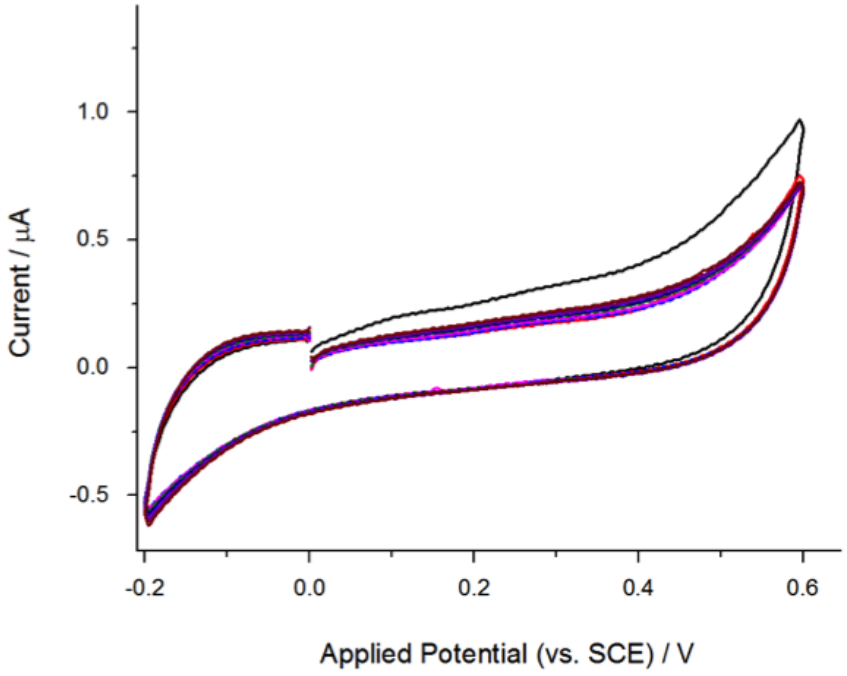

Figure 7.22: The variation of the capacitative current with increasing immersion time of the graphite/dioctly phthalate CPE in a deoxygenated borate buffer solution of pH 10.01 that contained 0.1 M KCl as the supporting electrolyte. Scans were obtained at 100 mV s^{-1} and 298 K.

7.3.3 Obtaining Analytical Limits of Detection for Phenol, 4-Phenoxyphenol and 4-Methoxyphenol

7.3.3.1 Testing the Selected Paste Over Wide a Phenol Concentration Range

Focussing on the optimum graphite/dioctyl phthalate paste electrode, the sensor was then tested with a wide concentration range of phenol. The aim was not only to obtain an

analytical limit of detection but to also investigate how high a phenol concentration could be detected through cyclic voltammetry, a task often limited in other electroanalyses due to rapid electrode surface fouling, especially with solid electrodes [33–35].

An analogous experiment as in Section 7.3.2.2 was thus carried out. The graphite/dioctyl phthalate paste electrode was immersed in a deoxygenated aqueous borate buffer solution of pH 10.01 that contained a known amount of phenol and 0.1 M KCl as the supporting electrolyte. This was again done under open circuit conditions, but this time the immersion time was fixed at 90 s, the previously identified equilibration time of this electrode with phenol, while the concentration of the source phenol solution was varied between 2.5 μM and 80 mM. Oxidative 100 mV s^{-1} scans were run in a deoxygenated aqueous borate buffer solution of pH 10.01, which contained 0.1 M KCl, in the potential range between -0.10 V and +0.70 V (vs. SCE); peaks due to the oxidation of phenol were seen at a peak potential of +0.52 V (vs. SCE).

The results are presented in Fig. 7.23, where the expected increase of the peak current with increasing phenol concentration is clearly seen up to phenol concentrations as high as 10 mM (Fig. 7.24); a plateau is reached when the phenol concentration is further increased. It was also observed that for the detection of concentrations lower than 7.0 μM the phenol solution had to be stirred and that, for up to 1.0 mM concentrations of phenol it was not necessary to refresh the paste before every scan to obtain reproducible results; renewing the surface only became important when larger phenol concentrations were used.

The above results are consistent with the paste being loaded with more and more phenol as the phenol concentration is increased and with phenol concentrations of or higher than 16 mM being large enough for their detection to be limited by the ability of

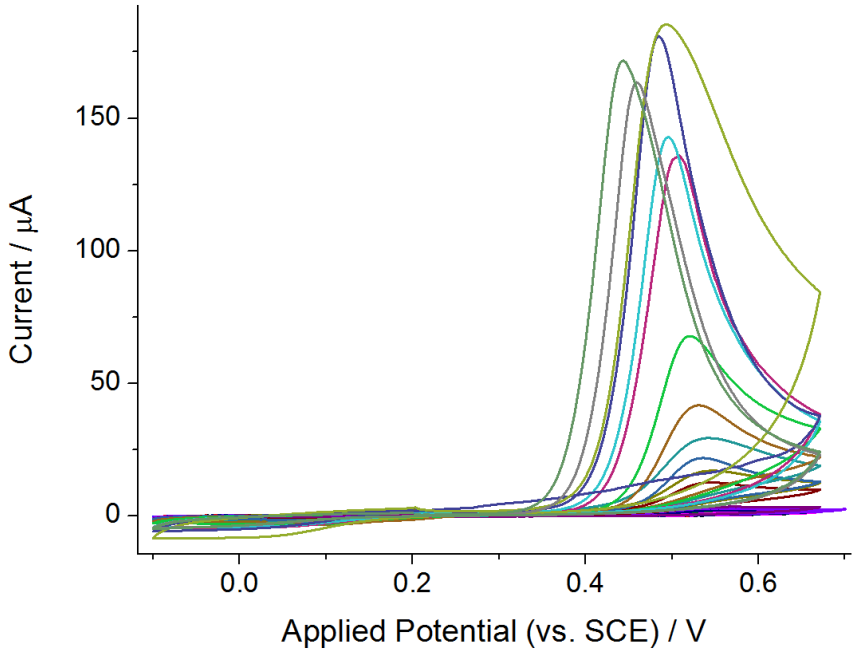

Figure 7.23: 100 mV s^{-1} cyclic voltammetric scans, obtained in a deoxygenated borate buffer solution, containing 0.1 M KCl, of pH = 10.01, after the graphite/dioctyl phthalate CPE had been immersed in identical solutions that also contained phenol at variable concentrations (2.5 μM to 80 mM) for 90 s.

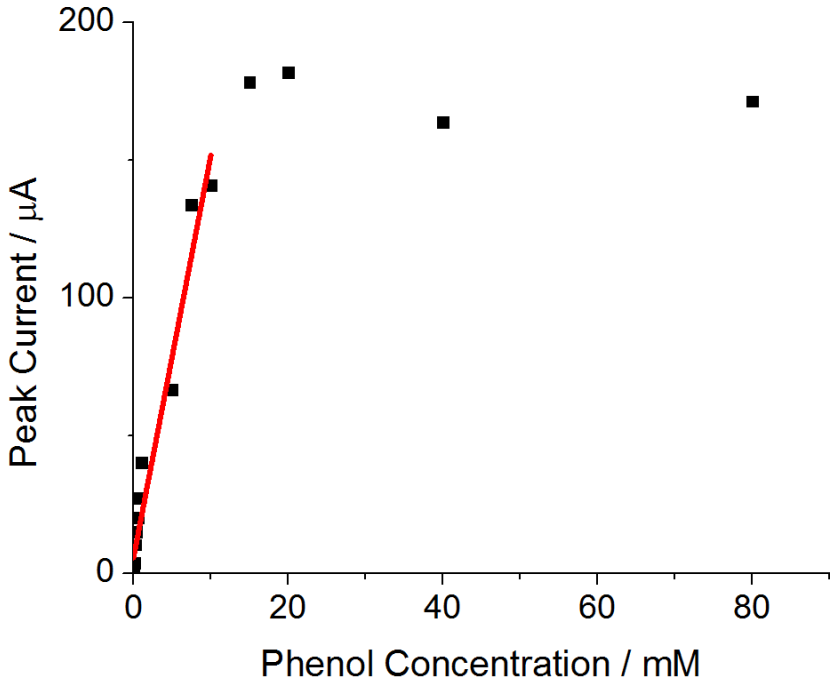

Figure 7.24: The increase of the peak current with increasing phenol concentration of the source solution.

the paste to "store" more of the analyte. A practical lower limit of detection of 2.5 μM that corresponds to phenol concentrations that can be practically detected was determined. Through the slope of the calibration curve the sensitivity of the sensor was also calculated as being 1.46 μA mM^{-1}. With regards to surface renewal, the observations indicate that the regularly observed problem of electrode surface fouling [33–35], known to increase

Theoretical LOD / μM	Method Used	Reference
0.006	ECD: Tyrosinase-Colloidal Au-Modified CPE	[27]
0.070	ECD: Tyrosinase-Au NP-Modified BDD Electrode	[41]
1.06	HPLC + ECD (Porous Graphite Electrodes)	[4]
1.10	ECD: MWCNT-DTDAB-Tyrosinase-Modified CPE	[6]
1.35	CLSM + ECD (Tyrosinase-MWCNTs-Modified Carbon SPEs)	[42]
2.00	IL film-Modified Pt wires	[43]
7.10	ECD: CPE Modified with pAP and MWCNTs	[5]
10.6	Capillary LC + ECD (GC Electrodes)	[44]
85	ECD: H_2 Plasma-pre-treated BDND Electrodes	[45]

Table 7.1: Literature values for phenol limits of detection. ECD: Electrochemical Detection, CPE: Carbon Paste Electrode, NP: Nanoparticle, BDD electrode: Boron Doped Diamond electrode, HPLC: High Performance Liquid Chromatography, MWCNT: Multi-Walled Carbon Nanotube, DTDAB: dimethylditetradecylammonium bromide, CLSM: Confocal Laser Scanning Microscopy, SPE: Screen Printed Electrode, IL: Ionic Liquid, pAP: p-Aminophenol, GO-Au-NP-tyrosinase: Graphene-Oxide-Gold-Nanoparticle film with immobilised tyrosinase, LC: Liquid Chromatography, BDND electrodes: Boron Doped Nanocrystalline Diamond electrodes.

with increasing phenol concentration [35] is not present for phenol concentrations of 1.0 mM or lower; this gives the developed sensor a great practical advantage.

Table 7.1 summarises the limits of detection for phenol found in literature [4, 5, 7, 27, 41–45]. As expected, when electrochemical methods are used to detect phenol, the electrodes are often modified; the most commonly chosen modifier is tyrosinase, due to the low limits of detection it can ensure. However, the reported values are theoretical limits of detection calculated from high concentration data that typically correspond to concentrations where signals cannot be seen. It is in this context that the practical limit of detection of 2.5 μM here obtained is very important, as it represents an observed signal.

7.3.3.2 Obtaining an Analytical Limit of Detection for 4-Phenoxyphenol and 4-Methoxyphenol

Analytical limits of detection were also obtained for the previously investigated 4-phenoxyphenol as well as for 4-methoxyphenol. The best suited paste electrode - graphite/dioctyl phthalate - acted as the working electrode. In the case of 4-phenoxyphenol, the previously determined 60 s equilibration time was used. The electrode was immersed in a deoxygenated aqueous borate buffer solution of pH 10.01 that contained a known amount of the target and 0.1 M KCl as the supporting electrolyte. Oxidative 100 mV s^{-1} scans were then carried out a in a deoxygenated aqueous borate buffer solution of pH 10.01, which contained 0.1 M KCl, in the potential range between 0.0 V and + 0.60 V (vs. SCE). A signal corresponding to the oxidation of 4-phenoxyphenol to benzoquinone was seen at a peak potential of +0.43 V (vs. SCE). This experiment was carried out with 4-phenoxyphenol solutions of concentrations of 2.5 to 40 μM.

In the case of 4-methoxyphenol, it was assumed that its behaviour would be similar

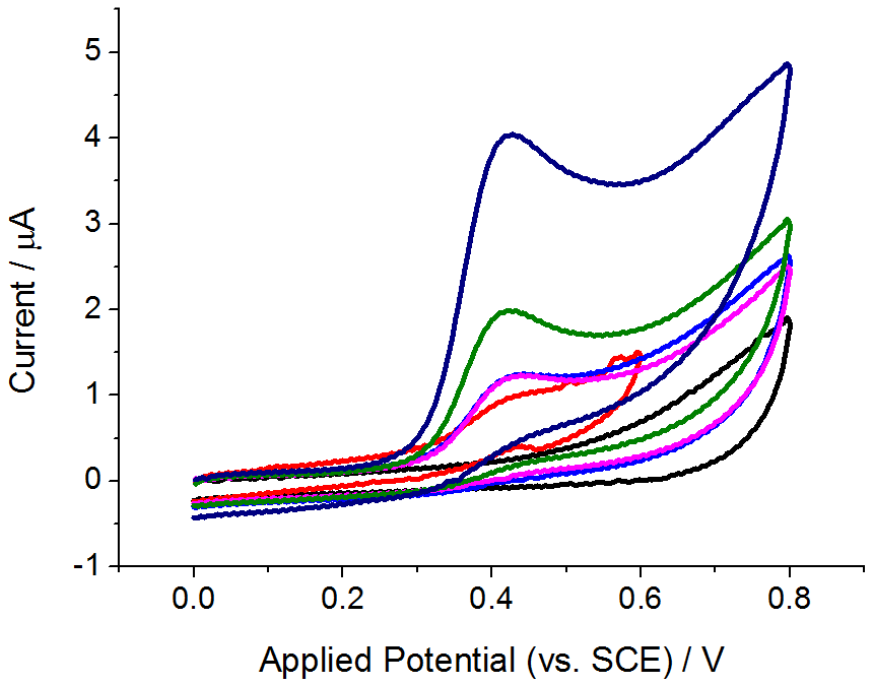

Figure 7.25: 100 mV s^{-1} cyclic voltammetric scans, obtained in a deoxygenated borate buffer solution, containing 0.1 M KCl, of pH = 10.01, after the graphite/dioctyl phthalate CPE had been immersed in identical solutions that also contained 4-phenoxyphenol at variable concentrations (2.5 to 40 μM) for 60 s.

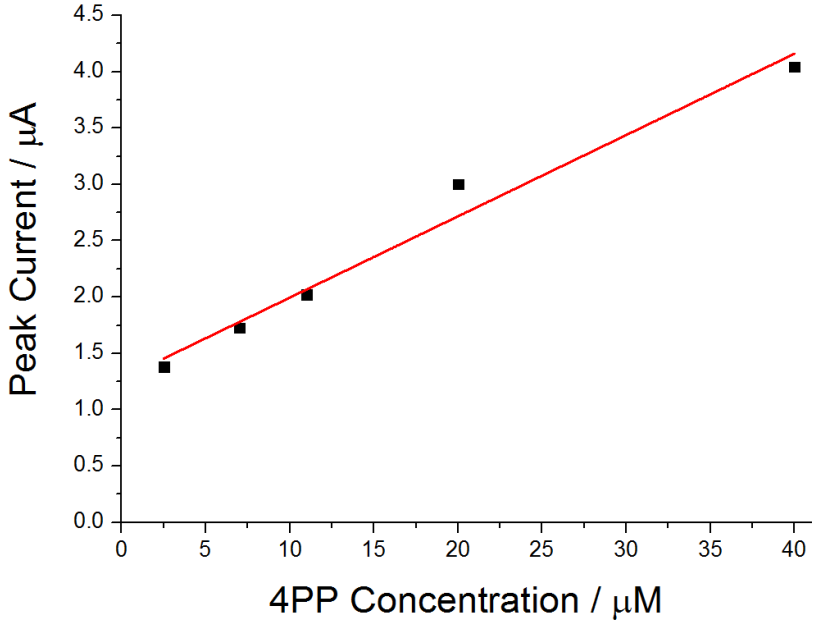

Figure 7.26: The increase of the peak current with increasing 4-phenoxyphenol concentration of the source solution.

to phenol and 4-phenoxyphenol and that the longer 90 s equilibration time determined for phenol could hence be used. The electrode was immersed in a deoxygenated aqueous borate buffer solution of pH 10.01 that contained a known amount of 4-methoxyphenol and 0.1 M KCl as the supporting electrolyte. It was then transferred into a deoxygenated aqueous borate buffer solution of pH 10.01, which only contained 0.1 M KCl, in which 100 mV s^{-1} oxidative scans were run, between -0.30 V and +0.50 V (vs. SCE). The peak due to the oxidation of 4-methoxyphenol to benzoquinone was observed at a peak potential of +0.30 V (vs. SCE). Here the target concentration was varied between 5.0 and 40 μM.

Starting from 4-phenoxyphenol, Fig. 7.25 shows the obtained results; as expected, the signal increased with increasing target concentration (Fig. 7.26). Similarly for 4-methoxyphenol, the results are presented in Fig. 7.27, with the expected dependency of the peak height on concentration being shown in Fig. 7.28. The analytical lower limits

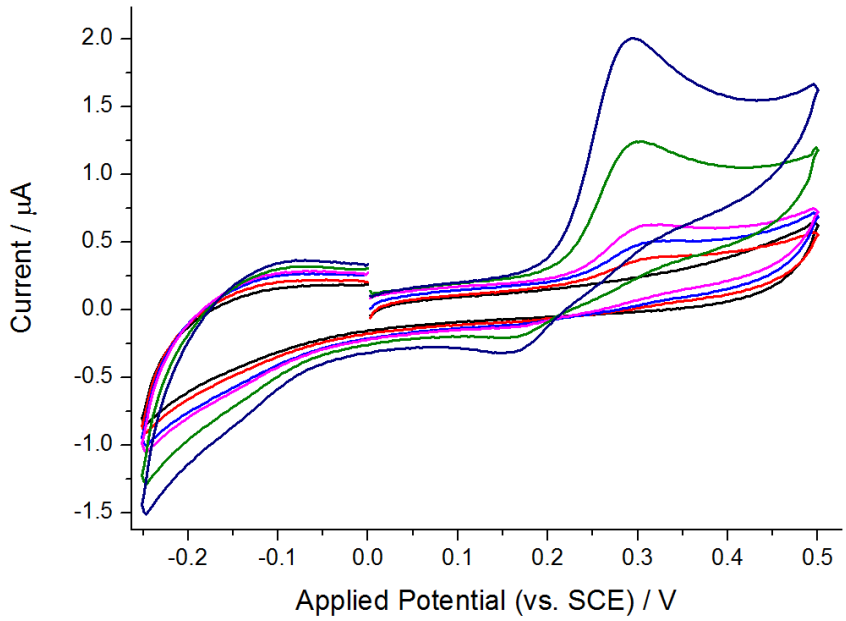

Figure 7.27: 100 mV s^{-1} cyclic voltammetric scans, obtained in a deoxygenated borate buffer solution, containing 0.1 M KCl, of pH = 10.01, after the graphite/dioctyl phthalate CPE had been immersed in identical solutions that also contained 4-methoxyphenol at variable concentrations (5.0 to 40 μM) for 90 s.

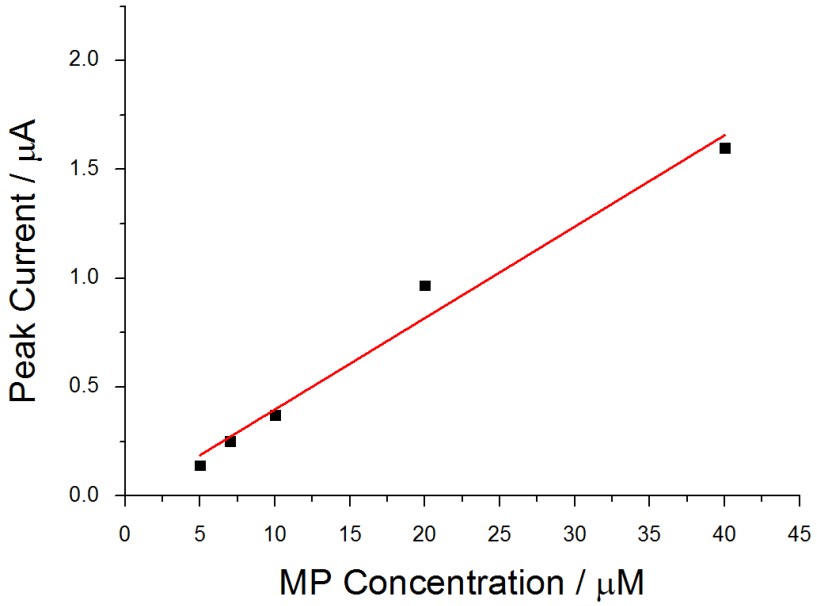

Figure 7.28: The increase of the peak current with increasing 4-methoxyphenol concentration of the source solution.

of detection were thus determined as being 2.5 μM and 5.0 μM for 4-phenoxyphenol and 4-methoxyphenol respectively. Values for the sensitivity were also extracted from the obtained calibration curves; these were 72.1 nA μM^{-1} and 42.0 $\mu M^{-1}1$ for 4-phenoxyphenol and 4-methoxyphenol respectively.

7.3.4 Using Square Wave Voltammetry for the Simultaneous Detection of Phenol, 4-Phenoxyphenol and 4-Methoxyphenol

To address the simultaneous detection of the three phenols, one further experiment was carried out in which a borate buffer solution of pH 10.01 was made that contained the three compounds (110 μM phenol, 110 μM 4-phenoxyphenol and 150 μM 4-methoxyphenol) as well as 0.1 M KCl. This was, as previously, deoxygenated and used to equilibrate the graphite/dioctyl phthalate paste with the three targets; an equilibration time of 90 s

was used. The electrode was then transferred into a deoxygenated borate buffer solution of the same pH that only contained supporting electrolyte (0.1 M KCl) and in which square wave voltammetric responses were obtained. Firstly, the square wave parameters were optimised. The frequency, as well as the step potential, were altered to achieve the highest peak current, while the amplitude was varied to achieve as best a peak separation as possible. The optimum values for each parameter were determined as being 100 Hz for the frequency, 25 mV for the amplitude and 1 mV for the step potential.

The square wave voltammogram that was recorded using the optimised parameters is shown in Fig. 7.29, where three peaks corresponding to the oxidation of 4-methoxyphenol, 4-phenoxyphenol and phenol can be seen at peak potentials of +0.28 V, +0.38 V and

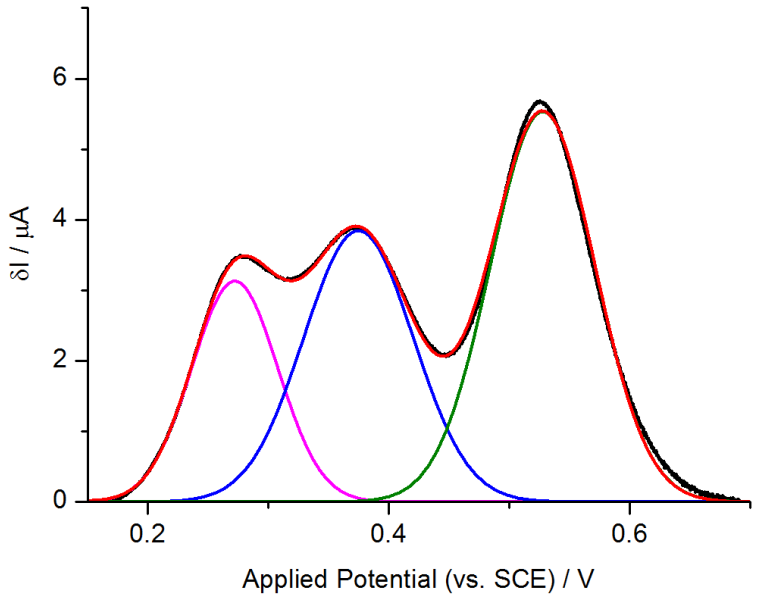

Figure 7.29: Baseline corrected square wave voltammograms (frequency: 100 Hz, amplitude: 25 mV, step potential: 1 mV) for the oxidation of 4-phenoxyphenol and phenol, seen at +0.28 V, +0.38 V and +0.53 V (vs. SCE) respectively, on the graphite/dioctyl phthalate paste electrode (black: experimental data, red: sum of the three Gaussian functions, olive, blue and magenta: the deconvoluted curves).Scans were obtained at 298 K in a deoxygenated borate buffer solution, containing 0.1 M KCl, of pH = 10.01, after the CPE had been immersed in an identical solution that also contained 110 μM phenol, 110 μM 4-phenoxyphenol and 150 μM 4-methoxyphenol for 90 s.

+0.53 V (vs. SCE), respectively, and where δI stands for the current difference between the forward and reverse scan. Even though the peak due to the oxidation of phenol is more clearly separated from the other two, there is some overlap with 4-phenoxyphenol response. At the same time, the responses of 4-phenoxyphenol and 4-methoxyphenol overlap greatly. Deconvolution of the square wave voltammograms was thus required, in order to be able to quantify the amount of each phenol. This was done using the Peak Analyser Function of OriginPro 9, where the voltammogram was modelled as a sum of three Gaussian functions. The sum of the Gaussian functions and the three deconvoluted curves are overlaid with the experimental data in Fig. 7.29.

7.3.5 Conclusions

A sensitive method, able to measure high target concentrations, for the separate and simultaneous detection of phenol, 4-phenoxyphenol and 4-methoxyphenol has been developed. The procedure relies on the use of an optimum carbon paste electrode, made of graphite powder and dioctyl phthalate. Immersion of the paste electrode to each aqueous phenol solution, for the determined equilibration times, allows the target compound to transfer from the source solution into the paste and the equilibration of the paste with the analyte. The oxidation signal of each phenol is used as the detection signal; the peak potentials were +0.60, +0.40 and +0.30 V (vs. SCE) for phenol, 4-phenoxyphenol and 4-methoxyphenol, respectively. We label the new approach "absorptive stripping voltammetry".

By carrying out pre-concentration experiments and fingerprinting the reduction of benzoquinone and orthoquinone, it was concluded that 4-phenoxyphenol undergoes a 2-electron 2-proton reduction to form benzoquinone. The oxidation of phenol was found

to result in the likely formation of polymeric products and not the monomers of oxidised catechol or 1,4-dihydroxybenzene.

Through calibration of the sensor in 2.5 μM to 80 mM phenol solutions, 2.5 - 40 μM 4-phenoxyphenol solutions and 5.0 - 40 μM 4-methoxyphenol solutions, analytical lower limits of detection (LODs) of 2.5 μM, 2.5 μM and 5.0 μM were obtained for phenol, 4-phenoxyphenol and 4-methoxyphenol respectively. As Table 7.1 clearly demonstrates, the practical limit of detection of 2.5 μM, here measured from an observed signal, is close to values found in the literature, with tyrosinase-based biosensors seemingly being able to detect even lower phenol concentrations. However, the values in Table 7.1 correspond to theoretical limits of detection that are calculated, usually by extrapolating the calibration curve and using the equation $LOD = \frac{3\sigma}{s}$, where σ is the measured standard deviation of the signal in the absence of the target and s is the sensitivity of the sensor [46]; the practical (measured) limit of detection of phenol of our new sensor is thus usefully low. Importantly, it was possible to determine phenol concentrations of up to 1.0 mM, without the measurements being compromised through electrode surface fouling, and concentrations of up to 10 mM, without being limited by the uptake of the analyte.

Square wave voltammetry enabled the study of systems containing all three phenol compounds. Through modelling of the experimental data as a sum of three Gaussian functions that can then be deconvoluted, simultaneous quantification of the three targets can be achieved.

This is the first time that such low phenol, 4-phenoxyphenol and 4-methoxyphenol concentrations have been detected using an unmodified surface. It is the sensitivity of this method, provided by absorptive pre-concentration, that leads to the term “absorptive stripping voltammetry”, by analogy to “adsorptive stripping voltammetry”. This work

opens up further studies into possible ways of exploiting carbon paste electrodes [47].

7.4 Absorptive Stripping Voltammetry Applied to Cannabis Detection

Building on the work reported in Section 7.3, the application of absorptive stripping voltammetry to the detection of low THC concentrations, in both aqueous solutions and in synthetic saliva is here discussed, with the aim of further illustrating the value of this approach, as well as its practical applicability. Following the same strategy, an optimum carbon paste electrode - fabricated by mixing graphite powder with mineral oil - is selected for the pre-concentration of the target; in light of the results obtained above, a pre-concentration time of three minutes was deemed adequate to equilibrate the paste with THC. Practically useful limits of detection were thus achieved, with the oxidation signal of THC, observed at peak potentials of ca. +0.35 V (vs. SCE), being used as the detection signal.

7.4.1 Selecting a Carbon Paste

The electrochemical oxidation of THC was first investigated using square wave voltammetry. Two carbon paste electrodes, fabricated by mixing graphite powder with dioctyl phthalate or mineral oil as described in Section 3.3, were used aiming to select the carbon paste electrode that would ensure the highest THC uptake.

Each carbon paste electrode was immersed for three minutes, under open circuit conditions, in a deoxygenated aqueous borate buffer solution of pH 10.0 that contained 7.0 - 80 μM THC and 0.1 M KCl as the supporting electrolyte. Each paste electrode was then

transferred to a deoxygenated aqueous borate buffer solution of pH 10.0, which only

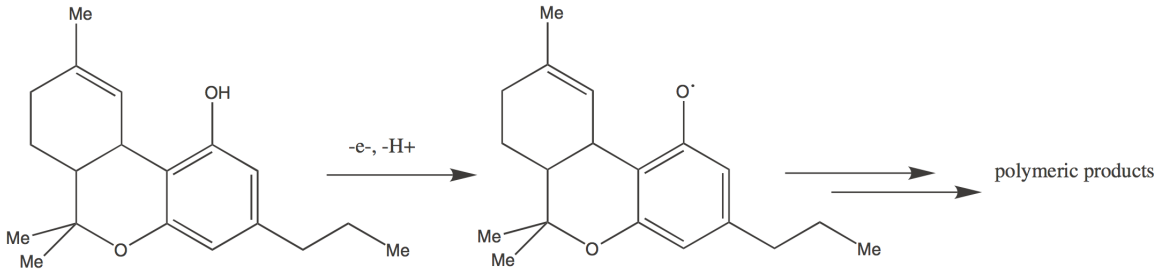

Figure 7.30: The oxidation of Δ^9-tetrahydrocannabinol (THC). THC, under oxidation, behaves as a typical phenol. [34, 48–50].

contained 0.1 M KCl. Oxidative square wave voltammetric scans were then run, between +0.25 V and + 0.52 V (vs. SCE) for the graphite/dioctyl phthalate paste electrode and between +0.20 V and +0.60 V (vs. SCE) in the case of the graphite/mineral oil paste electrode. The frequency and step potential used were 100 Hz and 1 mV, respectively, while the amplitude was set to 40 mV. Peaks due to the oxidation of THC, as shown in Fig. 7.30 [34, 48–50], were seen at peak potentials of +0.39 V and +0.37 V (vs. SCE) on the graphite/dioctyl phthalate and the graphite/mineral oil pastes respectively; typical responses are depicted in Fig. 7.31. Fig. 7.30 assumes that, under oxidation, THC behaves like a typical phenol [34]; to the best of the author's knowledge there is no literature reporting identification of further THC oxidation products.

As can be seen in Fig. 7.31 and 7.32, the peak current observed with the graphite/mineral oil paste was higher than that observed with the graphite/dioctyl phthalate paste, this reflecting the greater ability of mineral oil to accumulate THC. As depicted in Fig. 7.32, the current also increased with increasing analyte concentration, reflecting the increasing amount of THC transferring into the paste. Only the graphite/mineral oil paste electrode was used for further experiments to achieve a lower THC limit of detection.

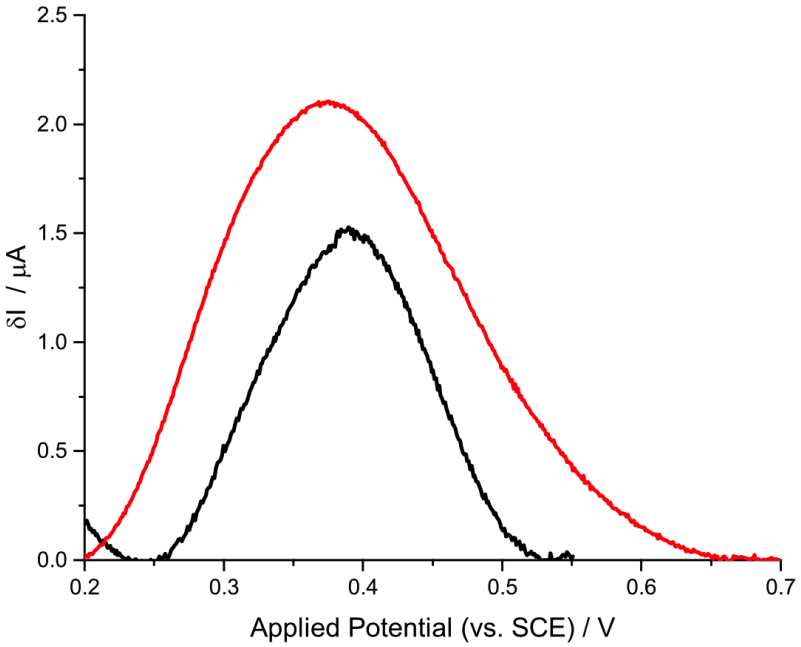

Figure 7.31: Square wave voltammograms (frequency: 100 Hz, amplitude: 40 mV, step potential: 1 mV) for the oxidation of THC on the graphite/dioctyl phthalate paste electrode (black line) and the graphite/mineral oil paste electrode (red line). Scans were obtained at 298 K in a deoxygenated borate buffer solution, containing 0.1 M KCl, of pH = 10.01, after each CPE had been immersed in an identical solution that also contained 80 μM THC for 180 s.

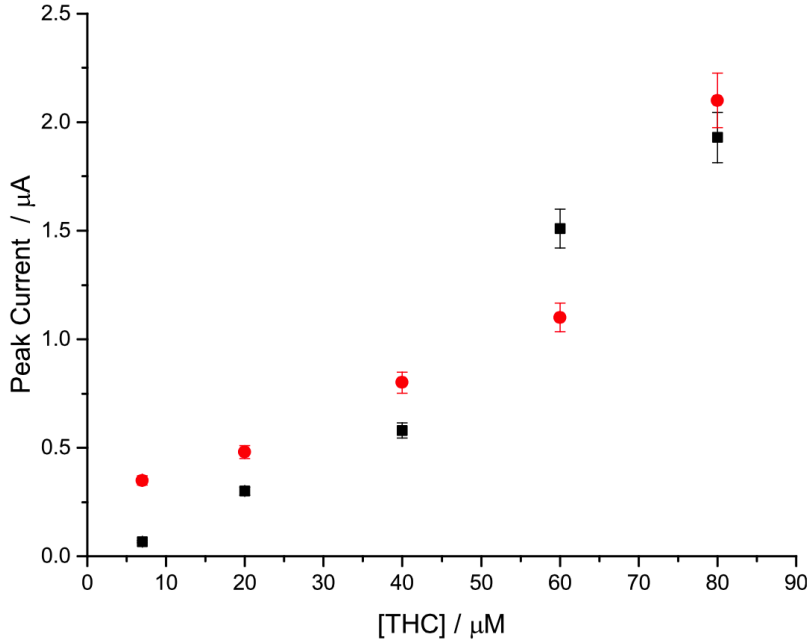

Figure 7.32: Comparison of the peak currents obtained with the two carbon paste electrodes (black squares: graphite/dioctyl phthalate paste, red circles: graphite/mineral oil paste).

7.4.2 Obtaining Analytical Limits of Detection for THC

7.4.2.1 Detecting THC in a Stationary vs. a Stirred Aqueous Solution

Focussing on lower THC concentrations, the graphite/mineral oil paste was tested in aqueous THC solutions of concentrations of 0.50 - 16 μM. Analogous experiments as in the Section above were thus carried out, where the pre-concentration time was increased to five minutes and where the amount of mineral oil used was doubled; the amount of graphite powder was kept constant. This was done to improve the uptake of THC and hence the sensitivity of the sensor.

The graphite/mineral oil carbon paste electrode was immersed in a stationary deoxygenated aqueous borate buffer solution of pH 10.0 that contained a known amount of THC

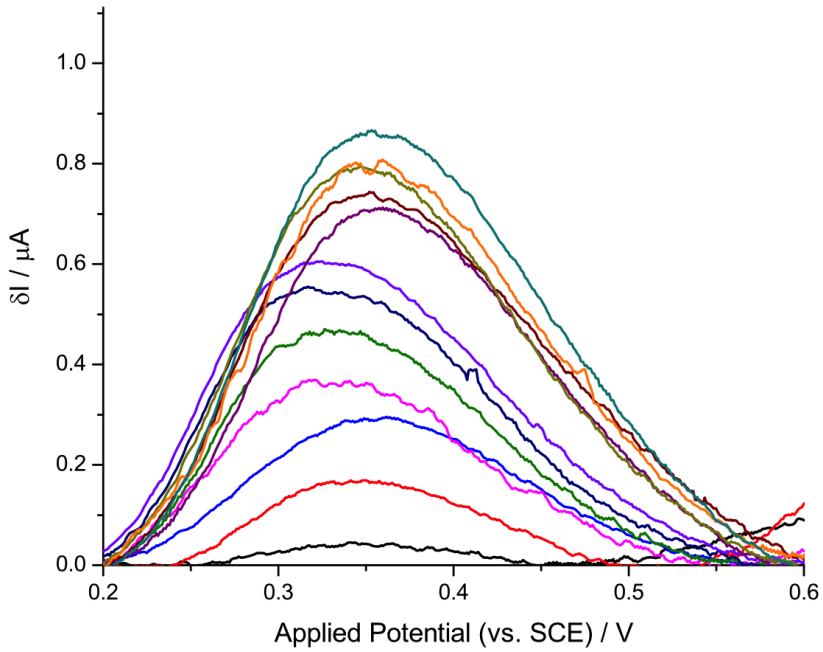

Figure 7.33: Square wave voltammograms (frequency: 100 Hz, amplitude: 40 mV, step potential: 1 mV) for the oxidation of THC on the graphite/mineral oil paste electrode. Scans were obtained at 298 K in a deoxygenated borate buffer solution, containing 0.1 M KCl, of pH = 10.01, after pre-concentrating the paste from an identical stationary solution that also contained THC (0.50 - 16 μM) for 300 s.

(between 0.50 and 16 μM) and 0.1 M KCl as the supporting electrolyte. This was again done under open circuit conditions. Oxidative square wave voltammetric scans were then run in a deoxygenated aqueous borate buffer solution of pH 10.0, which only contained 0.1 M KCl, in the same potential range (between +0.20 V and +0.60 V [vs. SCE]) and using the same values of 100 Hz, 1 mV and 40 mV for the frequency, step potential and amplitude, respectively, as in the Section above. The same procedure was then repeated, stirring the source THC solutions to lower the limit of detection of the sensor.

The results obtained from the stationary THC solution are presented in Fig. 7.33, where peaks corresponding to the oxidation of THC, as in Fig. 7.30, can be observed at a peak potential of ca. +0.35 V (vs. SCE). As can be seen in Fig. 7.34, the peak current shows a linear increase with increasing THC concentration up to THC concentrations of 5.0 μM; the peak height then levels off and a plateau is reached when the THC concen-

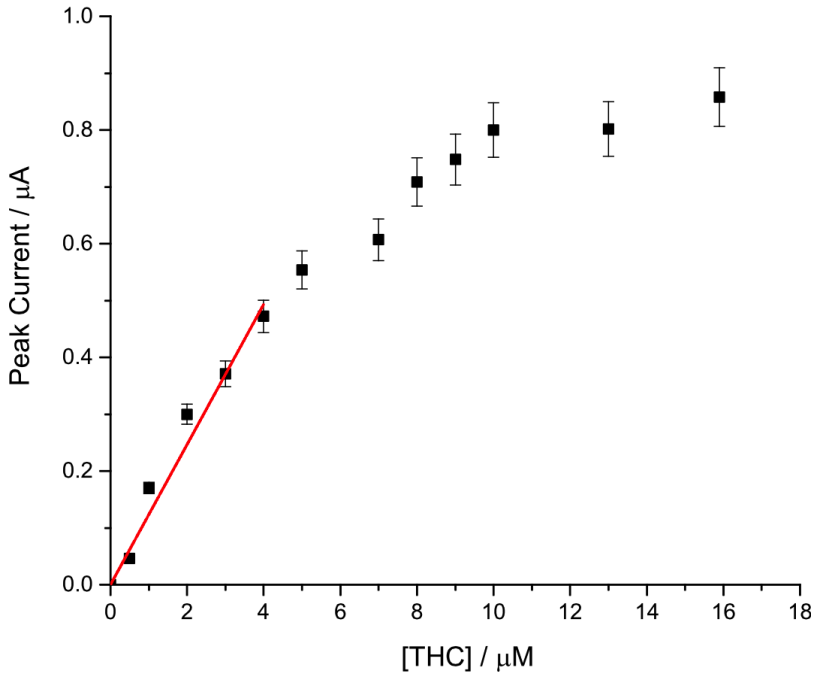

Figure 7.34: The increase of the peak current with increasing THC concentration of the stationary borate buffer source solution (black squares), with the correlation line through the linear range (red line, R2 = 0.95).

tration is further increased. Similarly, the results obtained from the stirred THC solution can be seen in Fig. 7.35, where the THC oxidation peak is seen at a peak potential of +0.37 V (vs. SCE). As previously, the peak current increases as the concentration of THC is increased, this time reaching a plateau at 4.0 μM (Fig. 7.36). The errors in the calibration curves relate to separate electrode preparations.

The above results are consistent with the fact that, as more THC is present in the source solution, more THC will accumulate into the paste, resulting in higher peak currents being observed. The fact that a plateau is reached indicates that, at some point, the paste is equilibrated with the analyte and thus no more THC can transfer into the binder. Comparing the THC concentration at which the plateau is reached under sta-

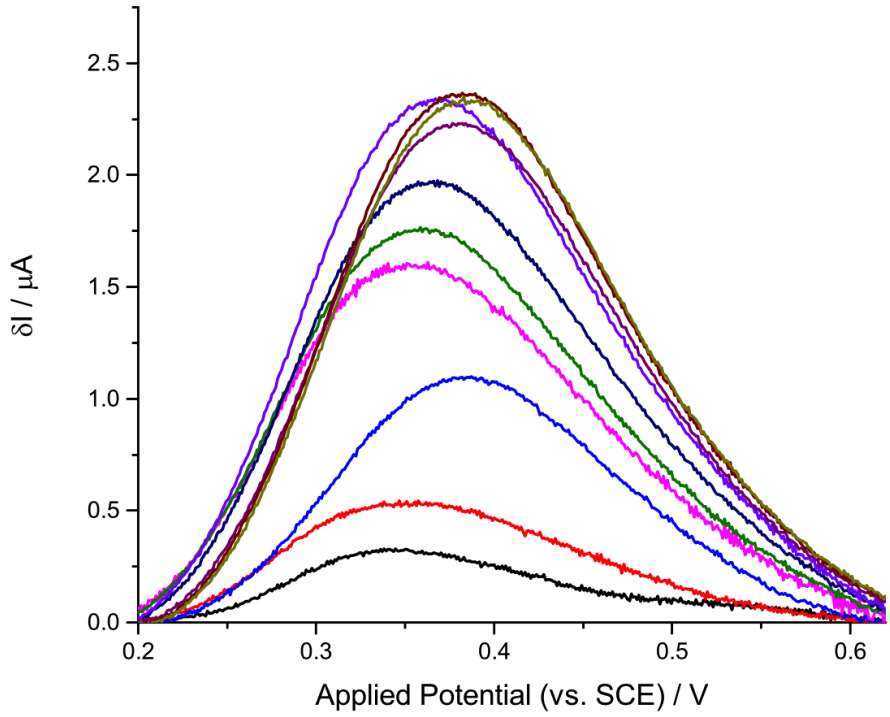

Figure 7.35: Square wave voltammograms (frequency: 100 Hz, amplitude: 40 mV, step potential: 1 mV) for the oxidation of THC on the graphite/mineral oil paste electrode. Scans were obtained at 298 K in a deoxygenated borate buffer solution, containing 0.1 M KCl, of pH = 10.01, after pre-concentrating the paste from an identical stirred solution that also contained THC (0.10 - 10 μM) for 300 s.

tionary vs. stirred conditions, the reason it is reached at lower THC concentrations when the solution is stirred is because the stirring replenishes the material that is depleted near the electrode surface, as the analyte transfers into the paste. This leads to more material accumulating into the paste at a given concentration.

Under stationary conditions, THC concentrations as low as 0.50 μM could be practically detected, while stirring the solution lowered the practical limit of detection to 0.10 μM; again this is due to the fact that stirring results in more material being present near the electrode surface and hence available to accumulate into the carbon paste. Theoretical limits of detection (LODs) were calculated by extrapolating the calibration curve and using the same equation as in Section 7.3: $LOD = \frac{3\sigma}{s}$ [46], where all the terms have been previously defined. These LOD values were determined as being 0.48 nM and 0.41 nM for the stationary and stirred THC aqueous buffer solutions respectively. Limits of

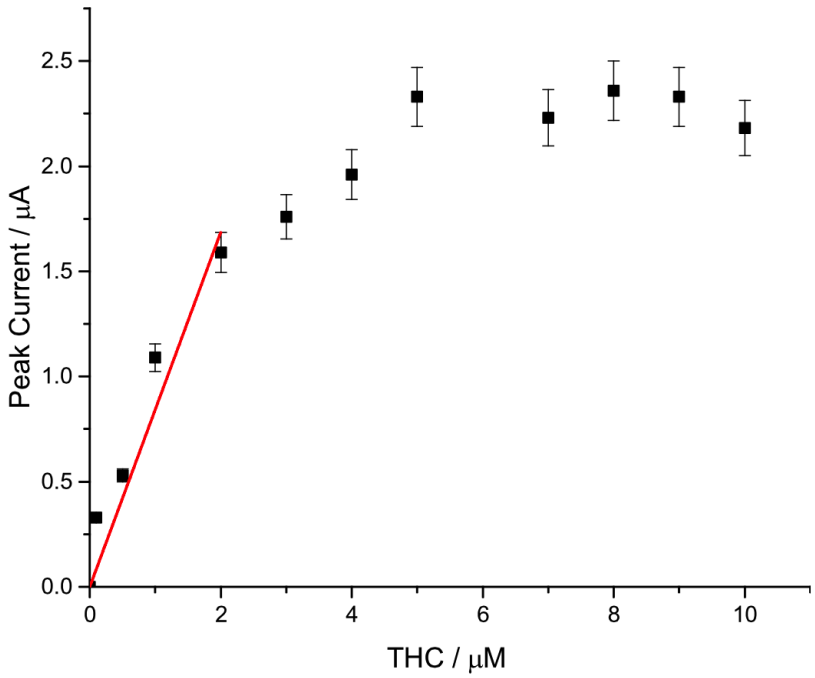

Figure 7.36: The increase of the peak current with increasing THC concentration of the stirred borate buffer source solution (black squares), with the correlation line through the linear range (red line, R2 = 0.96).

quantification (LOQ) were also calculated by again extrapolating the calibration curve but using the equation $LOQ = \frac{10\sigma}{s}$ [46], where the variables are the same as in the LOD equation. The calculated values were 1.61 nM and 1.38 nM for the stationary and stirred THC aqueous buffer solutions respectively. Lastly, the slope of each calibration curve gave values for the sensitivity of the sensor of 0.12 μA μM^{-1} and 0.84 μA μM^{-1} for the stationary and stirred THC aqueous buffer solutions respectively.

7.4.2.2 Detecting THC in a Stationary Synthetic Saliva Solution

Focussing on the same THC concentration range as above, the graphite/mineral oil paste was tested in THC synthetic saliva solutions of concentrations of 0.50 - 16 μM. The same conditions and carbon paste electrode as in the Section 7.4.2.1 were used.

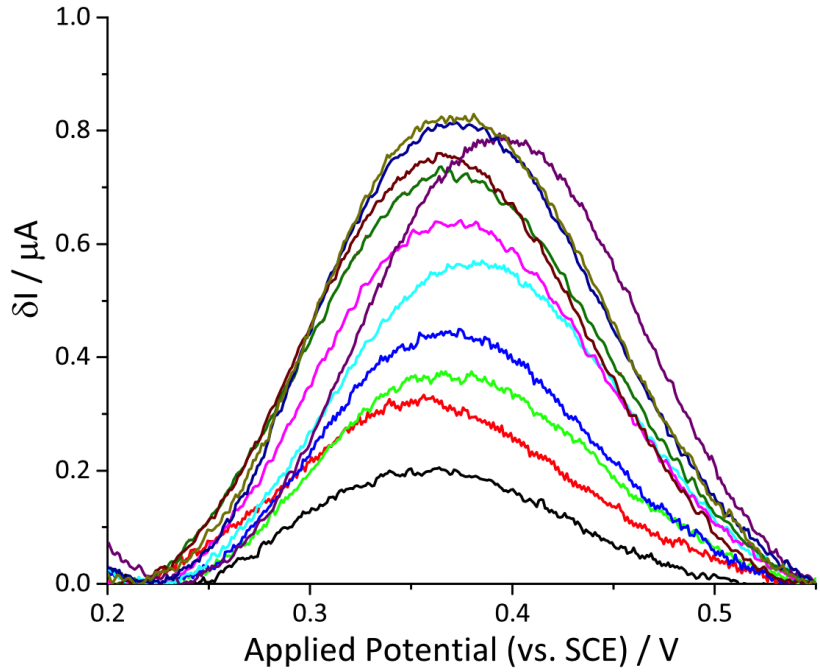

Figure 7.37: Square wave voltammograms (frequency: 100 Hz, amplitude: 40 mV, step potential: 1 mV) for the oxidation of THC on the graphite/mineral oil paste electrode. Scans were obtained at 298 K in a deoxygenated borate buffer solution, containing 0.1 M KCl, of pH = 10.01, after pre-concentrating the paste from an identical stationary synthetic saliva solution that also contained THC (0.50 - 16 μM) for 300 s.

The graphite/mineral oil carbon paste electrode was therefore immersed in a stationary deoxygenated synthetic saliva/borate buffer solutions of pH = 10.0 that contained a known amount of THC (between 0.50 and 16 μM) and 0.1 M KCl as the supporting electrolyte. This was again done under open circuit conditions, using the same fixed five minute pre-concentration time. Oxidative square wave voltammetric scans were then run in a deoxygenated aqueous borate buffer solution of pH 10.0, which only contained 0.1 M KCl, in the same potential range (between +0.20 V and +0.60 V [vs. SCE]) and using the same values of 100 Hz, 1 mV and 40 mV for the frequency, step potential and amplitude, respectively, as in Section 7.4.2.1 above.

The results obtained from the stationary THC solution are presented in Fig. 17.37, where peaks corresponding to the oxidation of THC, as in Fig. 7.30, can be observed at a peak potential of +0.37 V (vs. SCE). As can be seen in Fig. 7.38, the peak current

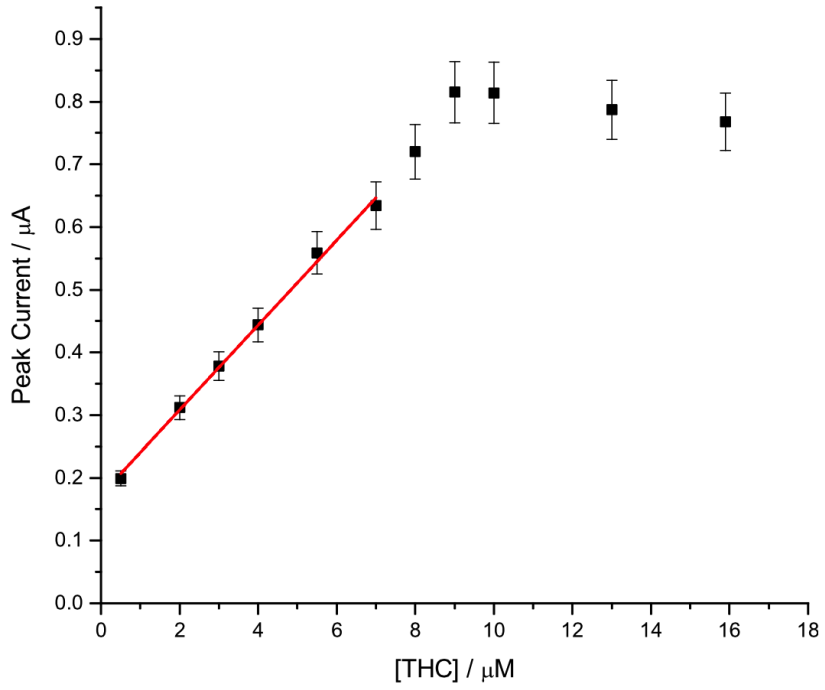

Figure 7.38: The increase of the peak current with increasing THC concentration of the source solution (black squares), with the correlation line through the linear range (red line, R2 = 0.99).

shows a linear increase with increasing THC concentration up to THC concentrations of 7.0 μM; a plateau is reached when the THC concentration is further increased. The errors in the calibration curves relate to separate electrode preparations.

The peak current increase was expected since more and more THC will accumulate into the paste if a higher amount of THC is present in the source solution. Again as expected, the uptake is at some point limited by the paste, this resulting in the observed plateau. THC concentrations as low as 0.50 μM could be practically detected while the slope of the calibration curve gave a value of 0.067 μA μM^{-1} for the sensitivity of the sensor. Theoretical LODs and LOQs were not here calculated as the linear range was between 0.5 and 7.0 μM.

Table 7.2 summarises the theoretical limits of detection for THC found in literature [22–24, 40, 50–52]. As expected, given the need for sensitive detection, sensitive methodologies do exist, with limits of detection of as low as 3.2 nM having been reported [49]. However, the LOD values for stirred and unstirred buffered matrices here calculated are much lower than those tabulated. It is worth highlighting that the low practical limits of detection here determined represent an observable signal.

7.4.3 Conclusions

"Absorptive stripping voltammetry" has been applied to the detection of THC in water and saliva. An optimised carbon paste, made of graphite powder and mineral oil, was exploited in the accumulation of THC, under open circuit conditions and using a five minute pre-concentration time.

By testing the sensor in water and synthetic saliva samples of known THC concentrations, analytical practical lower limits of detection (LODs) of 0.50 μM and 0.10 μM were

obtained for THC in stationary and stirred aqueous borate buffer solutions, respectively, and 0.50 μM for THC in stationary synthetic saliva solutions. Theoretical LOD values of 0.48 nM and 0.41 nM were also calculated for the stationary and stirred buffer systems respectively. As Table 7.4.2.2 clearly demonstrates, the theoretical limits of detection here determined are much lower than those reported in the literature. Importantly, the practical limit of detection of 0.50 μM determined in synthetic saliva, and which corresponds to an observed signal, is comparable to theoretical literature values, usually calculated. The limit of detection of 0.50 μM is also practically useful in terms of road side detection, this also clearly illustrating the value of absorptive stripping voltammetry. This work opens up further studies into different ways of taking advantage of the properties of carbon paste electrodes [47].

Reported LODs / nM	Sample	Method	Reference
3.2	oral samples	LC-MS	[49]
3.2	saliva	HPLC-ED	[22]
4.7	brain tissue	HPLC-ED	[50]
47	urine	GC	[51]
120	hair	HPLC/ED	[52]
1 x 10^3	saliva	ED	[23]
25 x 10^{3}	BBS	ED	[24]

Table 7.2: Literature values for THC and THC-COOH [28] limits of detection. LC: Liquid Chromatography, MS: Mass Spectrometry, HPLC: High Performance Liquid Chromatography, ED: Electrochemical Detection, GC: Gas Chromatography.

7.5 Overall Conclusions

It has been shown that the novel approach - absorptive stripping voltammetry - presented and discussed in this chapter allows very versatile sensing methodologies to be developed. Not only can usefully low analyte concentrations be detected, but higher concentrations that previously developed methods would have inherently been unable to assess can be determined. Through the application of absorptive stripping voltammetry to the detection of the above phenolic species, the value of carbon paste electrodes in electroanalysis has been illustrated.

References

[1] Nissim, R.; Compton, R. G. *Analyst* **2014**, *139*, 5911.

[2] Nissim, R.; Compton, R. G. *Chemistry Central Journal* **2015**, *9*, 41.

[3] Mohammadi, S.; Kargari, A.; Sanaeepur, H.; Abbassian, K.; Najafi, A.; Mofarrah, E. *Desalination and Water Treatment* **2015**, *53*, 2215.

[4] Achilli, G.; Cellerino, G. P. *Journal of Chromatography A* **1995**, *697*, 357–362.

[5] Ensafi, A. a.; Heydari-Bafrooei, E.; Rezaei, B. *Chinese Journal of Catalysis* **2013**, *34*, 1768–1775.

[6] Hashemnia, S.; Khayatzadeh, S.; Hashemnia, M. *Journal of Solid State Electrochemistry* **2012**, *16*, 473–479.

[7] Ramaekers, J. G.; Berghaus, G.; van Laar, M.; Drummer, O. H. *Alcohol and Drug Addiction* **2014**, *73*, 109.

[8] Pertwee, R. G. *British Journal of Pharmacology* **2006**, *147*, S163.

[9] Texeira, H.; Proenca, P.; Castanheira, A.; Santos, S.; Lopez-Rivadulla, M.; Corte-real, F.; Margues, E. P.; Vieira, D. N. *Forensic Science International* **2004**, *14S*, S61.

[10] Chariotti, M.; Costamanga, L. *Forensic Science International* **2000**, *114*, 1.

[11] Kelly, E.; Darke, S.; Ross, J. *Drug Alcohol Rev.* **2004**, *23*, 319.

[12] Notsu, H.; Tatsuma, T.; Fujishima, A. *Journal of Electroanalytical Chemistry* **2002**, *523*, 86–92.

[13] De Carvalho, R. M.; Mello, C.; Kubota, L. T. *Analytica Chimica Acta* **2000**, *420*, 109–121.

[14] Schiller, J. G.; Liu, C. C. *Analytical Biochemistry* **1978**, *33*, 25–33.

[15] Sachs, H.; Kintz, P. *J. Chromatogr. B. Biomed. Sci. Appl.* **1998**, *713*, 147.

[16] Lachenmeier, D. W.; Kroener, L.; Musshoff, F.; Madea, B. *Anal. Bioanal. Chem.* **2004**, *378*, 183.

[17] Brettell, T. A.; Inman, K.; Rudin, N.; Saferstein, R. *Anal. Chem.* **2001**, *73*, 2735.

[18] Fisher, D. H.; Broudy, M. I.; Fisher, L. M. *Biomedical Chromatography* **1996**, *10*, 161–166.

[19] Gunasingham, H.; Fleet, B. *Journal of Chromatography* **1983**, *261*, 43–53.

[20] Makuch, B.; Gazda, K.; Kamiśnski, M. *Analytica Chimica Acta* **1993**, *284*, 53–58.

[21] Nakahara, Y.; Sekine, H. *Journal of Analytical Toxicology* **1985**, *9*.

[22] Thompson, L. K.; Cone, E. J. *Journal of Chromatography* **1987**, *421*, 91.

[23] Kim, K.; Kim, D.; You, J.-M.; Han, H. S.; Jeon, S. *Electrochimica Acta* **2012**, *81*, 31.

[24] Goodwin, A.; Banks, C. E.; Compton, R. G. *Electroanalysis* **2006**, *18*, 1063.

[25] Lowe, E. R.; Banks, C. E.; Compton, R. G. *Analytical and Bioanalytical Chemistry* **2005**, *383*, 523–531.

[26] Backoffen, U.; Hoffmann, W.; Matysik, F.-M. *Chromatography* **2000**, 14.

[27] Liu, S.; Yu, J.; Ju, H. *Journal of Electroanalytical Chemistry* **2003**, *540*, 61–67.

[28] Rogers, K. R.; Becker, J. Y.; Cembrano, J. *Electrochimica Acta* **2000**, *45*, 4373–4379.

[29] Wang, J.; Lu, F.; Kane, S. A.; Choi, Y.-K. C.-K.; Smith, M. R.; Rogers, K. *Electroanalysis* **1997**, *9*, 1102.

[30] Hedenmo, M.; Narváez, A.; Domínguez, E.; Katakis, I. *Journal of Electroanalytical Chemistry* **1997**, *425*, 1–11.

[31] Ito, S.; Yamazaki, S.-i.; Kano, K.; Ikeda, T. *Analytica Chimica Acta* **2000**, *424*, 57–63.

[32] Fernández, L.; Borrás, C.; Carrero, H. *Electrochimica Acta* **2006**, *52*, 872–884.

[33] Koile, R. C.; Johnson, D. C. *Analytical Chemistry* **1979**, *51*, 741–744.

[34] Gattrell, M. *Journal of The Electrochemical Society* **1993**, *140*, 903.

[35] Carvalho, R. H.; Lemos, M. a. N. D. a.; Lemos, F.; Cabral, J. M. S.; Ribeiro, F. R. *Journal of Molecular Catalysis A: Chemical* **2006**, *253*, 170–175.

[36] Nissim, R.; Compton, R. G. *Physical Chemistry Chemical Physics* **2013**, *15*, 11918.

[37] Lowinsohn, D.; Gan, P.; Tschulik, K.; Foord, J. S.; Compton, R. G. *Electroanalysis* **2013**, *25*, 2435.

[38] Nissim, R.; Compton, R. G. *ChemElectroChem* **2014**, *1*, 763.

[39] Hart, J. P.; Spring, S. A.; Morgan, I. C. *Analyst* **1989**, *114*, 933.

[40] Jeng, C. Y.; Langer, S. H. *Journal of Chromatographic Science 27*, 549.

[41] Janegitz, B. C.; Medeiros, R. a.; Rocha-Filho, R. C.; Fatibello-Filho, O. *Diamond and Related Materials* **2012**, *25*, 128–133.

[42] Guix, M.; Pérez-López, B.; Sahin, M.; Roldán, M.; Ambrosi, A.; Merkoçi, A. *The Analyst* **2010**, *135*, 1918–1925.

[43] Toniolo, R.; Pizzariello, A.; Susmel, S.; Dossi, N.; Doherty, A. P.; Bontempelli, G. *Electroanalysis* **2007**, *19*, 2141–2148.

[44] Segovia-Martínez, L.; Moliner-Martínez, Y.; Campíns-Falcó, P. *Journal of Chromatography A* **2010**, *1217*, 7926–7930.

[45] Azevedo, A. F.; Souza, F. a.; Hammer, P.; Baldan, M. R.; Ferreira, N. G. *Journal of Nanoparticle Research* **2011**, *13*, 6133–6139.

[46] Analytical Methods Committee, E., Recommendations for the Definition; of the Detection Limit, U. *Analyst* **1987**, *112*, 119.

[47] Švancara, I.; Vytřas, K.; Kalcher, K.; Walcarius, A.; Wang, J. *Electroanalysis* **2009**, *21*, 7.

[48] Balbina, M. A.; de Menezes, M. M. T.; Eleotério, J. C.; Saczk, A. A.; Okumura, L. L.; ao, H. M. T.; de Oliveira, M. F. *Forensic Science International* **2012**, *221*, 29.

[49] Teixeira, H.; Verstraete, A.; Proenca, P.; Corte-Real, F.; Monsano, P.; Vieira, D. N. *Forensic Science International* **2007**, *170*, 148.

[50] Nyoni, E. C.; Sitaram, B. R.; Taylor, D. A. *Journal of Chromatography B* **1996**, *679*, 79.

[51] Krylova, E. N.; Tyurin, I. A.; Smirnov, A. V. *Mikroelementy v Meditsine* **2005**, *6*, 78.

[52] Backoffen, U.; Matysik, M.-F.; Lunte, C. E. *Journal of Chromatography A* **2002**, *942*, 259.

Chapter 8

Thesis Conclusions

In this thesis, the property of carbon paste electrodes to be able to accumulate species that are soluble and stable within the organic component of the material has been exploited both in fundamental electrochemical studies of the reduction of oxygen as well as more particularly in an analytical context, in the detection of the superoxide anion and substituted and unsubstituted phenols, including Δ^9-tetrahydrocannabinol (THC). The property of CTAB micelles to solubilise oxygen has also been studied, with the solubility of the species in the micelles having been measured. This thesis hence highlights the advantages of utilising accumulation steps in electroanalysis.

More specifically, Chapter 4 investigates the changed oxygen reduction pathway that is followed when a carbon paste electrode, rather than a glassy carbon substrate, is used, and it is concluded that the additional peak that is then observed is due to the one-electron reduction of oxygen to superoxide at the carbon-oil-water triple phase boundary. This alternative route is possible due to oxygen being able to accumulate in the utilised organic pasting liquid , dioctyl phthalate. Importantly, the proposed route accounts for both the "new" forward and reverse peaks but also for the potential loss of the anion radical into solution. The above findings are supported by the independence of the peak position on the solution pH as well as by the extracted kinetic and thermodynamic parameters.

Chapter 5, noting the lack of a simple and quantitative procedure to measure the solubility of oxygen in micelles [1–6], concludes that the monitoring of the oxygen uptake by CTAB micelles provides a simple and generally applicable micellar titration method for the reliable determination of the oxygen solubility in the CTAB micelles (6.7 ± 0.72 mM). The importance of this finding lies in the potential of using micelles as a biomimetic route through which to increase the solubility and mass transport of oxygen in aqueous systems.

The remaining chapters conclude that adjusting the paste composition, whether that be through the identity of the paste components or by altering the carbon-to-liquid ratio, is a significant consideration in the preparation of an assay. This is evidenced by the usefully sensitive sensing methodologies that can thus be developed, which can rely on either the direct or the indirect detection of the target species.

Chapter 6 is, to the best of the author's knowledge, the first electrochemical analogue of the NBT test and, additionally, one of the first examples of a non-enzymatic superoxide sensor that permits the assessment of superoxide concentrations as low as 59 pm. The work investigates the electrochemical behaviour of NBTC, elucidating the reduction mechanism of the species on a glassy carbon surface and subsquently applying the acquired knowledge to carbon paste electrodes. Through the pre-concentration of *both* superoxide and NBTC in the liquid binder of the substrate and the voltammetric observation of the chemically generated diformazan, the reaction between the two analytes as taking place *within* the pasting liquid is confirmed. The superoxide anion can thus successfully be detected using this set-up, allowing for a competitively low practical limit of detection to be obtained. A non-enzymatic approach to the electroanalysis of superoxide is hence concluded to be viable.

Finally Chapter 7 further advances the work of Chapter 6 with the development of a new approach, here termed "absorptive stripping voltammetry", for both the wide range *and* the sensitive detection of phenolic species in aqueous solutions and synthetic saliva samples. It is concluded that appropriate tunning of the paste recipe is essential in order for both analyte conctentrations in the low micromolar range as well as the higher millimolar end to be detected (LOD (phenol) = 2.5 μM, LOD (4-phenoxyphenol) = 2.5 μM, LOD (4-methoxyphenol) = 5.0 μM). The power and usefulness of absorptive stripping voltammetry is effectively illustrated through its application to the sensitive detection of THC, the active constituent of cannabis which also contains a phenol moiety. In this work, it is the different identity of the pasting liquid along with its addition in larger quantities that leads to the reliable detection of THC in synthetic saliva samples (LOD (THC in saliva) = 5.0 μM); this result is of major significance as it proves the practical applicability of the approach.

Absorptive stripping voltammetry thus provides a powerful and versatile electrochemical approach that enables the reliable, quantitative and sensitive detection of biologically and environmentally important molecules.

References

[1] Matheson, I. B.; King, A. *J. Colloid Interf. Sci.* **1978**, *66*, 464.

[2] Geiger, M. W.; Turro, N. J. *Photochem Photobiol* **1975**, *22*, 273.

[3] Petyaeo, I.; Hunt, J. *Biochim. Biophys. Acta* **1997**, *1345*, 293.

[4] Kameo, Y.; Takahashi, S.; Krieg-Kowald, M.; Ohmachi, T.; Takagi, S.; Inoue, H. *J. Phys. Chem. B* **1999**, *103*, 9562.

[5] An, Y.-J.; Carraway, E. J.; Schlautman, M. A. *Water Res.* **2002**, *36*, 300.

[6] Barillari, J.; Iori, R.; Papi, A.; Orlandi, M.; Bartolini, G.; Gabbanini, S.; Pedulli, G. F.; Valgmigli, L. *J. Agric. Food Chem.* **2008**, *56*, 7823.